nature portfolio

Peer Review File

Antisite Defect Unleashes Catalytic Potential in High-Entropy Intermetallics for Oxygen Reduction Reaction

Corresponding Author: Professor Dingguo Xia

This file contains all reviewer reports in order by version, followed by all author rebuttals in order by version.

Attachments originally included by the reviewers as part of their assessment can be found at the end of this file.

Version 0:

Reviewer comments:

Reviewer #1

(Remarks to the Author)
The manuscript reported a novel high entropy intermetallic electrocatalyst with antisite-defect and an average particle size of only 1.7 nm. The as-prepared electrocatalyst showed high mass activity of 4.12 A mgPt 1 toward the oxygen reduction reaction, which was 33 times that of the commercial Pt/C. PEMFC, assembled with PD-PZFCNC-HEI as the cathode (0.05 mgPt cm 2) exhibits a peak power density of 1.9 W cm 2 and a high mass activity of 2.2 A mgPt 1 at 0.9 V. The work is well-organized and significantly different from previously reported work. The evidence provided is comprehensive. I strongly recommend that Nature Communications accepts the manuscript with minor revisions:

1. The author should explain what Pt anti-site defects are so that readers can understand this concept.
2. Why Co, Fe, Ni, Zn, and Cr elements are chosen to construct the high-entropy intermetallics with Pt?
3. Related to question 2, what are the roles of Co, Fe, Ni, Zn, and Cr elements in the catalytic process?
4. For the aberration electron microscopy image in Figure 1d, the author should mark the Pt inversion defects to be described, otherwise it will be difficult for readers to know where the so-called Pt inversion defects are located.
5. For the preparation of PD-PZFCNC-HEI, it seems that there is a significant difference in the feeding ratio of each element during synthesis compared to the element ratio in the final product PD-PZFCNC-HEI. This is why?

Reviewer #2

(Remarks to the Author)
The manuscript by Chen et al. describes the application of Pt-based high-entropy intermetallic materials as catalysts for the oxygen reduction reaction. The optimized composition demonstrates superior mass and surface area-normalized ORR activity as compared to commercial Pt/C and other literature references, that in principle represents an impactful result. However, the content of the work is very similar to the previous study from the same group, where the material with a very similar composition (viz., PtIrFeCoCu) was already reported and studied for the same application [J. Am. Chem. Soc., 2023, 145, 11140] (the mentioned paper is not cited in the main text).
In the present study, authors claim that Pt sites occupying the antisite positions play an important role in activity enhancement, however there are no compelling experimental evidences for that, and even the DFT calculations (e.g. Pt d band center position) do not convincingly confirm this trend. Indeed, the ORR activity of the material obtained at 800 C is higher than that of other references, however the Reviewer would find it more plausible that changes of the coordination environment of Pt due to different temperature treatments (viz. differences in segregation/dispersion of the elements forming alloy) would have higher impact on the activity than the presence of the antisite defects. Furthermore, since TEM is a local probe technique, there is no strong proof that antisite defects (1) is an exclusive feature of the materials synthesized at 800 C, (2) do not present in other reference materials prepared by authors.
Other comments:
1) Authors demonstrate the operational stability of the materials however little is said about structural stability of the nanoparticles. Fig. S32 demonstrate that the structure is preserved, however it is also important to compare the elemental composition before and after activity tests as it is very likely that some non-noble elements would leach during operation in acidic condition that would indicate their rather minor role in activity enhancement.

2) ICP analysis of the electrolyte solution after activity test is necessary to monitor the structural integrity of the catalysts.
3) Fig. S13 shows that zinc is present in the system mainly in the form of (nanosized) oxide (and possibly complex with N-ligands), rather than in metallic state. In case of other elements, it should also be mentioned that the presence of the respective oxide phases cannot be ruled out based of the XAS data.

Reviewer #3

(Remarks to the Author)
The authors synthesized an ordered PtZnFeCoNiCr high-entropy intermetallic electrocatalyst with Pt antisite point defects, which exhibited superior ORR catalytic actives than commercial Pt/C. They also used theoretical calculations and in situ X-ray absorption fine structure to reveal the underlying mechanism. The research is interesting. However, there are also some points which must be addressed in the revised manuscript before further consideration.
1.In the introduction, the author should explain how does the defect design and growth control affect the catalytic activity. Additionally, the summary on the current researches is insufficient, and the outlined challenges lack distinct characteristics.
2.The authors should explain the elemental selection of PtZnFeCoNiCr.
3.In DFT modeling, despite the authors listed 10 different models in Fig.S40, how did the authors ensure the randomness of atomic distribution in the high-entropy model? By the use of randomization tools or other methods?
4.It is recommended to utilize the DFT+U approach to improve the description of systems with strongly correlated d electrons and enhance the result reliability. In addition, did the authors consider the spin-effect of each metal sites? The authors should adjust their computational methods accordingly.
5.Although PD-PZFCNC-HEI catalyst showed superior properties, the authors should add other references for comparison, such as the combination of bimetal, trimetal, and quaternary-metal catalysts with Pt anti-site defects to better explain the role of each metal.
6.For the average diameter analysis of the PD-PZFCNC-HEI catalyst, the error analysis of the measurement should be given. Did the heat treatment affect the morphology and particle size of PZFCNC-HEA, which may also the important factor for catalyst.
7.Longer stability tests with larger current density need to be provided to furtherly confirm its practical potentials. The sample under testing conditions shows significant fluctuations in Figure. S31, the author should explain it.
8.The authors should present more comparison on several relevant catalyst samples for mass activity and peak power density (Fig.3i)in the revised manuscript.
9.The authors should clarify the transformation mechanism of the precursors to the HEA/HEI under different calcination temperature.
10.In the catalytic process, the role of Fe, Co, Ni, and Cr in high entropy material in performance improvement and stability should be further explained.
11.The PD-PZFCNC-HEI nanoparticles exhibited significant compressive and tensile strains, which were attributed to the lattice distortion effects arising (Fig.1p-q). The authors should consider the strain effects on the electronic structures and the enhanced catalytic activates.

Reviewer #4

(Remarks to the Author)
The paper by Chen et al. reports on a high-entropy intermetallic compound for the oxygen reduction reaction (ORR). The catalyst has been thoroughly characterized and tested, showing very promising results. The experiments are supplemented by DFT calculations, however these are not performed and presented in a way that can support the associated conclusions. I therefore recommend major revisions, addressing the detailed comments given below, before the paper may be suitable for publication.

1. On p4 it says: “The selection of non-precious metal constituents is based on a comprehensive consideration of the atomic radii, formation enthalpy, and reported ORR activity of each component.” Given that the selection of elements to mix is one of the most challenging aspects of high entropy alloys, an elaboration of these considerations would be suitable
2. From the XPS data it looks like a significant fraction of Fe, Co and Ni atoms are oxidized. What is the origin of this oxidation?
3. The activity normalized by the electrochemical active surface area is reported for the Pt reference and for the PD-PZFCNC-HEI sample. Is it similar for the other HEI samples?
4. Figure 4c: It is impossible to see the difference in the inset figures of (what I assume is) the charge distribution in the pure metals and the HEI. Also, the colour bar has no label.
5. The insets in Figure 4g-h are likewise too small. However, if you zoom in it can be seen that the adsorbates are not in the same adsorption sites. Notably, the diagram which is stated to be a Zn adsorption site (Figure 4h) shows pictures where the adsorbates are never bound to Zn only. The other diagram (Figure 4g) appears to have *OH in a site that is not present in the pictures for *O and *OOH. Are these pictures taken from the optimized structures? Is the reason that Zn sites are found to be surprisingly active perhaps that the adsorbates move during optimisation?
6. For the pure Pt reference (figure S43) all adsorbates are positioned on top, while for the HEIs a mixture of top, bridge and hollow site adsorption sites are shown. On Pt, *O is usually more stable in the hollow site, while on a HEI the most stable site will depend on the neighbouring atoms, and the adsorbate will not necessarily relax to this position. Thus, different adsorption sites (top, bridge, hollow) as well as different adsorption environments for the HEI should be tested to be able to conclude anything. This is especially true considering the small energy differences presented here. Furthermore, it could provide substance to the claim that the Pt antisite defects are important.
7. It is unclear how the surface formation energies are calculated? The values are very large. For the calculation of antisite defects, as I understand it a random atom has been swapped for Pt in the original surface model. However, the defect

formation energy depends on the local environment, and conclusions cannot be made based on a single defect structure.
8. COHP calculations are performed for the adsorption of *OH, however it is unclear what insight they add. The meaning of the values is not explained, and in any case the rate limiting step is found to be the hydrogenation of O2.

Minor Comments
9. P2 L8: “However, the development of efficient oxygen reduction reaction catalysts hinders their practical applications.” I think this sentence was intended to have the opposite meaning
10. P7, line 2. “Pt occupies the non-metallic sites” There are no non-metallic sites?
11. P10: There are two references to Figure 40, this must be figure S40?
12. Figure 4a-b. There is no label for the colours of the different atoms

Version 1:

Reviewer comments:

Reviewer #1

(Remarks to the Author)
The authors have properly responded the reviewer's comments and clearly revised the manuscript. This reviewer strongly recommends the acceptance of this manuscript for the publication in Nature Communications.

Reviewer #2

(Remarks to the Author)
The authors satisfactorily addressed Reviewer's comments. Manuscript can be recommended for publication.

Reviewer #3

(Remarks to the Author)
Thanks to the authors for revising the manuscript to address the concerns/suggestions. I am satisfied with the revision and have no further comments.

Reviewer #4

(Remarks to the Author)
Overall, the revision has improved the manuscript and answered some of my concerns. However, a few points should be corrected or conveyed more clearly in the paper before it can be published. New comments are related to the answers to my previous comments and have been attached as a pdf for clarity.

Version 2:

Reviewer comments:

Reviewer #4

(Remarks to the Author)
The revision has addressed my concerns and the manuscript can now be recommended for publication.

Response to reviewers (NCOMMS-24-57617)

We gratefully thank all reviewers for their time spend making their constructive remarks and useful suggestions, which has significantly raised the quality of the manuscript and has enable us to improve the manuscript. Each suggested revision and comment, brought forward by the reviews was accurately incorporated and considered. Below the comments of the reviewers are addressed point by point and the revision are indicated.

Reviewers' comments:

Reviewer #1: The manuscript reported a novel high entropy intermetallic electrocatalyst with antisite-defect and an average particle size of only 1.7 nm. The as-prepared electrocatalyst showed high mass activity of 4.12 A mg_{Pt}^{-1} toward the oxygen reduction reaction, which was 33 times that of the commercial Pt/C. PEMFC, assembled with PD-PZFCNC-HEI as the cathode (0.05 mg_{Pt} cm^{-2}) exhibits a peak power density of 1.9 W cm^{-2} and a high mass activity of 2.2 A mg_{Pt}^{-1} at 0.9 V. The work is well-organized and significantly different from previously reported work. The evidence provided is comprehensive. I strongly recommend that Nature Communications accepts the manuscript with minor revisions:

Response: We sincerely appreciate the reviewer's positive comments on our work. We have provided point-by-point responses and made revisions based on the comments you raised.

Comment 1. The author should explain what Pt anti-site defects are so that readers can understand this concept.

Response: Thanks for reviewer's professional suggestions. Pt antisite defects refer to the phenomenon in the crystal structure of alloys or intermetallic compounds, where an element that is supposed to occupy a specific site (in this case, a non-precious metal element) is replaced by another element (such as Pt). Specifically, in the Pt-based high-entropy intermetallics synthesized in this work, Pt is typically expected to occupy the noble metal sites, but a small amount of Pt atoms may migrate to the non-noble metal sites, forming antisite defects. These defects can impact the structure and properties of the material, particularly in catalytic reactions, where Pt antisite defects can alter the electronic structure and local environment, thereby affecting catalytic activity.

Changes made in the revised manuscript:

In the revised manuscript, we added a description: "This suggests that a small amount of Pt has migrated into positions typically occupied by non-precious metals, resulting in Pt antisite defects. These defects may influence the material's structure and properties, particularly in catalytic reactions. Notably, Pt antisite defects were observed for the first time in Pt-based intermetallic catalysts."

Comment 2. Why Co, Fe, Ni, Zn, and Cr elements are chosen to construct the high-entropy intermetallics with Pt?

Response: Thanks for reviewer's professional suggestions. The research objective of this work is to explore low platinum and high activity oxygen reduction catalysts. Considering that Pt is the optimal catalytic element for ORR, our research aims to reduce the amount of platinum and enhance its catalytic activity through high-entropy alloying based on Pt. The selection of non-precious metals requires consideration of elements that can be alloyed with Pt and subsequently converted into intermetallic compounds with Pt. In addition, the selected elements ideally have similar atomic radii to alleviate lattice distortion effects in the resulting high-entropy alloy. Importantly, if the selected non-precious metal also exhibits favorable ORR catalytic activity, it would be advantageous. In light of these criteria, we opted for Zn, Fe, Co, Ni, and Cr, as these elements have been reported to possess high ORR activity and are amenable to alloying with Pt (*Angew Chem. Int. Ed. Engl.* **2021**, *60*, 21899; *Nat. Commun.* **2014**, *5*, 5185; *Adv. Mater.* **2022**, *34*, e2109188; *Advanced Energy Materials* **2020**,

10, 2000179; *Chemistry of Materials* **2015**, *27*, 7538). Additionally, they belong to neighboring transition metals in the fourth period, minimizing the disparity in atomic radii.

Changes made in the revised manuscript:

We added a revised description "The selection of non-precious metal constituents is based on a comprehensive consideration of the atomic radii, formation enthalpy, and reported ORR activity of each component, aiming to obtain highly active high-entropy intermetallic compounds." in the revised manuscript.

Comment 3. Related to question 2, what are the roles of Co, Fe, Ni, Zn, and Cr elements in the catalytic process?

Response: Thanks for reviewer's professional suggestions. From the PDOS results shown in Figures 4d-f, the non-precious metals Co, Fe, Ni, Zn, and Cr optimize the Pt d-band electron structure while lowering the d-band center. The lowering of the d-band center can optimize the adsorption energy of oxygen-containing intermediates on the PD-PZFCNC-HEI surface, thereby enhancing catalytic activity. On the other hand, in addition to Pt, non-precious metals such as Zn can also serve as active reaction sites. As shown in Figure 4h, the reaction energy barrier at the Zn site is significantly lower than that on the Pt (111) surface. Furthermore, as seen in Figure S53b, the reaction process at each active site involves not only the interaction between the oxygen-containing intermediates and the single metal, but also the synergistic effect of nearby metal atoms at the metal site, which jointly participates in the interaction with the intermediates.

In addition, based on the ADT tests of different reference samples, it was observed that the high-entropy intermetallic reference sample without Cr exhibited significant half-wave potential decay, whereas the reference sample containing Cr remained relatively stable (Figure S40). Therefore, it can be concluded that Cr serves as an important element for enhancing structural stability.

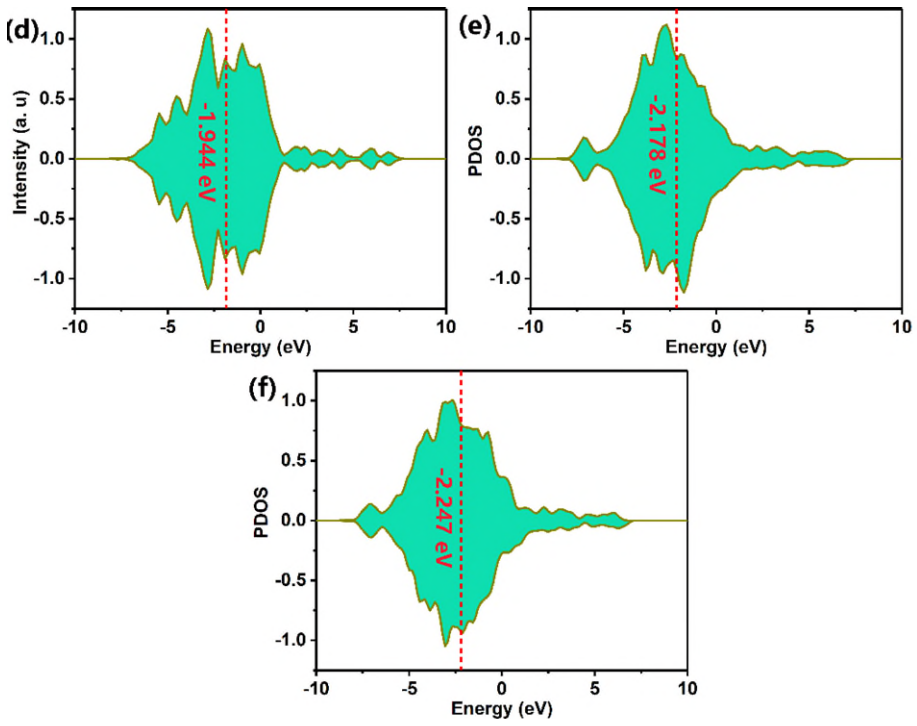

Figure 4. Partial density of states (PDOS) of the d-band for the surface Pt atoms in (d) Pt (111), (e) PZFCNC-HEI and (f) PD-PZFCNC-HEI surface.

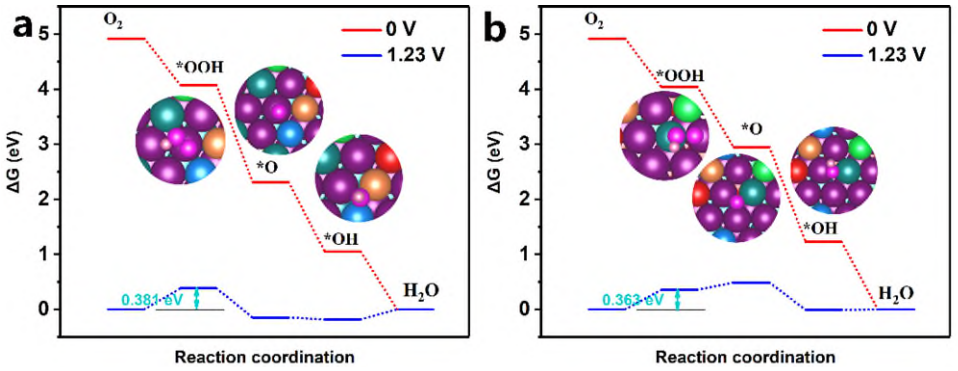

Figure 4g-h: The free energies of intermediates of (g) Pt and (h) Zn sites on the PD-PZFCNC-HEI surface for the ORR steps.

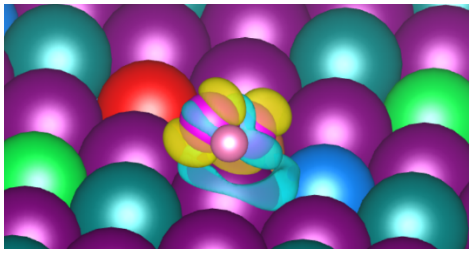

Figure S53b. Differential charge density ($\Delta\rho = \rho_{*OOH} - \rho_{*} - \rho_{OOH}$) of *OOH adsorbed system at the PD-PFCNCZ-HEI. The isosurface in blue and yellow represent charge accumulation and depletion, respectively.

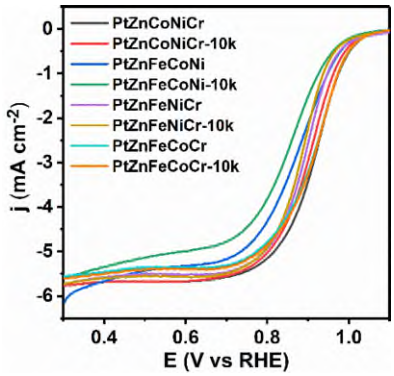

Figure S40. Polarization curves of some relevant quinary intermetallic reference samples after AST between 0.6 and 0.95 V at different cycle numbers.

Changes made in the revised manuscript:

In the revised supporting information, we added a description: "Supplementary Note 4: we controlled other conditions while varying the types and quantities of elements to prepare a series of binary, ternary, quaternary, and quinary catalyst reference samples. All the reference samples were tested for ORR catalytic performance in 0.1 M $HClO_4$ solution. As shown in Figure S37, the half-wave potentials ($E_{1/2}$) of the non-high-entropy samples PtZn, PtZnCr, PtZnCo, PtZnNi, PtZnFe, PtZnFeCo, PtZnCoNi, PtZnFeCr, PtZnFeNi, and PtZnCoCr are 0.86 V, 0.81 V, 0.848 V, 0.850 V, 0.881 V, 0.917 V, 0.903 V, 0.885 V, 0.850 V, and 0.829 V, respectively, all of which are significantly lower than the 0.948 V of PD-PZFCNC-HEI. Furthermore, from a structural perspective, taking the reference sample PtZnFe as an example, it is likely that due to the insufficient amount of non-precious metals, it tends to form an $L1_2$ structure (Figure S38a). Additionally, due to its relatively low configurational entropy, the surface of the sample is etched (Figure S38b) after treatment with 0.1 M $HClO_4$ solution.

This further demonstrates that high configurational entropy contributes to the enhanced corrosion resistance of PD-PZFCNC-HEI in acidic media. On the other hand, to better explain the role of each metal element in the alloy, we prepared a series of high-entropy intermetallic catalyst reference samples, including PtZnCoNiCr, PtZnFeCoNi, PtZnFeNiCr, and PtZnFeCoCr, with Fe, Cr, Co, and Ni individually omitted. The corresponding $E_{1/2}$ values of these samples are 0.921 V, 0.87 V, 0.90 V, and 0.917 V, respectively, as shown in Figure S39. Due to the unique introduction method of Zn in present work, it is not possible to prepare a quintary intermetallic alloy without Zn. However, the results of PtZn ($E_{1/2}$ = 0.87 V) and Pt/C ($E_{1/2}$ = 0.86 V) indicate that Zn slightly enhances the ORR activity of Pt-based catalysts, while its presence also increases the configurational entropy of the material. After 10,000 cycles, the $E_{1/2}$ values of PtZnCoNiCr, PtZnFeCoNi, PtZnFeNiCr, and PtZnFeCoCr decreased by 12 mV, 30 mV, 13 mV, and 1 mV, respectively (Figure S40). It means that the presence of Cr significantly reduces the extent of activity degradation. In summary, Zn, Fe, Co, Ni, and Cr all contribute to the modulation of Pt's electronic structure to enhance ORR catalytic activity, while Cr further improving the material's durability."

Comment 4. For the aberration electron microscopy image in Figure 1d, the author should mark the Pt inversion defects to be described, otherwise it will be difficult for readers to know where the so-called Pt inversion defects are located.

Response: Thanks for reviewer's professional suggestions. We have highlighted the Pt antisite defects in Figure 1d using red dashed circle and added the corresponding description in the revised manuscript.

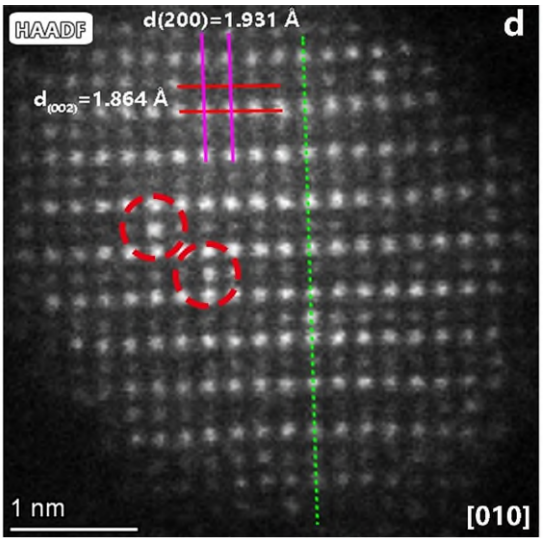

Figure 1d. High-angle annular dark-field scanning transmission electron microscopy images of PD-PZFCNC-HEI nanoparticle

Changes made in the revised manuscript:

In the revised supporting information, we added a description: "Moreover, a small amount of high-contrast Pt atoms is dispersed within the lower contrast non-precious metal layer (As indicated by the red dashed circle)."

Figure 1 is replaced as follow:

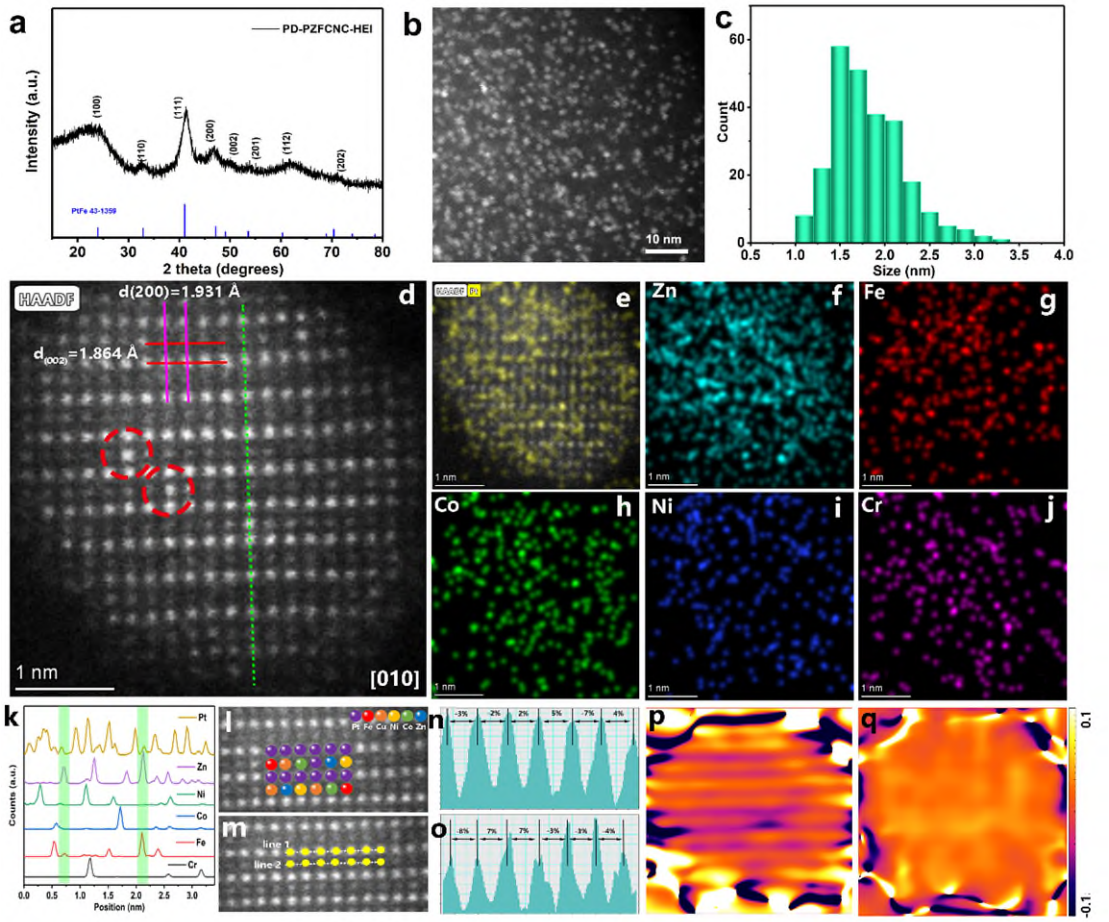

Figure 1. (a) X-ray diffraction (XRD) pattern of PD-PZFCNC-HEI; (b) Transmission electron microscopy images of PD-PZFCNC-HEI; (c) Particle size distribution histogram of PD-PZFCNC-HEI; (d) High-angle annular dark-field scanning transmission electron microscopy images of PD-PZFCNC-HEI nanoparticle; The corresponding atomic-resolution STEM-EDS mapping of (e) Pt, (f) Zn, (g) Fe, (h) Co, (i) Ni, and (j) Cr; (k) Line-scan profile of the PD-PZFCNC-HEI nanoparticle along the green line in Figure 1d; (l) and (m) Corresponding local structure image; Quantitative analysis on compressive and tensile strains within dislocation cores along (n) line 1 and (o) line 2 in Figure 1m, respectively; Strain distributions of (p) ε_{yy} and (q) ε_{xx} by geometric phase analysis.

Comment 5. For the preparation of PD-PZFCNC-HEI, it seems that there is a significant difference in the feeding ratio of each element during synthesis compared to the element ratio in the final product PD-PZFCNC-HEI. This is why?

Response: Thanks for reviewer's professional suggestions. During synthesis, we maintained a nearly 1:1 metal feed ratio for each element in the initial metal mixture. As a result, the amount of non-precious metals was intentionally in excess. This was done to ensure the complete formation of the $L1_0$-structured high-entropy alloy with non-precious metals. The excess non-precious metals tend to segregate, and therefore, we treated the final product with 0.1 M $HClO_4$ solution to dissolve the segregated non-precious metals, obtaining the final PD-PZFCNC. Consequently, the final elemental ratio will differ slightly from the initial feed ratio, with the non-precious metals being present in a smaller proportion than initially introduced.

Reviewer #2: The manuscript by Chen et al. describes the application of Pt-based high-entropy intermetallic materials as catalysts for the oxygen reduction reaction. The optimized composition demonstrates superior mass and surface area-

normalized ORR activity as compared to commercial Pt/C and other literature references, that in principle represents an impactful result. However, the content of the work is very similar to the previous study from the same group, where the material with a very similar composition (viz., PtIrFeCoCu) was already reported and studied for the same application [J. Am. Chem. Soc., 2023, 145, 11140] (the mentioned paper is not cited in the main text).

Response: We sincerely appreciate the reviewer's positive comments on our work. As you mentioned, our research group published a paper on high-entropy intermetallic ORR catalysts in 2023 (J. Am. Chem. Soc., 2023, 145, 11140). However, the work published in J. Am. Chem. Soc. is fundamentally different from the manuscript we are currently submitting to *Nature Communications*, with key distinctions in the following aspects:

1. Differences in Synthesis Strategy: In J. Am. Chem. Soc., 2023, 145, 11140, we employed a chemical co-reduction method. Metal ions were first dispersed in an aqueous solution, followed by co-reduction of the metal elements using sodium borohydride as a strong reducing agent to form high-entropy alloys, which were then sintered at 850°C to obtain the PtIrFeCoCu five-component high-entropy intermetallic. In contrast, in present work submitted to *Nature Communications*, we adopt an impregnation-reduction strategy combined with spatial confinement. First, metal ions are dispersed within the synthesized DPCN (porous nitrogen-doped carbon) matrix. The metal ions are then reduced at high temperature under H_2, and particle growth is confined to a small size, resulting in the formation of PtZnFeCoNiCr high-entropy intermetallic nanoparticles.
2. Difference in the Support: In J. Am. Chem. Soc., 2023, 145, 11140, we directly used Ketjen black carbon powder as the metal support, which primarily served to disperse the metal particles and provide electrical conductivity. In contrast, in present work, we employed DPCN (porous nitrogen-doped carbon) as the support material. The pore size distribution of DPCN is predominantly below 3 nm, as shown in Figure S7. By using DPCN as a confinement framework, the growth of the synthesized PtZnFeCoNiCr high-entropy intermetallic nanoparticles is restricted, ensuring that their particle size remains below 3 nm (as shown in Figure 1b), which allows for enhanced exposure of the precious metal. Additionally, nitrogen (N) atoms in the DPCN matrix form N-M bonds with the high-entropy metal nanoparticles (Figure 2l), anchoring the metal particles and preventing their migration during both the synthesis process and cycling.
3. Difference in Elemental Composition: In J. Am. Chem. Soc., 2023, 145, 11140, we selected five elements: Pt, Ir, Fe, Co, and Cu. The larger atomic radii of Pt and Ir occupied the same sites, while Fe, Co, and Cu occupied other non-precious metal sites. These elements were randomly arranged within their respective sites, with Pt and Ir atoms accounting for 50% of the total atomic composition, thus forming an $L1_0$-structured high-entropy intermetallic. In contrast, in present manuscript submitted to *Nature Communications*, we selected six elements: Pt, Zn, Fe, Co, Ni, and Cr. The Pt atomic content constitutes about 50%, while the remaining five non-precious metals account for the other 50%, also forming an $L1_0$ structure. It is well-known that the choice of elemental composition has a significant impact on the electronic structure and electrochemical performance of alloy catalysts. For example, although they belong to the same crystal structure, Pt_3Al (Adv. Funct. Mater., 2014) and Pt_3Co (Adv. Mater., 2023, 35, 2301310) exhibit distinct d-band electronic structures.
4. Differences in morphological characteristics: In J. Am. Chem. Soc., 2023, 145, 11140, the average particle size of the PtIrFeCoCu intermetallics reached 6 nm, with a wide size distribution ranging from 2 to 12 nm. In contrast, the PtZnFeCoNiCr high-entropy intermetallics synthesized in this study exhibit an average particle size of only 1.7 nm, with a size range between 1 and 3.5 nm. Clearly, the PtZnFeCoNiCr intermetallics developed in this work represent a significant breakthrough in the synthesis of high-entropy intermetallics, offering valuable insights for the synthesis of small-sized high-entropy intermetallics.
5. Differences in Catalytic Activity: In J. Am. Chem. Soc., 2023, 145, 11140, the PtIrFeCoCu intermetallics as ORR catalysts achieved only a half-wave potential ($E_{1/2}$) of 0.896 V in a half-cell, with the current density and mass activity approaching zero in a practical hydrogen-oxygen fuel cell at 0.9 V. In contrast, the PtZnFeCoNiCr high-entropy

intermetallics synthesized in this work exhibit a much higher $E_{1/2}$ of 0.948 V in the half-cell, and their mass activity in a practical hydrogen-oxygen fuel cell at 0.9 V remains as high as 3.0 A $mgPt^{-1}$. It is evident that the ORR activity of the PtZnFeCoNiCr high-entropy intermetallics prepared in this study has been significantly enhanced, marking a striking performance.

6. Differences in Catalytic Mechanisms: The high catalytic activity of PtIrFeCoCu high-entropy intermetallics prepared in J. Am. Chem. Soc. 2023, 145, 11140 is primarily attributed to the high activity of low-index facets (001). In contrast, the high ORR catalytic activity of PtZnFeCoNiCr, prepared in this work, is due to two factors: (i) the presence of Pt antisite defects, which induce compressive strain and thereby modulate the Pt d-band electrons, and (ii) the formation of multiple active sites.

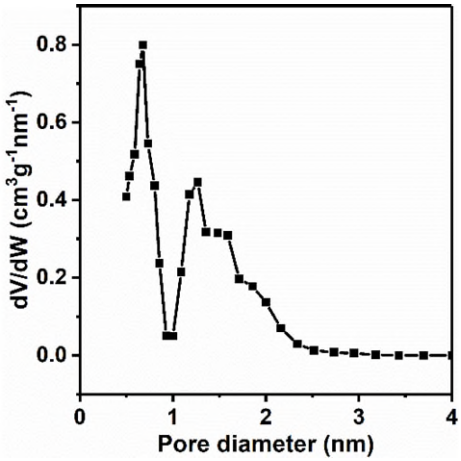

Figure S7. Pore size distribution of Zn-DPCN.

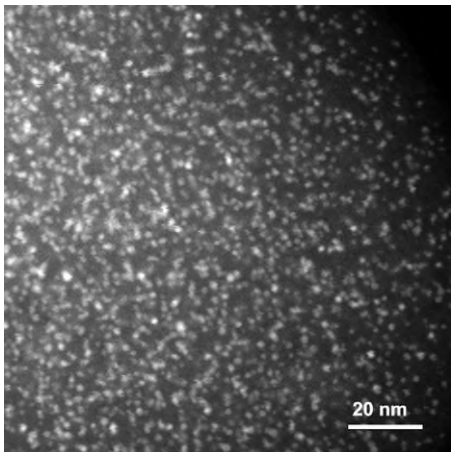

Figure 1b. TEM images of PD-PZFCNC-HEI.

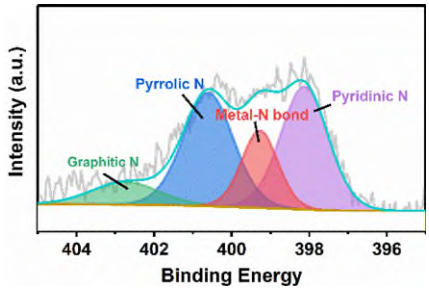

Figure 2l. X-ray photoelectron spectroscopy spectra collected at the N 1s edges for the PD-PZFCNC-HEI sample.

Comment 1: In the present study, authors claim that Pt sites occupying the antisite positions play an important role in activity enhancement, however there are no compelling experimental evidences for that, and even the DFT calculations (e.g. Pt d band center position) do not convincingly confirm this trend. Indeed, the ORR activity of the material obtained at 800 C is higher than that of other references, however the Reviewer would find it more plausible that changes of the coordination environment of Pt due to different temperature treatments (viz. differences in segregation/dispersion of the elements forming alloy) would have higher impact on the activity than the presence of the antisite defects.

Response: Thanks for reviewer's professional suggestions. In fact, we believe that the presence of Pt antisite defects is an important, but not the sole, reason for the high catalytic activity of PD-PZFCNC-HEI. As shown in Figure S28, for the sample synthesized under 900°C conditions without antisite defects, the half-wave potential ($E_{1/2}$) still reaches 0.926V, and the mass activity achieves 1.82 A $mgPt^{-1}$, which is 14.4 times that of commercial Pt/C. This indicates that even in the absence of antisite defects, the sample already exhibits relatively high catalytic activity. In the sample synthesized at 800°C, which contains Pt antisite defects, the $E_{1/2}$ is further enhanced to 0.948V. Therefore, it can be inferred that the presence of Pt antisite defects has contributed to the further improvement in catalytic activity. From the perspective of the d-band electronic structure of Pt (Figure 4d-f), in the PZFCNC-HEI without antisite defects, the d-band center of Pt (-2.178 eV) is lower compared to that of pure Pt (111) (-1.944 eV), suggesting a weaker interaction with reaction intermediates. Therefore, it can be observed that the d-band electronic structure of Pt in PZFCNC-HEI without antisite defects is optimized due to factors such as the ligand effect. Additionally, in PD-PZFCNC-HEI containing Pt antisite defects, the d-band center is further lowered to -2.247 eV, indicating that the presence of Pt antisite defects influences local strain, thereby further optimizing the d-band electronic structure. Hence, the high catalytic activity of PD-PZFCNC-HEI arises from multiple factors rather than a single cause. However, this study emphasizes the unique role of antisite defects, which enable PD-PZFCNC-HEI to achieve further improvement in catalytic performance.

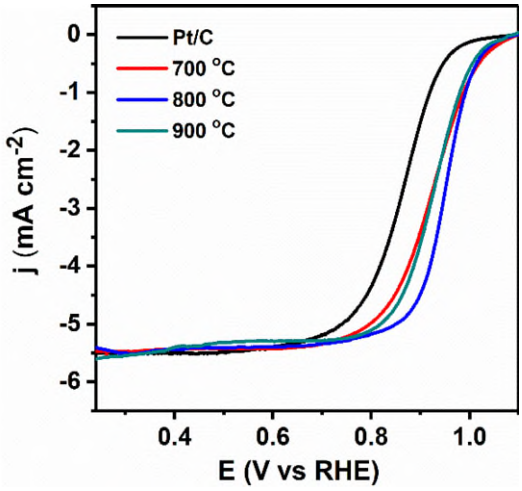

Figure S28. Oxygen reduction reaction (ORR) polarization curves of PD-PZFCNC-HEI synthesized at different temperatures.

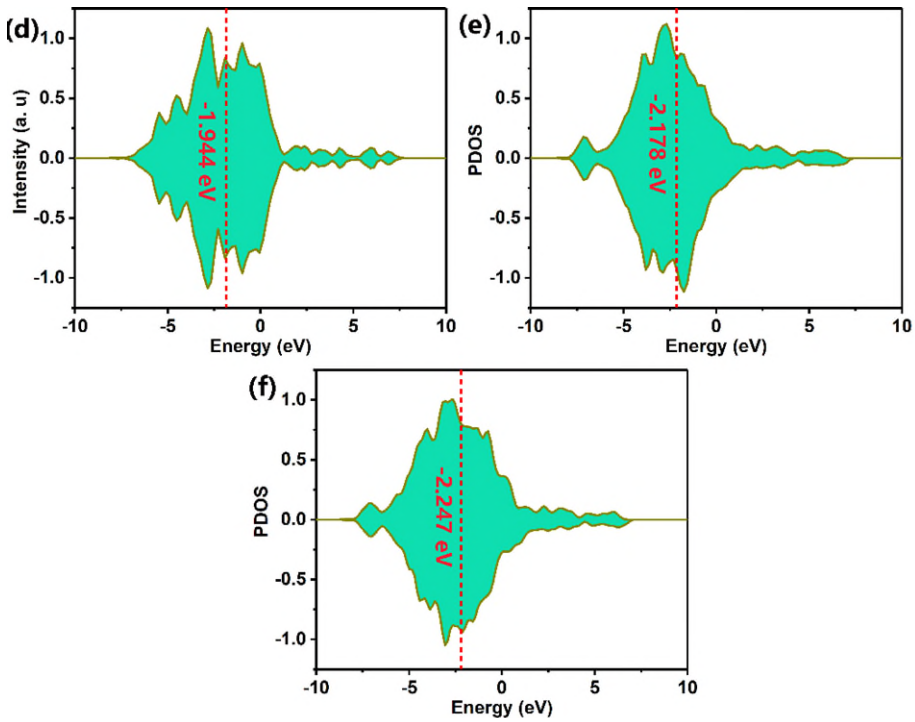

Figure 4. Partial density of states (PDOS) of the d-band for the surface Pt atoms in (d) Pt (111), (e) PZFCNC-HEI and (f) PD-PZFCNC-HEI surface.

Comment 2: Furthermore, since TEM is a local probe technique, there is no strong proof that antisite defects (1) is an exclusive feature of the materials synthesized at 800 ℃, (2) do not present in other reference materials prepared by authors.

Response: Thanks for reviewer's professional suggestions. Based on your considerations, we performed a fitting of the EXAFS results for the Pt element in the sample PZFCNC-HEI (Figure S25), prepared under 900°C conditions without antisite defects, and the defect-containing sample PD-PZFCNC-HEI (Figure S26), prepared under 800°C conditions. The local structural information was obtained by fitting the FT-EXAFS spectrum using Artemis software, mainly focusing on fitting the first coordination shell peak of PZFCNC-HEI and PD-PZFCNC-HEI owing to the signal-to-noise ratio of the absorption spectrum for our ultrasmall particles. The fitting structural parameters are shown in Table S2. The fitting results of PD-PZFCNC-HEI indicate that the average coordination number (CN) of the first shell of Pt is around 8, with Pt-Pt coordination number of 4.5 and Pt-M (M: non-precious metal) coordination number of 3.5, indicating the successful formation of a face-centered tetragonal (fct) ordered intermetallic structure in PFCNCZ-HEI (J. Am. Chem. Soc. 20181402926). Most importantly, the Pt-M coordination number in PD-PZFCNC-HEI (3.5) is slightly lower than that in PZFCNC-HEI (3.8), while the Pt-Pt coordination number in PD-PZFCNC-HEI (4.5) is significantly higher than in PZFCNC-HEI (4.0). This suggests that Pt antisite defects occupy some non-precious metal atomic sites, leading to an increase in the Pt-Pt coordination number in PD-PZFCNC-HEI, which macroscopically supports the presence of Pt antisite defects in PD-PZFCNC-HEI. On the other hand, the Pt-Pt bond length in PD-PZFCNC-HEI (2.70 Å) is slightly shorter than in PZFCNC-HEI (2.71 Å), further verifying the presence of Pt antisite defects, as the larger radius of the Pt defects compared to non-precious metals induces local compressive strain, thereby reducing the average Pt-Pt bond length.

On the other hand, Figure S22 shows the XRD spectra results of the modified high-entropy alloys prepared at different temperatures. It can be seen that the (110) crystal plane at 32.8° for the sample prepared at 700°C,which is characteristic of the intermetallic phase , is not prominent. In the solid solution structure, the occupancy of metal atoms is completely random (J.Am.Chem.Soc. 2024, 146, 3010−3022), thus no antisite defects can exist. When the temperature was increased

to 800°C and 900°C, the PD-PZFCNC-HEI and PZFCNC-HEI samples obtained respectively showed a distinct (110) crystal plane characteristic peak at 32.8°, indicating the formation of an ordered intermetallic structure. Furthermore, from the STEM images of the intermetallic particles, no Pt antisite defects were observed in the PZFCNC-HEI sample obtained at 900°C (Figure S23), while clear Pt antisite defects were evident in the PD-PZFCNC-HEI sample obtained at 800°C (Figure S20). Therefore, it can be inferred that Pt antisite defects are unique to the PD-PZFCNC-HEI sample obtained at 800°C.

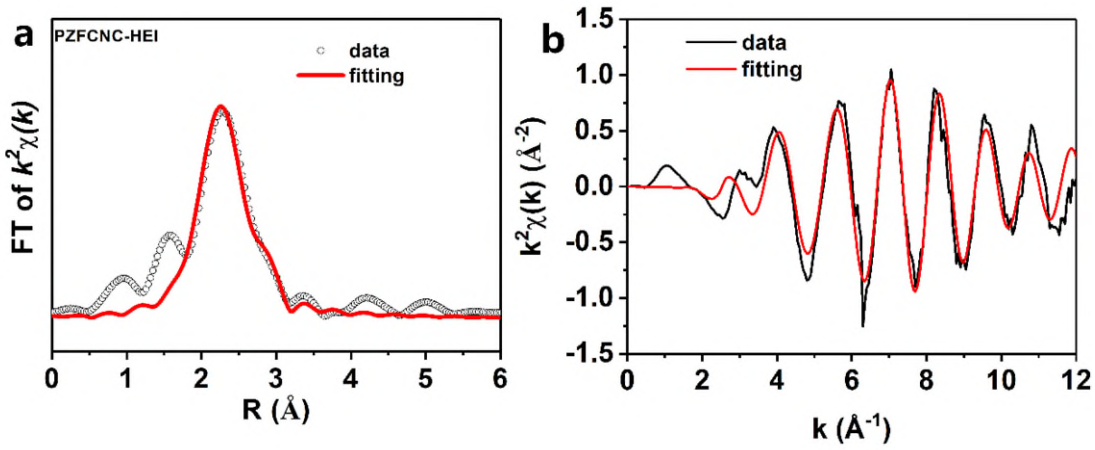

Figure S25. Comparison of the experimental k^2-weighted EXAFS and the fitting curves in the (a) R space and (b) K space for the as-prepared PZFCNC-HEI at Pt L_3-edge.

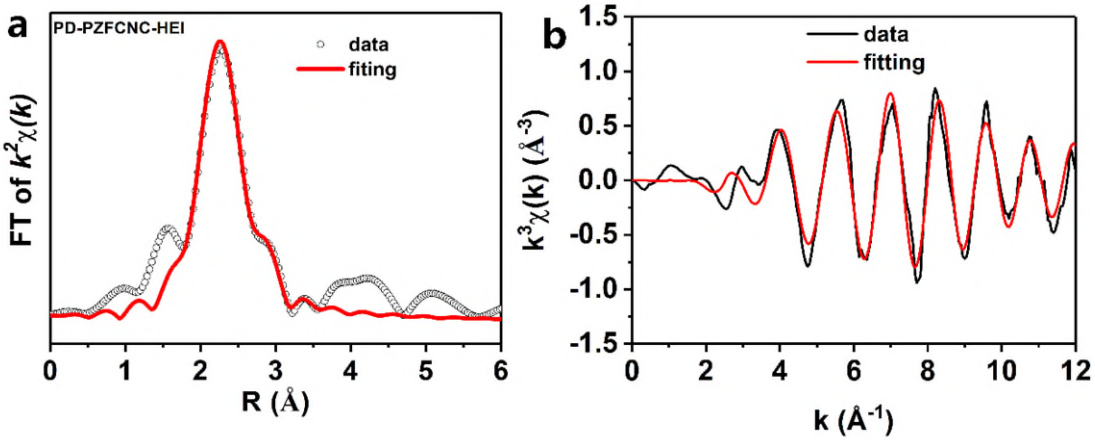

Figure S26. Comparison of the experimental k^2-weighted EXAFS and the fitting curves in the (a) R space and (b) K space for the as-prepared PD-PZFCNC-HEI at Pt L_3-edge.

Table S2. EXAFS fitting parameters at the Pt L-edge various samples (S_0^2=0.82).

samples	path	C. N.[a]	R (Å) [b]	σ^2 ($\times 10^{-3}$ Å^2) [c]	ΔE (eV) [d]	R factor[e]
PZFCNC-HEI	Pt-M	3.8±0.4	2.62±0.02	7.2±3.1	4.3±5.6	0.02
	Pt-Pt	4.0±0.7	2.71±0.02	5.1±2.0		
PD-PZFCNC-HEI	Pt-M	3.5±0.3	2.61±0.02	8.8±4.3	3.8±3.7	0.02
	Pt-Pt	4.5±0.5	2.70±0.02	9.8±4.4		

[a]C. N.: coordination numbers; [b]*R*: bond distance; [c]σ^2: Debye-Waller factors; [d]ΔE_0: the inner potential correction. [e]*R* factor:

goodness of fit.

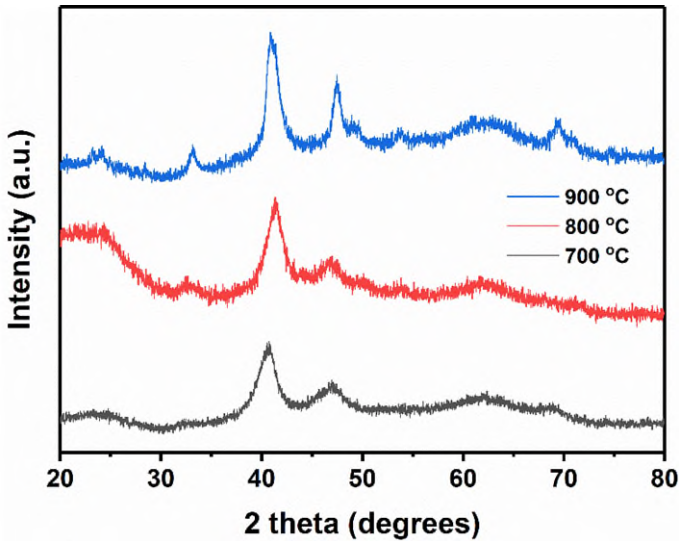

Figure S22. XRD patterns of PD-PZFCNC-HEI synthesized at different temperatures.

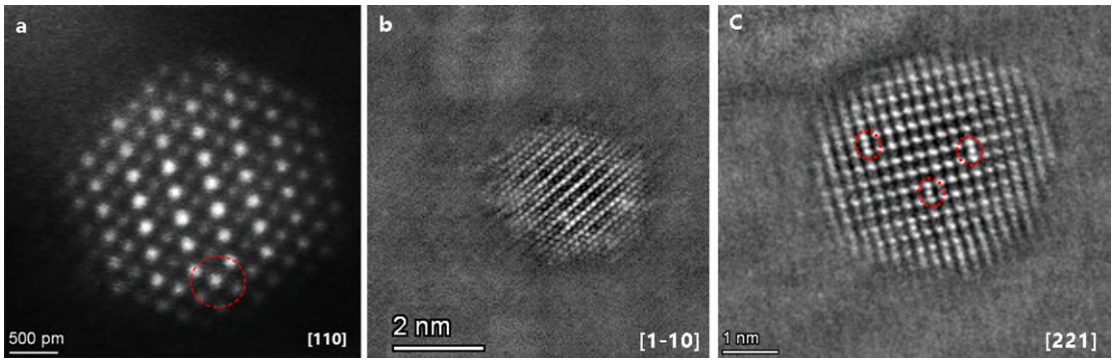

Figure S20. High-angle annular dark-field scanning transmission electron microscopy (HAADF-STEM) images of PD-PZFCNC-HEI nanoparticle along the (a) [110], (b) [1-10] and (c) [221] zone axis.

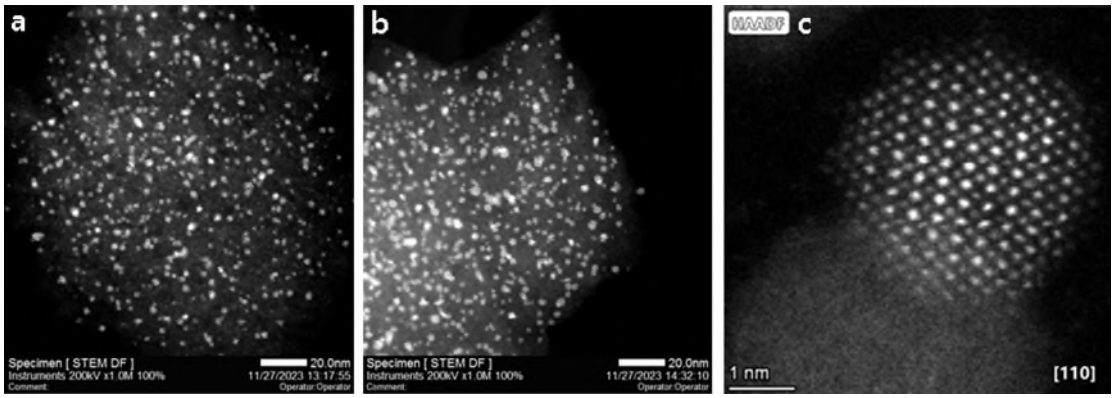

Figure S23. (a) and (b) STEM images of PZFCNC-HEI (900) reference synthesized at 900 °C; (c) HAADF-STEM image of PZFCNC-HEI (900 °C) reference.

Changes made in the revised manuscript:

In the revised manuscript, we added a description: "The local structural information was obtained by fitting the FT-EXAFS spectrum using Artemis software, mainly focusing on fitting the first coordination shell peak of PZFCNC-HEI (Figure S25) and PD-PZFCNC-HEI (Figure S26) owing to the signal-to-noise ratio of the absorption spectrum for our ultrasmall particles. The fitting structural parameters are shown in Table S2. The fitting results of PD-PZFCNC-HEI indicate that the average coordination number (CN) of the first shell of Pt is around 8, with Pt-Pt coordination number of 4.5 and Pt-M (M: non precious metal) coordination number of 3.5, indicating the successful formation of a face-centered tetragonal (fct) ordered intermetallic structure in PFCNCZ-HEI.[1] Most importantly, the Pt-M coordination number in PD-PZFCNC-HEI (3.5) is slightly lower than that in PZFCNC-HEI (3.8), while the Pt-Pt coordination number in PD-PZFCNC-HEI (4.5) is significantly higher than in PZFCNC-HEI (4.0). This suggests that Pt antisite defects occupy some non-precious metal atomic sites, leading to an increase in the Pt-Pt coordination number in PD-PZFCNC-HEI, which macroscopically supports the presence of Pt antisite defects in PD-PZFCNC-HEI. On the other hand, the Pt-Pt bond length in PD-PZFCNC-HEI (2.70 Å) is slightly shorter than in PZFCNC-HEI (2.71 Å), further verifying the presence of Pt antisite defects, as the larger radius of the Pt defects compared to non-precious metals induces local compressive strain, thereby reducing the average Pt-Pt bond length."

Figure S25, Figure S26 and Table S2 were added in supporting information as follows:

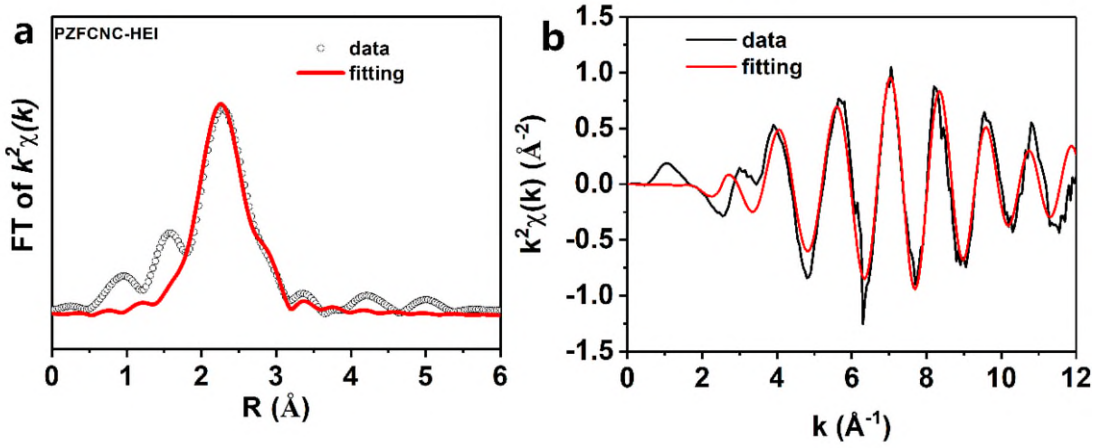

Figure S25. Comparison of the experimental k^2-weighted EXAFS and the fitting curves in the (a) R space and (b) K space for the as-prepared PZFCNC-HEI at Pt L_3-edge.

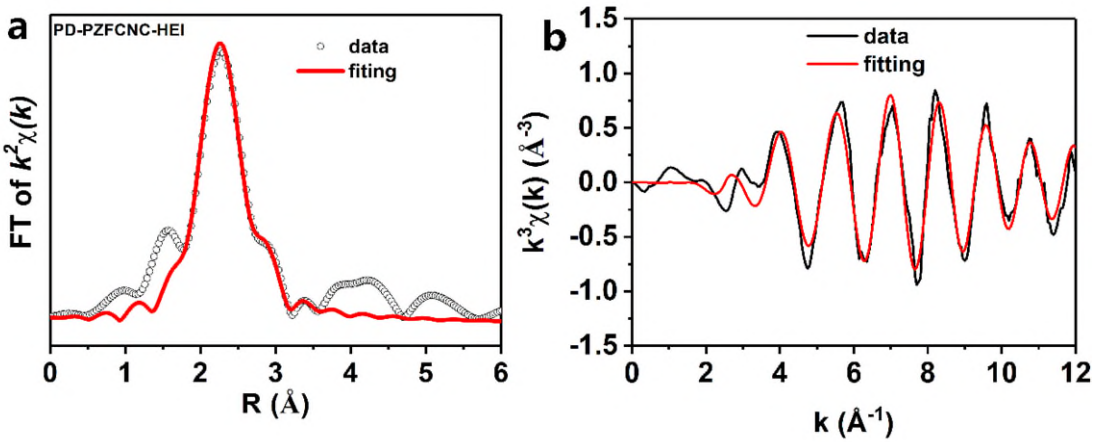

Figure S26. Comparison of the experimental k^2-weighted EXAFS and the fitting curves in the (a) R space and (b) K space for the as-prepared PD-PZFCNC-HEI at Pt L_3-edge.

Table S2. EXAFS fitting parameters at the Pt L-edge various samples (S_0^2=0.82).

samples	path	C. N.[a]	R (Å) [b]	σ^2 ($\times 10^{-3}$ Å^2) [c]	ΔE (eV) [d]	R factor[e]
PZFCNC-HEI	Pt-M	3.8±0.4	2.62±0.02	7.2±3.1	4.3±5.6	0.02
	Pt-Pt	4.0±0.7	2.71±0.02	5.1±2.0		
PD-PZFCNC-HEI	Pt-M	3.5±0.3	2.61±0.02	8.8±4.3	3.8±3.7	0.02
	Pt-Pt	4.5±0.5	2.70±0.02	9.8±4.4		

[a]C. N.: coordination numbers; [b]*R*: bond distance; [c]σ^2: Debye-Waller factors; [d]ΔE_0: the inner potential correction. [e]*R* factor: goodness of fit.

Comment 3: Authors demonstrate the operational stability of the materials however little is said about structural stability of the nanoparticles. Fig. S32 demonstrate that the structure is preserved, however it is also important to compare the elemental composition before and after activity tests as it is very likely that some non-noble elements would leach during operation in acidic condition that would indicate their rather minor role in activity enhancement.

Response: Thanks for reviewer's professional suggestions. In the PD-PZFCNC-HEI sample, the Pt atoms benefit from optimized d-band electron distribution due to ligand and strain effects, making Pt sites the dominant active sites for the reaction. With a noble metal Pt content of 50%, it is evident that Pt serves as the primary catalytic active site. Although some non-noble metal sites also contribute to the catalytic activity and can further enhance performance, the dissolution of a small amount of non-noble metals after the reaction has a relatively minor impact on the overall catalytic activity. Based on your suggestion, we performed ICP-MS testing on the PD-PZFCNC-HEI sample after cycling. As shown in Table S4, the elemental ratio of PD-PZFCNC-HEI after cycling shows minimal change, and the material still retains its high-entropy structure. Calculations show that its configurational entropy remains at 1.52R (greater than 1.5R). Compared to the reported literature, the atomic ratio change of PD-PZFCNC-HEI after AST testing is relatively small. This further supports the preservation of the non-precious metal sites.

Table S4. The atomic ratio calculated based on the ICP-MS results of sample A before and after AST testing.

sample	Cr	Fe	Co	Ni	Zn	Pt	
PD-PZFENC-HEI	0.105	0.095	0.084	0.093	0.26	0.5	This work
PD-PZFENC-HEI-AST	0.107	0.07	0.076	0.082	0.25	0.5	
PtFe		0.23				0.5	Small 2022, 18, 2202916
PtFe-AST		0.09				0.5	
PtNiMo/C				0.22		0.5	ACS Catal. 2019, 9, 8682
PtNiMo/C-ADT				0.13		0.5	
PtCo			0.5			0.5	J. Mater. Chem. A, 2024,
PtCo-ADT			0.11			0.5	12, 27979

Changes made in the revised manuscript:

In the revised manuscript, we added a description: "In addition, after the AST testing, the PD-PZFCNC-HEI sample still retains a relatively high configurational entropy (Table S4 and S5)."

Table S4 is added in supporting information as follow:

Table S4. The atomic ratio calculated based on the ICP-MS results of sample A before and after AST testing.

sample	Cr	Fe	Co	Ni	Zn	Pt	
PD-PZFENC-HEI	0.105	0.095	0.084	0.093	0.26	0.5	This work
PD-PZFENC-HEI-AST	0.107	0.07	0.076	0.082	0.25	0.5	
PtFe		0.23				0.5	Small 2022, 18, 2202916
PtFe-AST		0.09				0.5	
PtNiMo/C				0.22		0.5	ACS Catal. 2019, 9, 8682
PtNiMo/C-ADT				0.13		0.5	

PtCo	0.5	0.5	J. Mater. Chem. A, 2024,
PtCo-ADT	0.11	0.5	12, 27979

Comment 4: ICP analysis of the electrolyte solution after activity test is necessary to monitor the structural integrity of the catalysts.

Response: Thanks for reviewer's professional suggestions. Based on your suggestion, we performed an AST test on 10 mg of the PD-PZFCNC-HEI sample and measured the metal content in the 200 mL electrolyte. The test results are shown in Figure S5. As can be seen, the metal leaching is minimal, demonstrating a clear advantage compared to the literature. Furthermore, the PD-PZFCNC-HEI retains its high-entropy configuration after the AST test (Table S4), further supporting the high structural stability of PD-PZFCNC-HEI.

Table S5. Metal content of a 10 mg sample in 200 mL electrolyte after AST testing, compared with values reported in the literature under the same conditions.

Sample	Cr (mg/L)	Fe (mg/L)	Co (mg/L)	Ni (mg/L)	Zn (mg/L)	Pt (mg/L)	Ref.
Pt nanoparticles						0.144	ACS Catal. 2020, 10, 6281
PtNi/C				0.345		0.288	Electrochimica Acta, 2024, 487, 144200
PtCo			0.4			0.115	Electrochimica Acta, 2024, 487, 144200
PtFe		0.21					Small 2022, 18, 2202916
PD-PZFCNC-HEI	0.003	0.092	0.093	0.04	0.031	0.093	This work

Changes made in the revised manuscript:

In the revised manuscript, we added a description: "In addition, after the AST testing, the PD-PZFCNC-HEI sample still retains a relatively high configurational entropy (Table S4 and S5)."

Table S5. Metal content of a 10 mg sample in 200 mL electrolyte after AST testing, compared with values reported in the literature under the same conditions.

Sample	Cr (mg/L)	Fe (mg/L)	Co (mg/L)	Ni (mg/L)	Zn (mg/L)	Pt (mg/L)	Ref.
Pt nanoparticles						0.144	ACS Catal. 2020, 10, 6281
PtNi/C				0.345		0.288	Electrochimica Acta, 2024, 487, 144200
PtCo			0.4			0.115	Electrochimica Acta, 2024, 487, 144200
PtFe		0.21					Small 2022, 18, 2202916
PD-PZFCNC-HEI	0.003	0.092	0.093	0.04	0.031	0.093	This work

Comment 5: Fig. S13 shows that zinc is present in the system mainly in the form of (nanosized) oxide (and possibly complex with N-ligands), rather than in metallic state. In case of other elements, it should also be mentioned that the presence of the respective oxide phases cannot be ruled out based of the XAS data.

Response: Thanks for reviewer's professional suggestions. Although part of the Zn exists in the form of Zn-N coordination, the EXAFS results for other elements show relatively weaker M-N coordination signals compared to the metal-N coordination signals. Additionally, since the XAS signal is a bulk-sensitive signal, it indicates that the other metals mainly exist in their metallic state. Based on your suggestion, we have made appropriate revisions to the relevant descriptions in the manuscript to make them more reasonable.

Changes made in the revised manuscript:

In the revised manuscript, we changed a description: "The extended X-ray absorption fine structure (EXAFS) results for all elements show strong metal-metal coordination peaks, further indicating they primarily exist in the metallic state (Figures 2e–h, Figures S13a and S13b)."

Reviewer #3: The authors synthesized an ordered PtZnFeCoNiCr high-entropy intermetallic electrocatalyst with Pt antisite point defects, which exhibited superior ORR catalytic actives than commercial Pt/C. They also used theoretical calculations and in situ X-ray absorption fine structure to reveal the underlying mechanism. The research is interesting. However, there are also some points which must be addressed in the revised manuscript before further consideration.

Response: We sincerely appreciate the reviewer's positive comments on our work.

Comment 1: In the introduction, the author should explain how does the defect design and growth control affect the catalytic activity. Additionally, the summary on the current researches is insufficient, and the outlined challenges lack distinct characteristics.

Response: We sincerely appreciate the reviewer's valuable comments. Regarding how defect design and growth control affect catalytic activity, we have further elaborated in the manuscript on the role of defects in modulating the surface electronic structure of catalysts. The introduction of defects can lead to local strain, which significantly influences the electronic structure and adsorption properties of the catalyst surface.(Joule 2018, 2, 2551-2582; Angewandte Chemie International Edition 2017, 56, 3594-3598) Specifically, the presence of defects such as vacancies, antisite defects, and grain boundaries introduces local strain that modifies the coordination environment of metal atoms, changing the d-band structure and enhancing the interaction between the catalyst and reaction intermediate. This local strain not only facilitates the adsorption and reduction of oxygen molecules but also leads to a more favorable adsorption energy, thus improving the overall ORR performance. Moreover, defects can create additional active sites by altering the local electronic environment, which can further boost the catalytic activity. These active sites, generated by strain fields around defects, are critical for optimizing the adsorption of ORR intermediates and enhancing reaction kinetics.

Regarding the summary of current research and the outlined challenges, we have provided a more detailed review of the existing progress in the manuscript, particularly regarding how alloying and defect engineering can enhance ORR catalytic performance. However, we also emphasize the challenges faced in defect control in high-entropy intermetallic catalysts, particularly the prevention of excessive grain growth and aggregation during high-temperature synthesis, and the effective stabilization of defect structures to maintain high catalytic activity during reactions.

We have expanded these discussions in the manuscript and ensured that these challenges are presented with clear characteristics, aiming to provide more targeted contributions to the existing literature.

Changes made in the revised manuscript:

In the revised manuscript, we added a description: "On the other hand, the kinetically controlled metal diffusion process results in various types of defects in alloys.[2,3] The presence of defects induces stress due to lattice mismatch, which can affect the surface electronic structure and the adsorption ability toward adsorbates.[4,5] To date, the synthesis of intermetallic nanocrystals with controlled defect structures remains challenging, partly due to the complex growth and ordering processes.[6,7] Conversely, **t**he presence of hysteresis diffusion effect in high-entropy intermetallic compounds further increases the likelihood of generating various defects.[8-10]"

Comment 2: The authors should explain the elemental selection of PtZnFeCoNiCr. The authors should explain the elemental selection of PtZnFeCoNiCr.

Response: We sincerely appreciate the reviewer's valuable comments. The research objective of this work is to explore low platinum and high activity oxygen reduction catalysts. Considering that Pt is the optimal catalytic element for ORR,

our research aims to reduce the amount of platinum and enhance its catalytic activity through high-entropy alloying based on Pt. The selection of non-precious metals requires consideration of elements that can be alloyed with Pt and subsequently converted into intermetallic compounds with Pt. In addition, the selected elements ideally have similar atomic radii to alleviate lattice distortion effects in the resulting high-entropy alloy. Importantly, if the selected non-precious metal also exhibits favorable ORR catalytic activity, it would be advantageous. In light of these criteria, we opted for Zn, Fe, Co, Ni, and Cr, as these elements have been reported to possess high ORR activity and are amenable to alloying with Pt (*Angew Chem. Int. Ed. Engl.* **2021**, *60*, 21899; *Nat. Commun.* **2014**, *5*, 5185; *Adv. Mater.* **2022**, *34*, e2109188; *Advanced Energy Materials* **2020**, *10*, 2000179; *Chemistry of Materials* **2015**, *27*, 7538). Additionally, they belong to neighboring transition metals in the fourth period, minimizing the disparity in atomic radii.

Changes made in the revised manuscript:

We added a revised description "The selection of non-precious metal constituents is based on a comprehensive consideration of the atomic radii, formation enthalpy, and reported ORR activity of each component, aiming to obtain highly active high-entropy intermetallic compounds." in the revised manuscript.

Comment 3: In DFT modeling, despite the authors listed 10 different models in Fig.S40, how did the authors ensure the randomness of atomic distribution in the high-entropy model? By the use of randomization tools or other methods?

Response: We sincerely appreciate the reviewer's valuable comments. The high-entropy model was constructed using Python's pymatgen and random modules by randomly replacing the Fe sites in the PtFe (111) surface structure. Specifically, we first determined the atomic numbers and quantities of atoms in the optimized PtFe (111) surface structure. Based on the elemental ratios obtained from experimental characterization (Pt:Cr:Fe:Co:Ni:Zn = 1:0.137:0.171:0.123:0.115:0.445), we calculated the number of atoms to be replaced for each of the five elements (Cr, Fe, Co, Ni, Zn). We then used the random module to generate a random array of these five elements and employed pymatgen methods to perform the element substitution in the PtFe (111) surface structure, aiming to simulate the disordered distribution of multiple elements in a high-entropy structure. Using this random construction method, we generated 10 different (4 × 4 × 4) unit cells, with energy differences less than 0.5 eV, indicating that their distribution has minimal impact on the stability of the bulk structure, as shown in Figure S47a-j. By further comparing their energies, we selected the structure with the lowest energy, i.e., the thermodynamically most stable structure, to further construct the Pt-defective high-entropy structure.

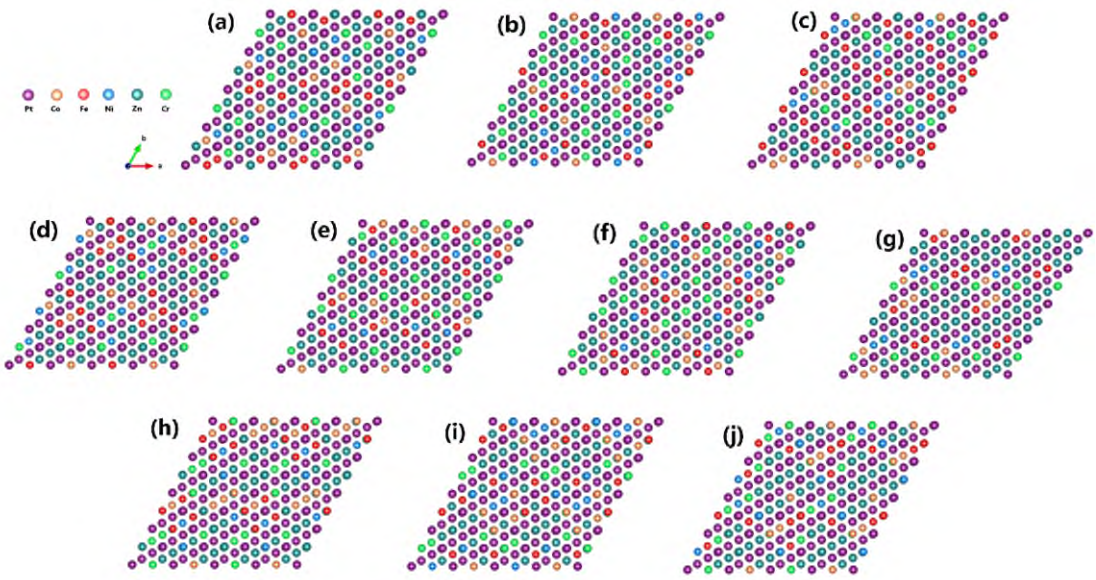

Figure S47. Constructed a series of defect free PFCNZ-HEI (111) surface models. The energies for (a)-(j) were -377.69 eV, -376.53 eV, -376.74 eV, -376.09 eV, -377.33 eV, -374.75 eV, -376.59 eV, -375.51 eV, 377.37 eV, -377.6 eV, respectively.

Changes made in the revised manuscript:

We added a revised description in the revised supporting information: "The high-entropy model was constructed using Python's pymatgen and random modules by randomly replacing the Fe sites in the PtFe (111) surface structure. Specifically, we first determined the atomic numbers and quantities of atoms in the optimized PtFe (111) surface structure. Based on the elemental ratios obtained from experimental characterization (Pt:Cr:Fe:Co:Ni:Zn = 1:0.137:0.171:0.123:0.115:0.445), we calculated the number of atoms to be replaced for each of the five elements (Cr, Fe, Co, Ni, Zn). We then used the random module to generate a random array of these five elements and employed pymatgen methods to perform the element substitution in the PtFe (111) surface structure, aiming to simulate the disordered distribution of multiple elements in a high-entropy structure. Using this random construction method, we generated 10 different (4 × 4 × 4) unit cells, with energy differences less than 0.5 eV, indicating that their distribution has minimal impact on the stability of the bulk structure, as shown in Figure S47a-j. By further comparing their energies, we selected the structure with the lowest energy, i.e., the thermodynamically most stable structure, to further construct the Pt-defective high-entropy structure."

Comment 4: It is recommended to utilize the DFT+U approach to improve the description of systems with strongly correlated d electrons and enhance the result reliability. In addition, did the authors consider the spin-effect of each metal sites? The authors should adjust their computational methods accordingly.

Response: We sincerely appreciate the reviewer's valuable comments. On the Applicability of the DFT+U Method: The DFT+U method is typically used to describe strongly correlated systems, particularly localized electrons in transition metal oxides or compounds.[11] When transition metals are in an oxidized state, their d-electrons can exhibit strong correlation effects, and the introduction of the U parameter helps improve the description of the electronic structure. However, in high-entropy alloy systems, the metal atoms studied are typically in their metallic state. In the metallic state, the d-electrons are delocalized and do not exhibit strong correlation effects.[12] Therefore, introducing U in such systems does not significantly improve the computational accuracy and may instead lead to over-constraint of the model, which could affect the reliability of the results. After careful consideration, we have opted not to use the DFT+U method in this study.

On the Spin Effect: For each metal site in the metallic system, we have considered spin polarization in our calculations to ensure accurate description of the magnetic properties of the system. In high-entropy alloys, the spin states of different metal elements may vary, and thus we have thoroughly accounted for the impact of spin effects on catalytic performance. Additionally, we have specified in the DFT calculation details that spin polarization has been incorporated.

Comment 5: Although PD-PZFCNC-HEI catalyst showed superior properties, the authors should add other references for comparison, such as the combination of bimetal, trimetal, and quaternary-metal catalysts with Pt anti-site defects to better explain the role of each metal.

Response: We sincerely appreciate the reviewer's valuable comments. Based on your suggestion, we controlled other conditions while varying the types and quantities of elements to prepare a series of binary, ternary, quaternary, and quinary catalyst reference samples. All the reference samples were tested for ORR catalytic performance in 0.1 M $HClO_4$ solution. As shown in Figure S37, the half-wave potentials ($E_{1/2}$) of the non-high-entropy samples PtZn, PtZnCr, PtZnCo, PtZnNi, PtZnFe, PtZnFeCo, PtZnCoNi, PtZnFeCr, PtZnFeNi, and PtZnCoCr are 0.86 V, 0.81 V, 0.848 V, 0.850 V, 0.881 V, 0.917 V, 0.903 V, 0.885 V, 0.850 V, and 0.829 V, respectively, all of which are significantly lower than the 0.948 V of PD-PZFCNC-HEI. Furthermore, from a structural perspective, taking the reference sample PtZnFe as an example, it is likely that due to

the insufficient amount of non-precious metals, it tends to form an $L1_2$ structure (Figure S38a). Additionally, due to its relatively low configurational entropy, the surface of the sample is etched (Figure S38b) after treatment with 0.1 M $HClO_4$ solution. This further demonstrates that high configurational entropy contributes to the enhanced corrosion resistance of PD-PZFCNC-HEI in acidic media. This demonstrates the enhancement of catalytic activity due to entropy modification and defect engineering. On the other hand, to better explain the role of each metal element in the alloy, we prepared a series of high-entropy intermetallic catalyst reference samples, including PtZnCoNiCr, PtZnFeCoNi, PtZnFeNiCr, and PtZnFeCoCr, with Fe, Cr, Co, and Ni individually omitted. The corresponding $E_{1/2}$ values of these samples are 0.921 V, 0.87 V, 0.90 V, and 0.917 V, respectively, as shown in Figure S39. Due to the unique introduction method of Zn in this synthesis, it is not possible to prepare a quintary intermetallic alloy without Zn. However, the results of PtZn ($E_{1/2}$ = 0.87 V) and Pt/C ($E_{1/2}$ = 0.86 V) indicate that Zn slightly enhances the ORR activity of Pt-based catalysts, while its presence also increases the configurational entropy of the material. Overall, it can be seen that the absence of any single element leads to a slight decrease in catalytic activity. After 10,000 cycles, the $E_{1/2}$ values of PtZnCoNiCr, PtZnFeCoNi, PtZnFeNiCr, and PtZnFeCoCr decreased by 12 mV, 30 mV, 13 mV, and 1 mV, respectively (Figure S40). It was observed that the presence of Cr significantly reduces the extent of activity degradation, as the sample without Cr, PtZnFeCoNi, exhibits the largest $E_{1/2}$ degradation. In summary, Zn, Fe, Co, Ni, and Cr all contribute to the modulation of Pt's electronic structure to enhance ORR catalytic activity, with Cr further improving the material's durability.

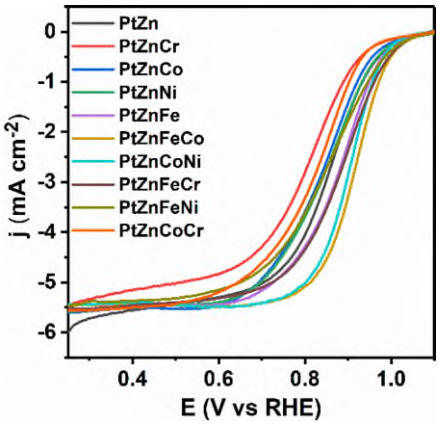

Figure S37. The ORR polarization curves of some relevant binary, ternary, and quaternary intermetallic reference samples.

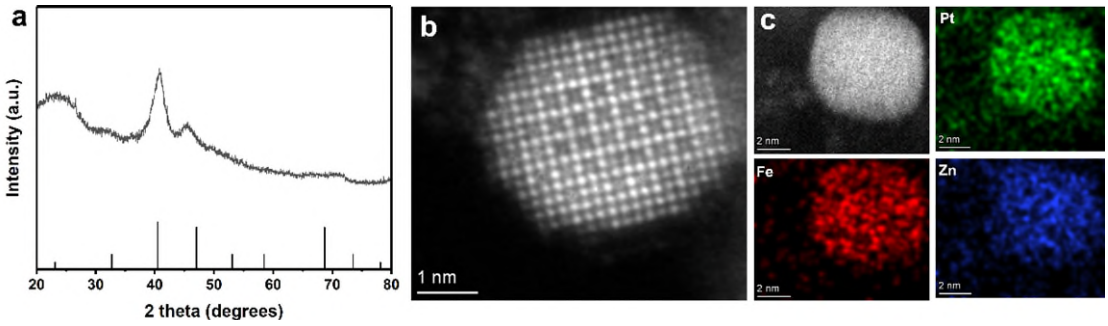

Figure S38. (a) XRD result of the PtZnFe reference sample; HAADF-STEM image of PtZnFe; (c) The corresponding atomic-resolution STEM-EDS mapping of Pt, Fe and Zn elements.

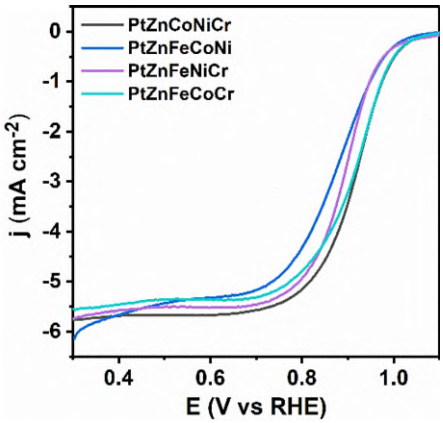

Figure S39. The ORR polarization curves of some relevant quinary intermetallic reference samples.

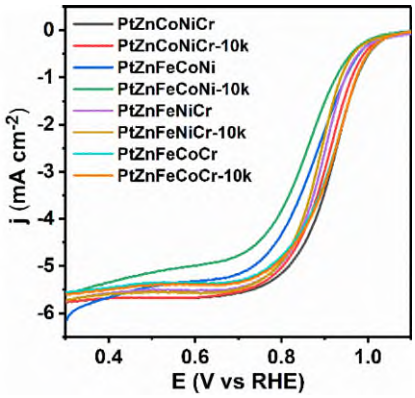

Figure S40. Polarization curves of some relevant quinary intermetallic reference samples after AST between 0.6 and 0.95 V at different cycle numbers.

Changes made in the revised manuscript:

In the revised supporting information supporting information, we added a description: "Supplementary Note 4: we controlled other conditions while varying the types and quantities of elements to prepare a series of binary, ternary, quaternary, and quinary catalyst reference samples. All the reference samples were tested for ORR catalytic performance in 0.1 M $HClO_4$ solution. As shown in Figure S37, the half-wave potentials ($E_{1/2}$) of the non-high-entropy samples PtZn, PtZnCr, PtZnCo, PtZnNi, PtZnFe, PtZnFeCo, PtZnCoNi, PtZnFeCr, PtZnFeNi, and PtZnCoCr are 0.86 V, 0.81 V, 0.848 V, 0.850 V, 0.881 V, 0.917 V, 0.903 V, 0.885 V, 0.850 V, and 0.829 V, respectively, all of which are significantly lower than the 0.948 V of PD-PZFCNC-HEI. Furthermore, from a structural perspective, taking the reference sample PtZnFe as an example, it is likely that due to the insufficient amount of non-precious metals, it tends to form an $L1_2$ structure (Figure S38a). Additionally, due to its relatively low configurational entropy, the surface of the sample is etched (Figure S38b) after treatment with 0.1 M $HClO_4$ solution. This further demonstrates that high configurational entropy contributes to the enhanced corrosion resistance of PD-PZFCNC-HEI in acidic media. On the other hand, to better explain the role of each metal element in the alloy, we prepared a series of high-entropy intermetallic catalyst reference samples, including PtZnCoNiCr, PtZnFeCoNi, PtZnFeNiCr, and PtZnFeCoCr, with Fe, Cr, Co, and Ni individually omitted. The corresponding $E_{1/2}$ values of these samples are 0.921 V, 0.87 V, 0.90 V, and 0.917 V, respectively, as shown in Figure S39. Due to the unique introduction method of Zn in this synthesis, it is not possible to prepare a quintary intermetallic alloy without Zn. However, the results of PtZn ($E_{1/2}$ = 0.87 V) and Pt/C ($E_{1/2}$ = 0.86 V) indicate that Zn slightly enhances the ORR activity of Pt-based catalysts, while its presence also increases the configurational entropy of the material. Overall, it can be seen

that the absence of any single element leads to a slight decrease in catalytic activity. After 10,000 cycles, the $E_{1/2}$ values of PtZnCoNiCr, PtZnFeCoNi, PtZnFeNiCr, and PtZnFeCoCr decreased by 12 mV, 30 mV, 13 mV, and 1 mV, respectively (Figure S40). It was observed that the presence of Cr significantly reduces the extent of activity degradation, as the sample without Cr, PtZnFeCoNi, exhibits the largest $E_{1/2}$ degradation. In summary, Zn, Fe, Co, Ni, and Cr all contribute to the modulation of Pt's electronic structure to enhance ORR catalytic activity, with Cr further improving the material's durability."

Figure S37, Figure S38, Figure S39 and Figure S40were added in supporting information as follows:

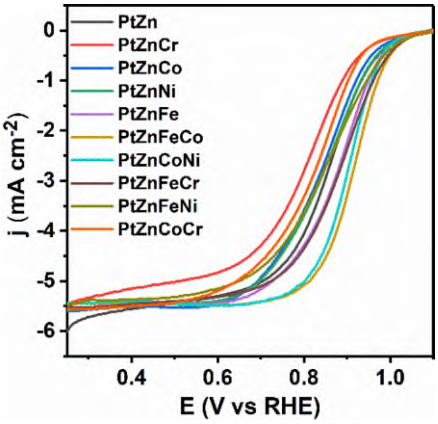

Figure S37. The ORR polarization curves of some relevant binary, ternary, and quaternary intermetallic reference samples.

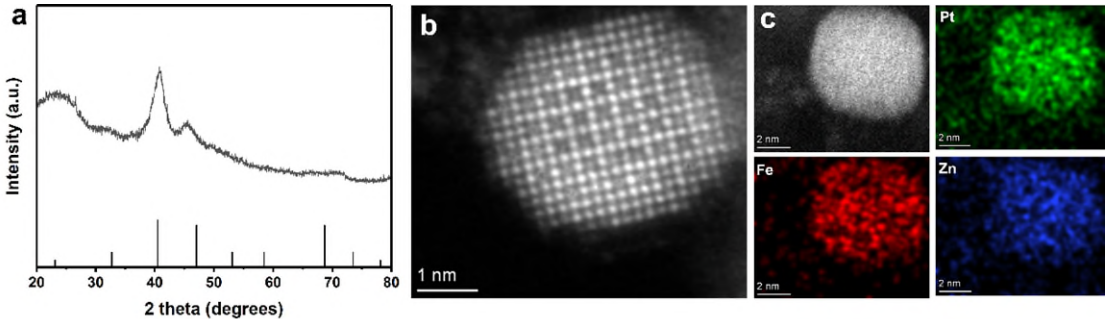

Figure S38. (a) XRD result of the PtZnFe reference sample; HAADF-STEM image of PtZnFe; (c) The corresponding atomic-resolution STEM-EDS mapping of Pt, Fe and Zn elements.

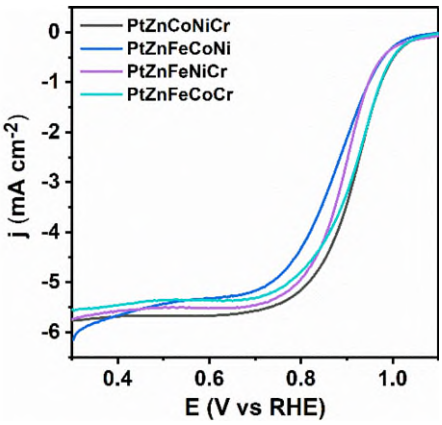

Figure S39. The ORR polarization curves of some relevant quinary intermetallic reference samples.

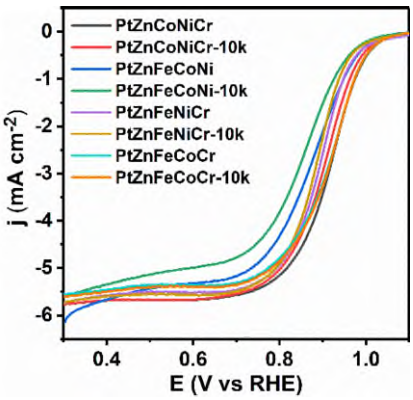

Figure S40. Polarization curves of some relevant quinary intermetallic reference samples after AST between 0.6 and 0.95 V at different cycle numbers.

Comment 6. For the average diameter analysis of the PD-PZFCNC-HEI catalyst, the error analysis of the measurement should be given. Did the heat treatment affect the morphology and particle size of PZFCNC-HEA, which may also the important factor for catalyst.

Response: We sincerely appreciate the reviewer's valuable comments. Based on your suggestion, we continued to randomly select 250 PD-PZFCNC-HEI particles for particle size measurement using ImageJ software. The particle size distribution results are shown in Figures R1a and R1b, with corresponding average particle sizes of 1.76 nm and 1.72 nm, respectively. Combining these with the 1.7 nm obtained in the first measurement, the average particle size is 1.726 nm, and the measured standard deviation is 0.025 nm.

In addition, based on your suggestion, we observed the morphology and structure of PZFCNC-HEA (700) using STEM standards, as shown in Figure S24. The particles are uniformly dispersed (Figures S24a and S24b), and their overall size is less than 3 nm (Figure S24d). According to particle size statistics, the average particle size is only 1.66 nm, which is similar to that of PD-PZFCNC-HEI. However, no obvious ordered structure is observed in PZFCNC-HEA (700) (Figure S24c). Considering the catalytic activity differences between PD-PZFCNC-HEI and PZFCNC-HEA (700), it can be speculated that the outstanding electrochemical performance of PD-PZFCNC-HEI is related to its unique structure.

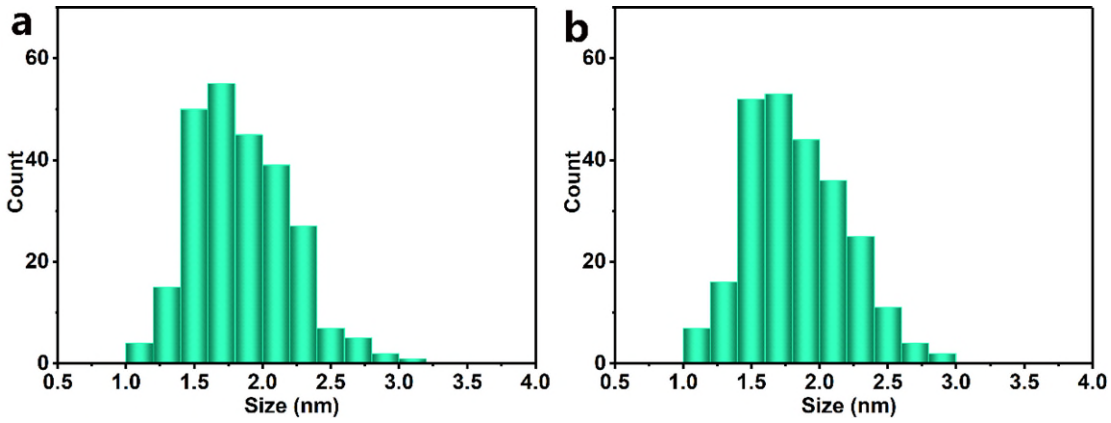

Figure R1. The particle size distribution diagrams from the (a) second and (b) third calculations.

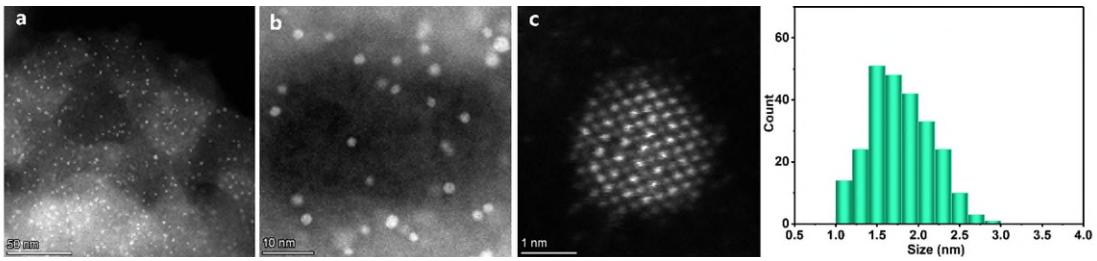

Figure S24. (a) and (b) STEM images of PZFCNC-HEA (700) reference synthesized at 700 °C; (c) HAADF-STEM image of PZFCNC-HEI (700 °C) reference; (d) Particle size distribution histogram of PZFCNC-HEA (700).

Changes made in the revised manuscript:

In the revised manuscript, we added a description: "Transmission electron microscopy (TEM) images show that the average diameter of the as-prepared PD-PZFCNC-HEI particles is 1.726 nm (measured standard deviation is 0.025 nm) with a uniform distribution" and "In addition, the reference sample prepared at 700°C, denoted as PZFCNC-HEA (700), shows no apparent structural ordering (Figure S24), with an average particle size of 1.66 nm."

Figure S24 were added in supporting information as follows:

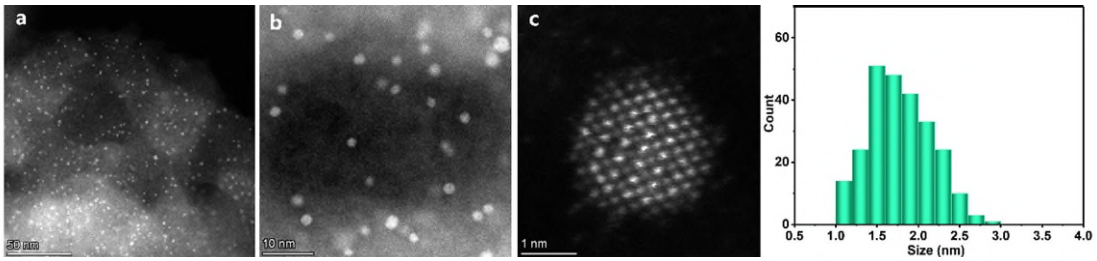

Figure S24. (a) and (b) STEM images of PZFCNC-HEA (700) reference synthesized at 700 °C; (c) HAADF-STEM image of PZFCNC-HEI (700 °C) reference; (d) Particle size distribution histogram of PZFCNC-HEA (700).

Comment 7. Longer stability tests with larger current density need to be provided to furtherly confirm its practical potentials. The sample under testing conditions shows significant fluctuations in Figure. S31, the author should explain it.

Response: We sincerely appreciate the reviewer's valuable comments. In the longer stability tests of PD-PZFCNC-HEI and Pt/C, we selected Chronoamperometric measurements conducted at 0.7V (Figure 3e). Based on their polarization curve characteristics (Figure 3a), the current at 0.7V is already near the limiting current for both PD-PZFCNC-HEI and Pt/C, so it is not possible to further increase the current for testing.

Regarding the current fluctuation in Figure S31 (now Figure S34), we believe several factors contribute to this. To reduce concentration polarization and ensure a good mass transfer process, the stability test was performed using a rotating disk electrode at a rotation speed of 1600 rad/s. Since this test involves an ORR reaction, continuous O_2 supply to the solution is required. The introduction of O_2 causes slight fluctuations in the liquid, which in turn affects the current density. Additionally, during the testing process, we observed minor evaporation of the electrolyte. To address this, we adjusted the position of the O_2 inlet, which led to some current fluctuations.

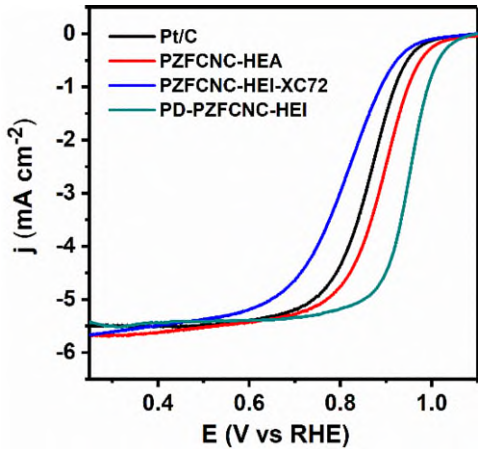

Figure 3a. ORR polarization curves of the PD-PZFCNC-HEI, PZFCNC-HEA, and commercial 20 wt% Pt/C catalysts.

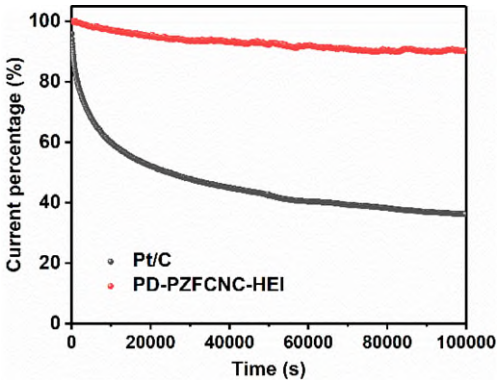

Figure 3e. Normalized chronoamperometric curves of the PD-PZFCNC-HEI and Pt/C catalysts tested at a constant potential of 0.7 V.

Comment 8. The authors should present more comparison on several relevant catalyst samples for mass activity and peak power density (Fig.3l) in the revised manuscript.

Response: We sincerely appreciate the reviewer's valuable comments. According to your suggestion, we have added more comparative catalyst samples in Figure 3l and Table 5. As can be seen, the PD-PZFCNC-HEI catalyst we synthesized shows significant advantages over a range of industry-leading catalysts.

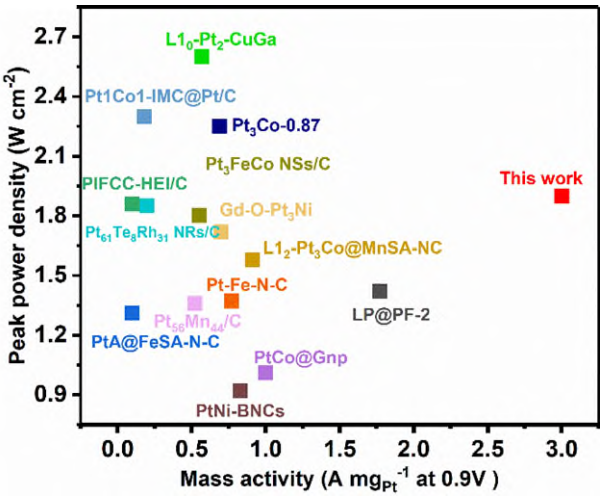

Figure 3l. Comparison of mass activity and peak power density as fuel cell cathode catalysts between this work and previous works base on Table S5.

Table S5. Comparison of key performance metrics in H_2–O_2 fuel cell for PD-PZFCNC-HEI versus. the state-of-the-art in the literature.

Catalysts	Load (mg$_{Pt}$ cm^{-2})	backpressure (bar)	Peak power density (W cm^{-1})	MA@0.9 V (A mg$_{Pt}^{-1}$)	Rated power normalized by mass (W mg$_{Pt}^{-1}$)	reference
LP@PF-2	0.035	2.0 bar	1.42	1.77	40	Science 2018, 362, 1276
Pt1Co1-IMC@Pt/C	0.1	1.0 bar	2.30	0.18	23	Energy Environ. Sci., 2022, 15, 278
PtA@FeSA-N-C	0.13	1.0 bar	1.31	~0.1	10.1	Energy Environ. Sci. 2020, 13, 3032
PIFCC-HEI/C	0.1	2.0 bar	1.86	~0.1	18.6	J. Am. Chem. Soc. 2023, 145, 11140
PtCo@Gnp	0.076	1.5 bar	1.01	~1.0	13.2	Nat. Nanotechnol. 2022, 17, 968
L1$_2$-Pt$_3$Co@MnSA-NC	0.1	1.5 bar	1.58	0.91	15.8	J. Am. Chem. Soc. 2023, 145, 17643
Pt$_{61}$Te$_8$Rh$_{31}$ NRs/C	0.3	1.0 bar	1.85	~0.2	6.16	Energy Environ. Sci. 2022, 15, 3877
PtNi-BNCs	0.15	3.0 bar	0.92	~0.83	6.13	Science 2019, 366, 850
Pt3FeCo NSs/C	0.18	2.0 bar	1.8	~0.55	10	Adv. Mater. 2023, 35, 2208672
Pt-Fe-N-C	0.1	2.5 bar	1.37	0.77	13.7	Nat. Catal. 2022, 5, 503
Pt$_3$Co-0.87	0.08	3.0 bar	2.25	0.69	28.125	ACS Energy Lett.2023,8,628
Gd-O-Pt$_3$Ni	0.1	2.0 bar	2.05	1.58	20.5	Angew.Chem.2024,136,e202315119
Pt$_{1.5}$Ni$_{1-x}$/Ni-N-C	0.05	2.0 bar	1.72	0.70	34.4	Energy Environ. Sci., 2023, 16, 148
L1$_0$-Pt$_2$-CuGa	0.1	2.0 bar	2.6	0.57	26	Angew.Chem.2023,135,e202302134
Pt$_{56}$Mn$_{44}$/C	0.1	2.0 bar	1.36	0.52	13.6	Angew. Chem. 2024, 136, e20231798
PD-PZFCNC-HEI	0.05	2.0 bar	1.90	3.0	38	This work

Changes made in the revised manuscript:

In the revised manuscript, Figure 3 was replaced as follows:

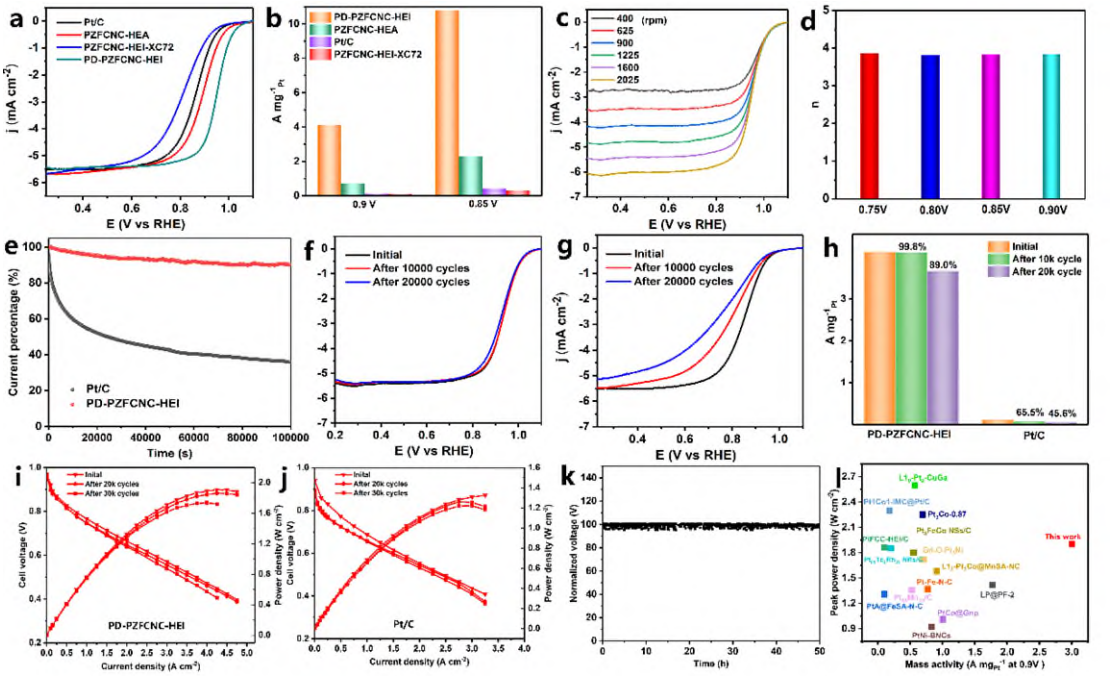

Figure 3. (a) ORR polarization curves of the PD-PZFCNC-HEI, PZFCNC-HEA, and commercial 20 wt% Pt/C catalysts; (b) Mass activities at 0.9 V vs. reversible hydrogen electrode; (c) Polarization curves of PD-PZFCNC-HEI at different rotation rates; (d) Charge transfer number of PD-PZFCNC-HEI. (e) Normalized chronoamperometric curves of the PD-PZFCNC-HEI and Pt/C catalysts tested at a constant potential of 0.7 V; Polarization curves of (f) PD-PZFCNC-HEI and (g) Pt/C after AST between 0.6 and 0.95 V at different cycle numbers; (h) Mass activity before and after AST; The I–V polarization curves and power density of the H_2–O_2 fuel cell of the (i) PD-PZFCNC-HEI and (k) Pt/C sample with the cathode Pt loading of 0.05 mg_{Pt} cm^{-2} before and after AST. (k) Long-term stability of the H_2-Air fuel cell with PZ-PZFCNC-HEI as the cathode at a current density of 500 mA cm^{-2}; (l) Comparison of mass activity and peak power density as fuel cell cathode catalysts between this work and previous works base on Table S5.

Table S5 was replaced in supporting information as follows:

Table S5. Comparison of key performance metrics in H_2–O_2 fuel cell for PD-PZFCNC-HEI versus. the state-of-the-art in the literature.

Catalysts	Load (mg_{Pt} cm^{-2})	backpressure (bar)	Peak power density (W cm^{-1})	MA@0.9 V (A mg_{Pt}^{-1})	Rated power normalized by mass (W mg_{Pt}^{-1})	reference
LP@PF-2	0.035	2.0 bar	1.42	1.77	40	Science 2018, 362, 1276
Pt1Co1-IMC@Pt/C	0.1	1.0 bar	2.30	0.18	23	Energy Environ. Sci., 2022, 15, 278
PtA@FeSA-N-C	0.13	1.0 bar	1.31	~0.1	10.1	Energy Environ. Sci. 2020, 13, 3032
PIFCC-HEI/C	0.1	2.0 bar	1.86	~0.1	18.6	J. Am. Chem. Soc. 2023, 145, 11140
PtCo@Gnp	0.076	1.5 bar	1.01	~1.0	13.2	Nat. Nanotechnol. 2022, 17, 968
$L1_2$-Pt_3Co@MnSA-NC	0.1	1.5 bar	1.58	0.91	15.8	J. Am. Chem. Soc. 2023, 145, 17643
$Pt_{61}Te_8Rh_{31}$ NRs/C	0.3	1.0 bar	1.85	~0.2	6.16	Energy Environ. Sci. 2022, 15, 3877
PtNi-BNCs	0.15	3.0 bar	0.92	~0.83	6.13	Science 2019, 366, 850
Pt3FeCo NSs/C	0.18	2.0 bar	1.8	~0.55	10	Adv. Mater. 2023, 35, 2208672
Pt-Fe-N-C	0.1	2.5 bar	1.37	0.77	13.7	Nat. Catal. 2022, 5, 503
Pt_3Co-0.87	0.08	3.0 bar	2.25	0.69	28.125	ACS Energy Lett.2023,8,628

Gd-O-Pt_3Ni	0.1	2.0 bar	2.05	1.58	20.5	Angew.Chem.2024,136,e202315119
$Pt_{1.5}Ni_{1-x}$/Ni-N-C	0.05	2.0 bar	1.72	0.70	34.4	Energy Environ. Sci., 2023, 16, 148
$L1_0$-Pt_2-CuGa	0.1	2.0 bar	2.6	0.57	26	Angew.Chem.2023,135,e202302134
$Pt_{56}Mn_{44}$/C	0.1	2.0 bar	1.36	0.52	13.6	Angew. Chem. 2024, 136, e20231798
PD-PZFCNC-HEI	0.05	2.0 bar	1.90	3.0	38	This work

Comment 9. The authors should clarify the transformation mechanism of the precursors to the HEA/HEI under different calcination temperature.

Response: We sincerely appreciate the reviewer's valuable comments. Based on your suggestion, we conducted STEM analysis on the PZFCNC-HEA (700) reference sample prepared at 700°C, as shown in Figure S24. Combined with the XRD results in Figure S22, it can be observed that the metallic nanoparticle structure shows no obvious ordering at 700°C. When the temperature is raised to 800°C, the particles transform into an ordered intermetallic structure. However, due to the hysteresis diffusion effect in the high-entropy alloy, some Pt antisite defects fail to diffuse in time, as shown in Figure S20. Upon further heating to 900°C, the Pt antisite defects disappear, and the structure becomes an ordered intermetallic without defects (Figure S23). As reported in previous studies, the transition from the disordered solid solution to the ordered intermetallic structure is a process determined by both thermodynamics and kinetics (Figure R2)[13]. The kinetics of this transition primarily depend on the competition between the thermodynamic driving force and the kinetic energy barriers that the system must overcome to reach the thermodynamic minimum. Based on our observations, 800°C is the optimal temperature for forming high-entropy intermetallics with antisite defects, as it provides a balance between the thermodynamic driving force for ordering and the time required for the diffusion of defects.

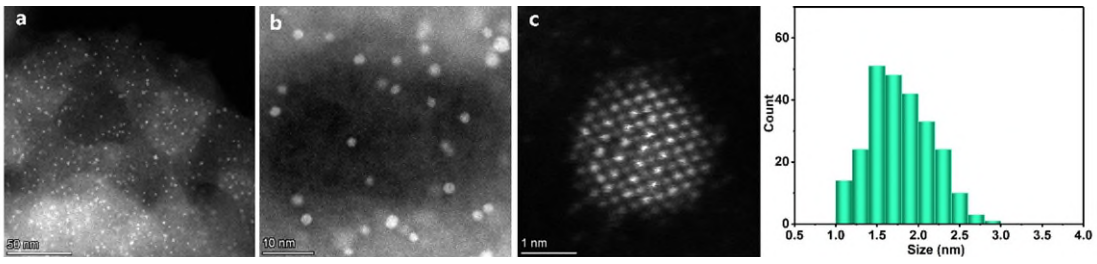

Figure S24. (a) and (b) STEM images of PZFCNC-HEA (700) reference synthesized at 700 °C; (c) HAADF-STEM image of PZFCNC-HEI (700 °C) reference; (d) Particle size distribution histogram of PZFCNC-HEA (700).

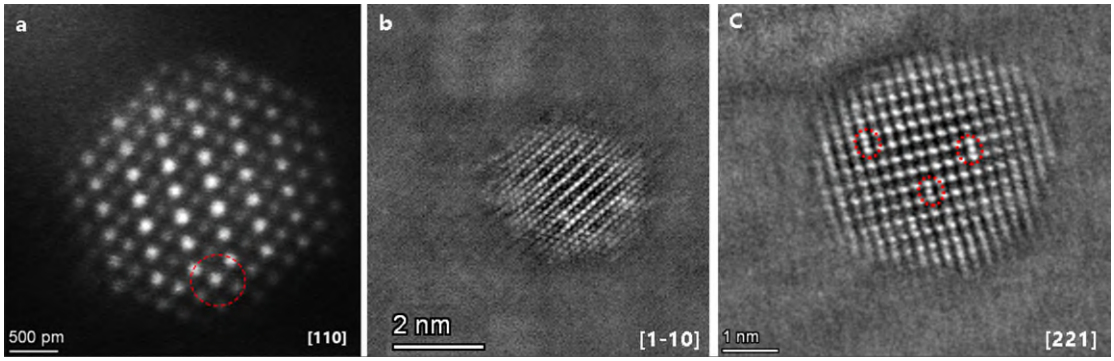

Figure S20. High-angle annular dark-field scanning transmission electron microscopy (HAADF-STEM) images of PD-PZFCNC-HEI nanoparticle along the (a) [110], (b) [1-10] and (c) [221] zone axis.

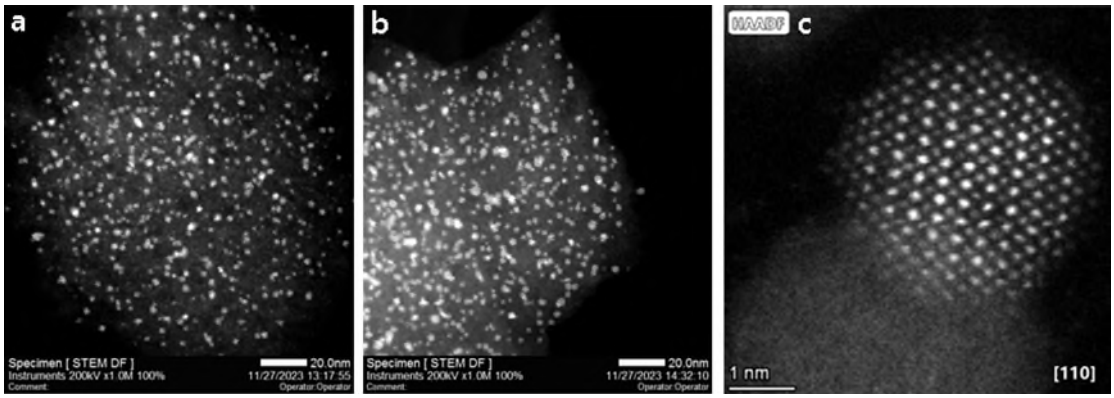

Figure S23. (a) and (b) STEM images of PZFCNC-HEI (900) reference synthesized at 900 °C; (c) HAADF-STEM image of PZFCNC-HEI (900 °C) reference.

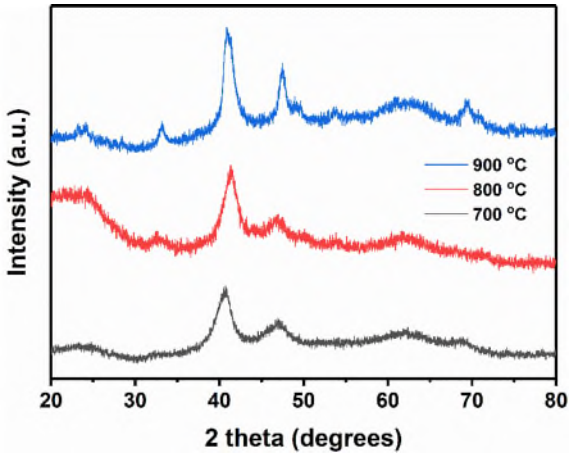

Figure S22. XRD patterns of PD-PZFCNC-HEI synthesized at different temperatures.

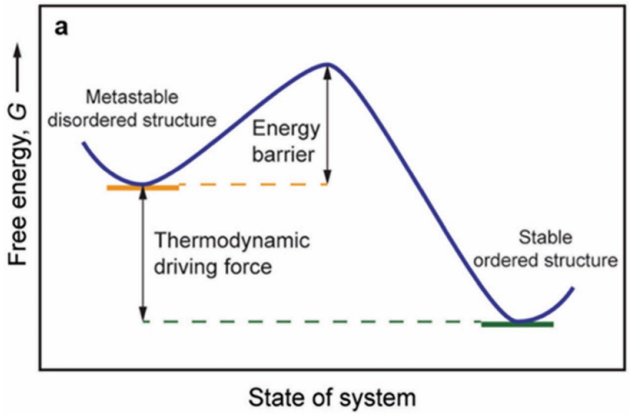

Figure R2. Schematic illustration of the transition from a metastable disordered phase to a stable ordered phase, in which the transition kinetics is determined by the competition between the energy barrier and the thermodynamic driving force.[13]

Changes made in the revised manuscript:

In the revised manuscript, we added a description: "Therefore, it can be concluded that 800°C is the optimal temperature for forming high-entropy intermetallics with antisite defects, as it provides a balance between the thermodynamic driving force for ordering and the diffusion energy barriers of defects."

Comment 10. In the catalytic process, the role of Fe, Co, Ni, and Cr in high entropy material in performance improvement and stability should be further explained.

Response: We sincerely appreciate the reviewer's valuable comments. Given that Pt is presently the optimal catalytic element for ORR, our objective is to enhance its catalytic activity and utilization by building upon the Pt element. The selection of non-precious metals necessitates consideration of elements capable of alloying with Pt, and subsequently converting into intermetallic compounds with Pt. Furthermore, the chosen elements ideally possess similar atomic radii to mitigate lattice distortion effects in the resulting high-entropy alloys. Importantly, if the chosen non-precious metals also exhibit favorable ORR catalytic activity, it would be advantageous. In light of these criteria, we opted for Zn, Fe, Co, Ni, and Cr, as these elements have been reported to possess high ORR activity and are amenable to alloying with Pt (*Angew Chem. Int. Ed. Engl.* **2021**, *60*, 21899; *Nat. Commun.* **2014**, *5*, 5185; *Adv. Mater.* **2022**, *34*, e2109188; *Advanced Energy Materials* **2020**, *10*, 2000179; *Chemistry of Materials* **2015**, *27*, 7538). They belong to neighboring transition metals in the fourth period, minimizing the disparity in atomic radii. In addition, based on the ADT tests of different reference samples, it was observed that the high-entropy intermetallic reference sample without Cr exhibited significant half-wave potential decay, whereas the reference sample containing Cr remained relatively stable (Figure S40). Therefore, it can be concluded that Cr serves as an important element for enhancing structural stability.

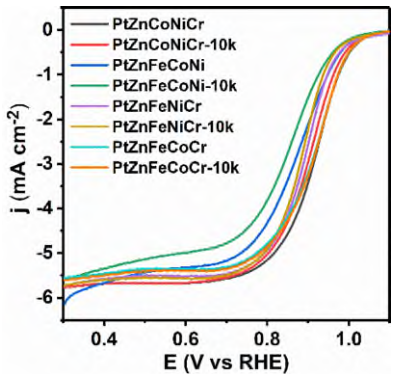

Figure S40. Polarization curves of some relevant quinary intermetallic reference samples after AST between 0.6 and 0.95 V at different cycle numbers.

Comment 11. The PD-PZFCNC-HEI nanoparticles exhibited significant compressive and tensile strains, which were attributed to the lattice distortion effects arising (Fig.1p-q). The authors should consider the strain effects on the electronic structures and the enhanced catalytic activates.

Response: We sincerely appreciate the reviewer's valuable comments. As shown in Figures 1p-q, localized stress is indeed present in the PD-PZFCNC-HEI. Therefore, we also considered strain effects when studying its electronic structure. As shown in Figure 4d, the d-band center of pure Pt (111) is -1.944 eV. In the PZFCNC-HEI reference sample without antisite defects (Figure 4e), the combined effect of overall ligand and strain effects results in the Pt d-band center shifting to -2.178 eV. In PD-PZFCNC-HEI (Figure 4f), the presence of Pt antisite defects leads to localized compressive strain, causing the Pt d-band electrons to shift further down to -2.247 eV. Overall, the presence of Pt defects results in further compression of the Pt d-band electrons, causing the Fermi level to rise and consequently lowering the Pt d-band center. The downward shift of the d-band center helps reduce the adsorption energy of Pt-O, thereby enhancing the reactivity of the reaction.

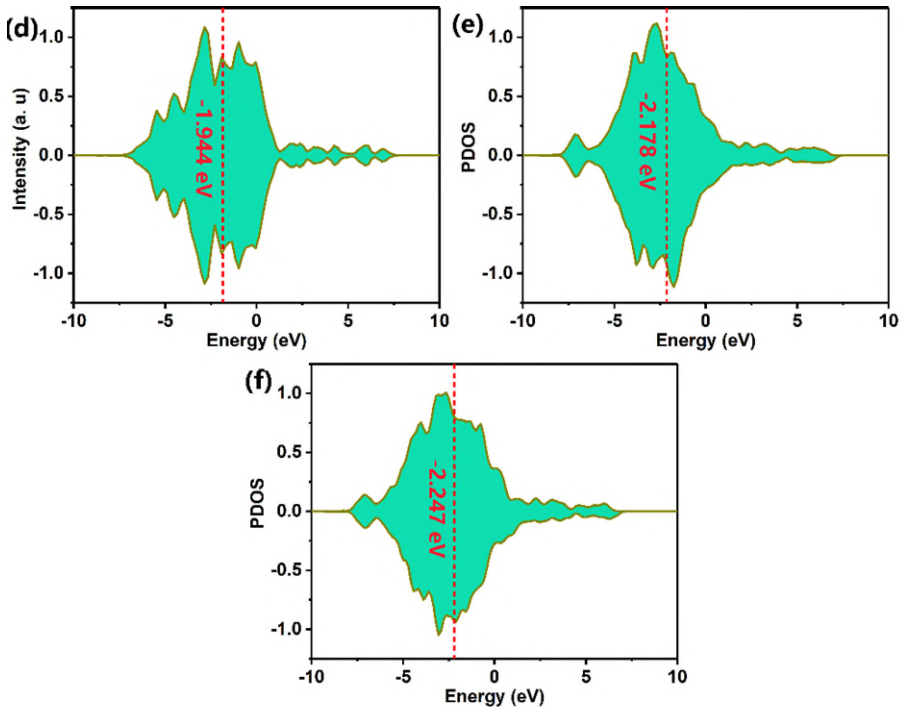

Figure 4d-f. Partial density of states (PDOS) of the d-band for the surface Pt atoms in (d) Pt (111), (e) PZFCNC-HEI and (f) PD-PZFCNC-HEI surface.

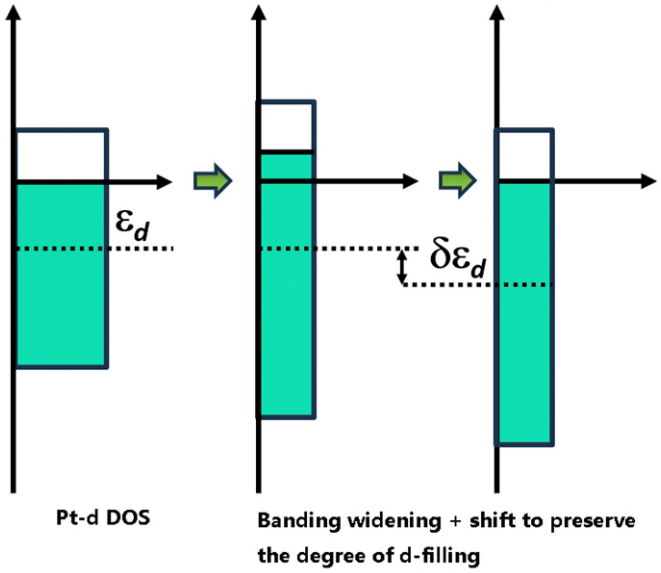

Figure 4l. Variation of Pt d-band structure with compressive strain.

Changes made in the revised manuscript:

In the revised manuscript, we added a description: "Overall, the presence of Pt defects results in further compression of the Pt d-band electrons, causing the Fermi level to rise and consequently lowering the Pt d-band center."

Reviewer #4: The paper by Chen et al. reports on a high-entropy intermetallic compound for the oxygen reduction reaction (ORR). The catalyst has been thoroughly characterized and tested, showing very promising results. The experiments are supplemented by DFT calculations, however these are not performed and presented in a way that can support the associated conclusions. I therefore recommend major revisions, addressing the detailed comments given below, before the paper may be suitable for publication.

Response: We sincerely appreciate the reviewer's positive comments on our work. Based on your suggestions, we have made the corresponding revisions.

Comment 1: On p4 it says: "The selection of non-precious metal constituents is based on a comprehensive consideration of the atomic radii, formation enthalpy, and reported ORR activity of each component." Given that the selection of elements to mix is one of the most challenging aspects of high entropy alloys, an elaboration of these considerations would be suitable.

Response: We sincerely appreciate the reviewer's valuable comments. The research objective of this work is to explore low platinum and high activity oxygen reduction catalysts. Considering that Pt is the optimal catalytic element for ORR, our research aims to reduce the amount of platinum and enhance its catalytic activity through high-entropy alloying based on Pt. The selection of non-precious metals requires consideration of elements that can be alloyed with Pt and subsequently converted into intermetallic compounds with Pt. In addition, the selected elements ideally have similar atomic radii to alleviate lattice distortion effects in the resulting high-entropy alloy. Importantly, if the selected non-precious metal also exhibits favorable ORR catalytic activity, it would be advantageous. In light of these criteria, we opted for Zn, Fe, Co, Ni, and Cr, as these elements have been reported to possess high ORR activity and are amenable to alloying with Pt (*Angew Chem. Int. Ed. Engl.* **2021**, *60*, 21899; *Nat. Commun.* **2014**, *5*, 5185; *Adv. Mater.* **2022**, *34*, e2109188; *Advanced Energy Materials* **2020**, *10*, 2000179; *Chemistry of Materials* **2015**, *27*, 7538). Additionally, they belong to neighboring transition

metals in the fourth period, minimizing the disparity in atomic radii.

Changes made in the revised manuscript:

We added a description in the supporting information: "Considering that Pt is the optimal catalytic element for ORR, our research aims to reduce the amount of platinum and enhance its catalytic activity through high-entropy alloying based on Pt. The selection of non-precious metals requires consideration of elements that can be alloyed with Pt and subsequently converted into intermetallic compounds with Pt. In addition, the selected elements ideally have similar atomic radii to alleviate lattice distortion effects in the resulting high-entropy alloy. Importantly, if the selected non-precious metal also exhibits favorable ORR catalytic activity, it would be advantageous. In light of these criteria, we opted for Zn, Fe, Co, Ni, and Cr, as these elements have been reported to possess high ORR activity and are amenable to alloying with Pt."

Comment 2: From the XPS data it looks like a significant fraction of Fe, Co and Ni atoms are oxidized. What is the origin of this oxidation.

Response: We sincerely appreciate the reviewer's valuable comments. There are mainly two reasons: 1. In high-entropy intermetallics, non-precious metal atoms such as Fe, Co, Ni, Zn, and Cr form various coordination environments with the precious metal Pt. The differing electronegativities and lattice interactions between these metal atoms result in the non-precious metals not being in a fully metallic zero-valent state.[14,15]

2. Since the PD-PZFCNC-HEI particles are dispersed on the DPCN support, which is rich in highly electronegative nitrogen atoms, charge transfer occurs between the metal particles and the support. Figure S19 and Figure 2l show the XPS results of nitrogen elements on the support before and after loading high-entropy intermetallic nanoparticles. After loading the metal nanoparticles, a distinct metal-N peak appears. This further supports the charge transfer between the metal and the support, leading to a slight increase in the metal oxidation state.

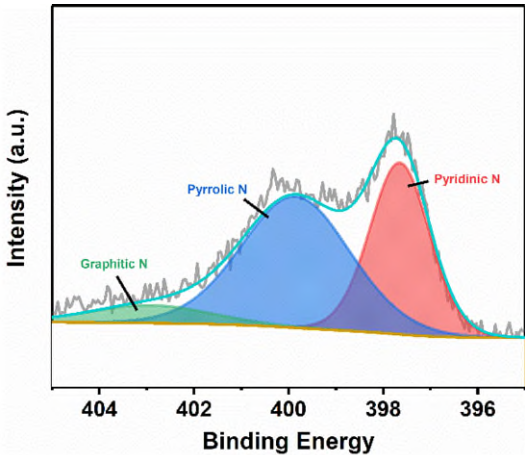

Figure S19. XPS spectra collected at the N 1s edges for the Zn-DPCN.

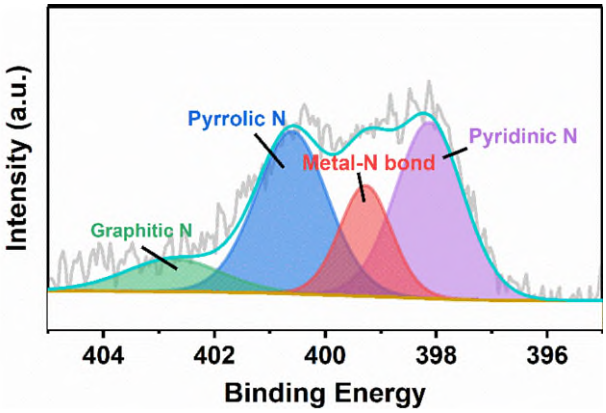

Figure 2l. X-ray photoelectron spectroscopy spectra collected at the N 1s edges for the PD-PZFCNC-HEI sample.

Comment 3: The activity normalized by the electrochemical active surface area is reported for the Pt reference and for the PD-PZFCNC-HEI sample. Is it similar for the other HEI samples?

Response: We sincerely appreciate the reviewer's valuable comments. Due to the challenges in synthesizing high-entropy intermetallics (HEIs), there have been relatively few reports on the successful preparation of HEI catalysts for ORR catalysis to date. In Table S6, we have compiled almost all the existing literature on the application of HEIs in ORR. As shown, the PD-PZFCNC-HEI catalyst we prepared achieves internationally leading performance in all relevant metrics. It is worth noting that, among all the reported HEI catalysts, the majority have not been successfully applied in practical hydrogen-oxygen fuel cells. In contrast, the PD-PZFCNC-HEI catalyst we synthesized has not only been successfully applied in practical hydrogen-oxygen fuel cells, but also exhibits the highest catalytic activity among all reported HEI catalysts, demonstrating excellent prospects for practical applications. On the other hand, it is also evident that our exploration of the PD-PZFCNC-HEI catalyst is relatively comprehensive compared to other reported HEIs.

Table S6. Comparison of catalytic performance of high-entropy intermetallics for ORR with other reported catalysts.

Catalysts	MA at 0.9V in half cell (A $mg_{noble\ metal}^{-1}$)	Cycle number	Decay of $E_{1/2}$ (mV)	$E_{1/2}$ (V. vs RHE)	MA@0.9V in fuel cell (A mg_{Pt}^{-1})	Reference
MHEI-PtPdFeCoNi	R	50k	Unknown	0.91	Unknown	Adv. Energy Mater. 2024, 14, 2303923
OHEA-mNC	2.03	10k	10	0.90	Unknown	Adv. Mater. 2022, 34, 2110128
$Pt_4FeCoCuNi$	3.78	30K	7	0.943	Unknown	Adv. Mater. 2023, 35, 2302067
PIFCC-HEI/C	7.14	60k	9	0.894	~0.1	J. Am. Chem. Soc. 2023, 145, 11140
PFCNCZ HEI	2.403	10k	0	0.906	1.1	J.Am.Chem.Soc. 2024,146,1174
$Pt(FeCoNiCu)_3/C$	4.09	5k	13	Unknown	Unknown	Angew.Chem.2024,136,e202411123
$L1_2$-$Pt(FeCoNiCuZn)_3$	0.7	30K	2	0.922	Unknown	J. Energy Chem. 2023. 86. 158
PD-PZFCNC-HEI	4.12	20K	7	0.948	3.0	This work

Changes made in the revised manuscript:

We added a description "It also demonstrates significant application advantages compared to other HEIs in the same field (Table S6)." in the revised manuscript.

Table S6 were added in supporting information as follows:

Table S6. Comparison of catalytic performance of high-entropy intermetallics for ORR with other reported catalysts.

Catalysts	MA at 0.9V in half cell (A $mg_{noble\ metal}^{-1}$)	Cycle number	Decay of $E_{1/2}$ (mV)	$E_{1/2}$ (V. vs RHE)	MA@0.9V in fuel cell (A mg_{Pt}^{-1})	Reference
MHEI-PtPdFeCoNi	R	50k	Unknown	0.91	Unknown	Adv. Energy Mater. 2024, 14, 2303923
OHEA-mNC	2.03	10k	10	0.90	Unknown	Adv. Mater. 2022, 34, 2110128
$Pt_4FeCoCuNi$	3.78	30K	7	0.943	Unknown	Adv. Mater. 2023, 35, 2302067
PIFCC-HEI/C	7.14	60k	9	0.894	~0.1	J. Am. Chem. Soc. 2023, 145, 11140
PFCNCZ HEI	2.403	10k	0	0.906	1.1	J.Am.Chem.Soc. 2024,146,1174
$Pt(FeCoNiCu)_3/C$	4.09	5k	13	Unknown	Unknown	Angew.Chem.2024,136,e202411123
$L1_2$-$Pt(FeCoNiCuZn)_3$	0.7	30K	2	0.922	Unknown	J. Energy Chem. 2023. 86. 158
PD-PZFCNC-HEI	4.12	20K	7	0.948	3.0	This work

Comment 4: Figure 4c: It is impossible to see the difference in the inset figures of (what I assume is) the charge distribution in the pure metals and the HEI. Also, the colour bar has no label.

Response: We sincerely appreciate the reviewer's valuable comments. Due to the fact that the deviation in the number of outermost electrons of PD-PZFCNC-HEI compared to pure metals is generally between 0.05 and 0.2 electrons, the electron transfer is minimal. Therefore, it is difficult to discern any significant difference in the charge distribution spherical diagram. Based on your suggestion, we are considering removing the inserted charge distribution spherical diagram from Figure 4c.

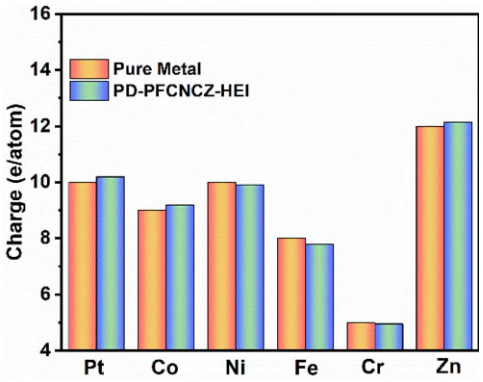

Figure 4c. The number of outer electrons in the surface atoms of PD-PZFCNC-HEI and the corresponding pure metal from Bader charge analysis.

Changes made in the revised manuscript:

Figure 4 are replaced as follow in the revised manuscript:

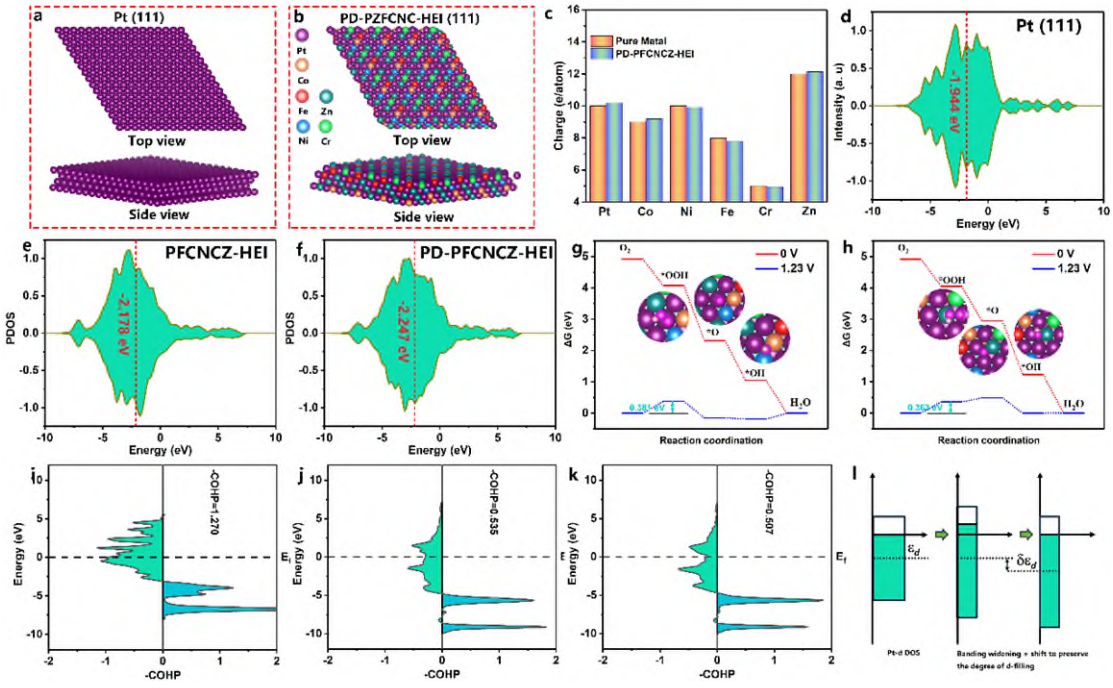

Figure 4. Mechanistic insights into the ORR catalytic reaction by PD-PZFCNC-HEI. The top and side views of the (a) Pt (111) and (b) PD-PZFCNC-HEI (111) surface models; (c) The number of outer electrons in the surface atoms of PD-PZFCNC-HEI and the corresponding pure metal from Bader charge analysis; Partial density of states (PDOS) of the d-band for the surface Pt atoms in (d) Pt (111), (e) PZFCNC-HEI and (f) PD-PZFCNC-HEI surface; The free energies of intermediates of (g) Pt and (h) Zn sites on the PD-PZFCNC-HEI surface for the ORR steps; COHP and ICOHP for *OH adsorption intermediates at (i) Pt (111), (j) the Pt and (k) the Zn sites on PD-PZFCNC-HEI; (l) Variation of Pt d-band structure with compressive strain.

Comment 5: The insets in Figure 4g-h are likewise too small. However, if you zoom in it can be seen that the adsorbates are not in the same adsorption sites. Notably, the diagram which is stated to be a Zn adsorption site (Figure 4h) shows pictures where the adsorbates are never bound to Zn only. The other diagram (Figure 4g) appears to have *OH in a site that is not present in the pictures for *O and *OOH. Are these pictures taken from the optimized structures? Is the reason that Zn sites are found to be surprisingly active perhaps that the adsorbates move during optimisation?

Response: We sincerely appreciate the reviewer's valuable comments. Based on your suggestion, we have enlarged the 4g and Figure 4h illustrations. As can be seen, the intermediates are not fully localized at their corresponding sites, as we have provided the optimized structure. The improvement in catalytic activity is certainly related to the final optimized adsorption positions of the species, so presenting the optimized positions is the most reasonable approach. In fact, the adsorption process of intermediates at each site on the high-entropy intermetallic surface is not isolated, but rather influenced by multiple metal atoms. As shown in Figure S53, when *OOH adsorbs on the Pt reactive sites of the PD-PZFCNC-HEI surface, charge transfer occurs not only between *OOH and Pt but also between *OOH and neighboring non-precious metal atoms. This also explains that part of the high catalytic activity of PD-PZFCNC-HEI results from the synergistic effect of multiple elements.

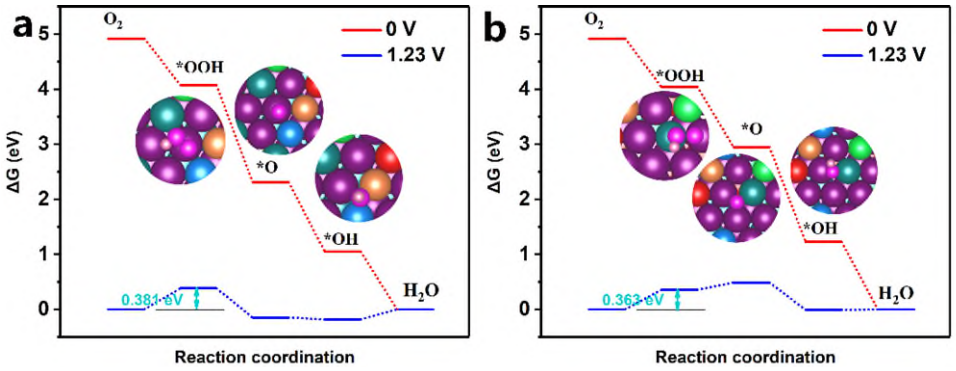

Figure 4g-h: The free energies of intermediates of (g) Pt and (h) Zn sites on the PD-PZFCNC-HEI surface for the ORR steps.

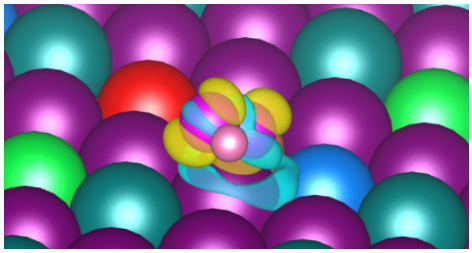

Figure S53b. Differential charge density ($\Delta\rho = \rho_{*OOH} - \rho_{*} - \rho_{OOH}$) of *OOH adsorbed system at the PD-PFCNCZ-HEI. The isosurface in blue and yellow represent charge accumulation and depletion, respectively.

Changes made in the revised manuscript:

Figure 4 are replaced as follow in the revised manuscript:

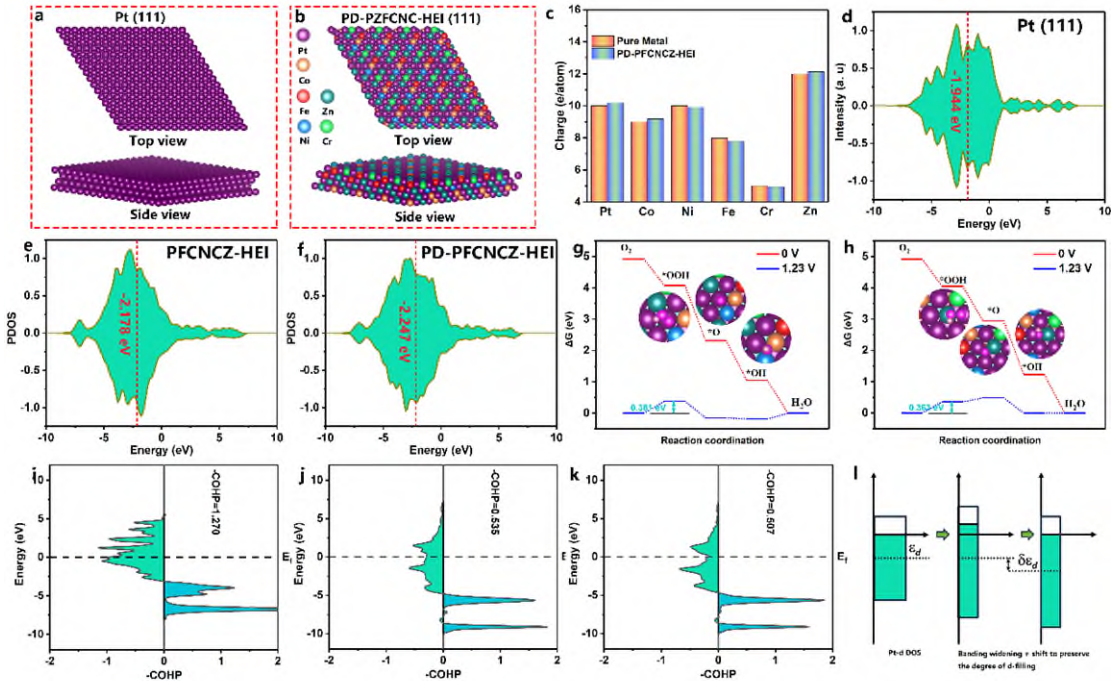

Figure 4. Mechanistic insights into the ORR catalytic reaction by PD-PZFCNC-HEI. The top and side views of the (a) Pt (111) and (b) PD-PZFCNC-HEI (111) surface models; (c) The number of outer electrons in the surface atoms of PD-PZFCNC-HEI and the corresponding pure metal from Bader charge analysis; Partial density of states (PDOS) of the d-band for the surface Pt atoms in (d) Pt (111), (e) PZFCNC-HEI and (f) PD-PZFCNC-HEI surface; The free energies of

intermediates of (g) Pt and (h) Zn sites on the PD-PZFCNC-HEI surface for the ORR steps; COHP and ICOHP for *OH adsorption intermediates at (i) Pt (111), (j) the Pt and (k) the Zn sites on PD-PZFCNC-HEI; (l) Variation of Pt d-band structure with compressive strain.

Comment 6: For the pure Pt reference (figure S43) all adsorbates are positioned on top, while for the HEIs a mixture of top, bridge and hollow site adsorption sites are shown. On Pt, *O is usually more stable in th. For the pure Pt reference (figure S43) all adsorbates are positioned on top, while for the HEIs a mixture of tope hollow site, while on a HEI the most stable site will depend on the neighbouring atoms, and the adsorbate will not necessarily relax to this position. Thus, different adsorption sites (top, bridge, hollow) as well as different adsorption environments for the HEI should be tested to be able to conclude anything. This is especially true considering the small energy differences presented here. Furthermore, it could provide substance to the claim that the Pt antisite defects are important.

Response: We sincerely appreciate the reviewer's valuable comments. Based on your suggestion, in order to consider the reaction sites for *O more comprehensively, we have also calculated the reaction pathways for the *O intermediate at the bridge and hollow sites on Pt (111), as shown in Figure S51. As can be seen, the reaction barriers for *O at the bridge and hollow sites are higher than that at the top site, indicating that the reaction pathway on the top site will still be preferred on the Pt (111) surface.

On the other hand, for PD-PZFCNC-HEI, the reaction intermediates undergo natural optimization relaxation, and theoretically, they will relax to their most stable positions. Therefore, the *O intermediate could be at the bridge site (as shown in Figure 4g) or at the hollow site (as shown in Figure 4h). It can be stated that during the optimization process, the adsorbates naturally move to more stable adsorption positions, and whether or not the adsorbates were initially placed at the bridge or hollow sites on the high-entropy surface model does not affect our current results. Moreover, the current results are sufficient to explain the existing experimental observations.

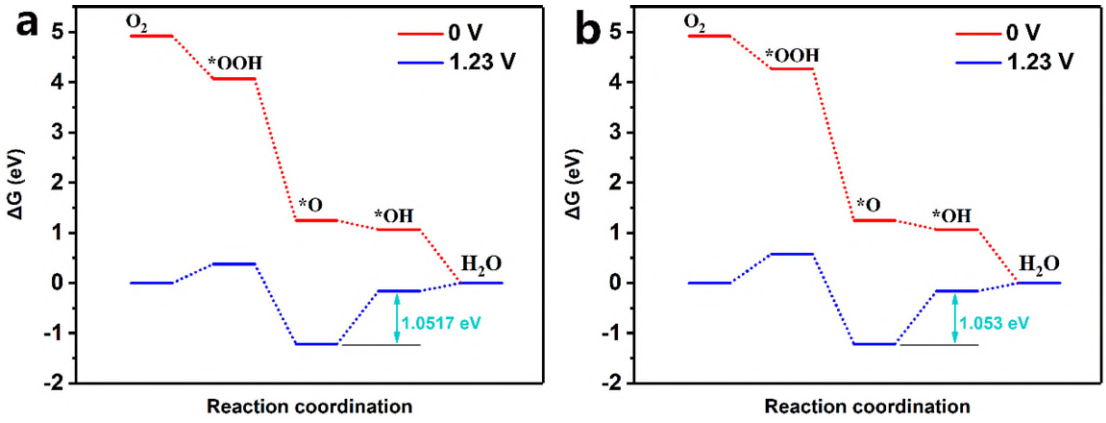

Figure S51. The reaction pathways for the intermediate *O on the Pt(111) surface at (a) the bridge site and (b) the hollow site during the ORR.

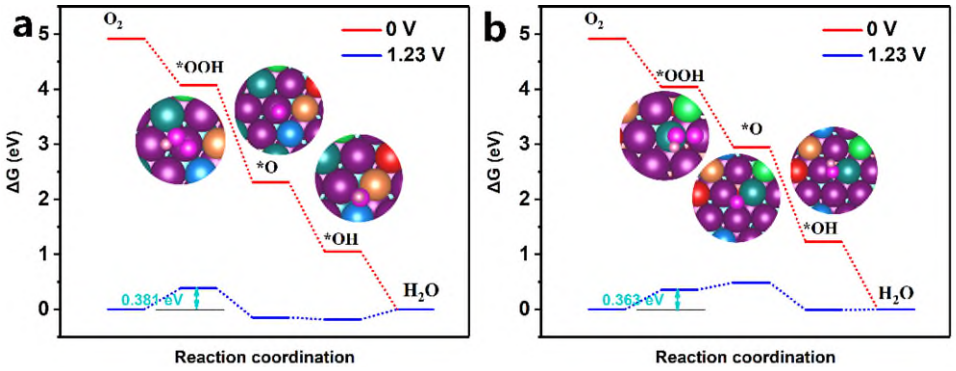

Figure 4g-h: The free energies of intermediates of (g) Pt and (h) Zn sites on the PD-PZFCNC-HEI surface for the ORR steps.

Changes made in the revised manuscript:

We added a description in supporting information: "The reaction barriers at both the bridge and hollow sites are higher than that at the top site shown in Figure S51, thus the reaction pathway for the *O intermediate is more likely to occur at the top site."

Figure S51 were added in supporting information as follows:

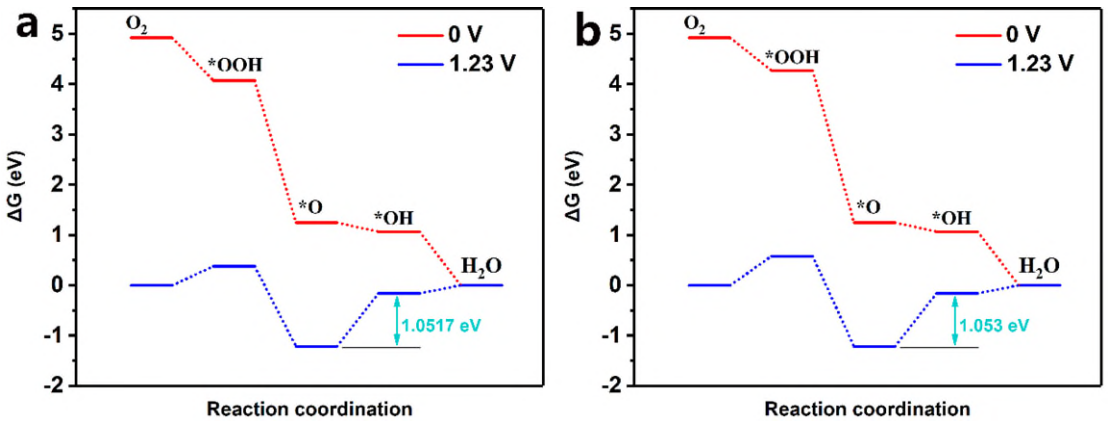

Figure S51. The reaction pathways for the intermediate *O on the Pt(111) surface at (a) the bridge site and (b) the hollow site during the ORR.

Comment 7: It is unclear how the surface formation energies are calculated? The values are very large. For the calculation of antisite defects, as I understand it a random atom has been swapped for Pt in the original surface model. However, the defect formation energy depends on the local environment, and conclusions cannot be made based on a single defect structure.

Response: We sincerely appreciate the reviewer's valuable comments. This is an error in our statement. What we calculated are the structural energies of these structures, not the surface formation energies. Surface formation energy refers to the energy required to transform a material from its bulk state to a surface state, which requires the energy information of the bulk phase. However, the models we have constructed here are primarily based on the (111) crystal plane to study the catalytic process on this surface[16]. Therefore, surface formation energy cannot be calculated in this case. Instead, we computed the energies of the constructed structures to identify the most stable structural model.

For the construction of the Pt antisite defect model, we first built the PtFe (111) surface structure based on the P4/mmm space group of the PtFe bulk phase. Then, by randomly substituting Fe sites in the PtFe (111) surface structure with other non-precious metal elements, we obtained the defect-free PZFCNC-HEI reference model, with elemental ratios derived from experimental results (Pt:Cr:Fe:Co:Ni:Zn = 1:0.137:0.171:0.123:0.115:0.445). Next, we generated 10 different defect-

free (4 × 4 × 4) PZFCNC-HEI unit cells, with energy differences of less than 0.5 eV, indicating that their distribution has minimal impact on the stability of the bulk structure, as shown in Figure S47a-j. Among these models, we selected Figure S47a, which has the lowest energy (-477.76 eV) and is therefore considered the most stable structure, as the PZFCNC-HEI model, with its surface shown in Figure S48. Considering that Pt antisite defects can replace any non-precious metal atom, we sequentially constructed Pt antisite defect models by substituting Zn, Fe, Co, Ni, and Cr sites on the PZFCNC-HEI (111) model surface. Subsequently, these models were optimized, and each exhibited stable energy convergence, as shown in Figure S49. The energies of these models were -382.18 eV, -377.76 eV, -376.15 eV, -381.19 eV, and -375.02 eV, respectively. It can be inferred that the inverse defect structure where Zn sites are replaced has the lowest energy and the most stable structure. Therefore, the model shown in Figure S47a was selected as the defect model PD-PZFCNC-HEI for subsequent studies.

To further illustrate the impact of Pt defects on the performance of HEIs, we selected the defect-free HEI structure with the second-lowest Gibbs free energy, shown in Figure S47j. Based on this structure, we sequentially replaced non-precious metal atoms (Zn, Fe, Co, Ni, Cr) with Pt atoms to construct defect models, as shown in Figure S54a-e. Among these, the model with the lowest energy, shown in Figure S54a, was selected for further exploration and designated as PD-PZFCNC-HEI-2, as detailed in Figure S55. By calculating the Gibbs free energy of the surface reaction intermediates for PD-PZFCNC-HEI-2, we found that the rate-determining step is the hydrogenation process of O_2, with an energy barrier of 0.354 eV, which is still significantly lower than the barrier for the Pt (111) surface (0.406 eV, Figure S50). This further supports the validation of the defect structure in enhancing catalytic activity.

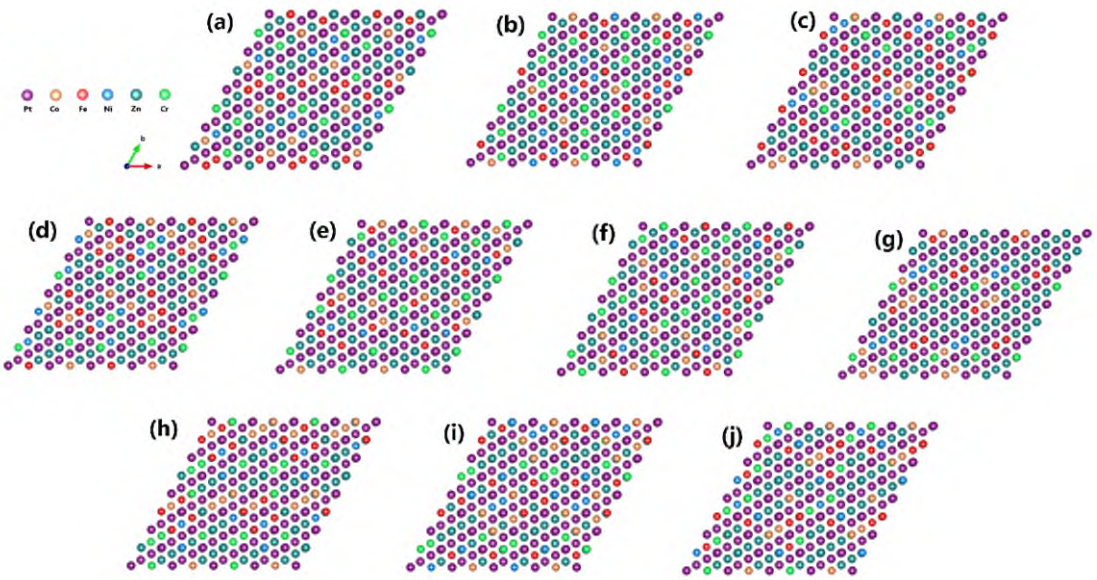

Figure S47. Constructed a series of defect free PFCNZ-HEI (111) surface models. The energies for (a)-(j) were -377.69 eV, -376.53 eV, -376.74 eV, -376.09 eV, -377.33 eV, -374.75 eV, -376.59 eV, -375.51 eV, 377.37 eV, -377.6 eV, respectively.

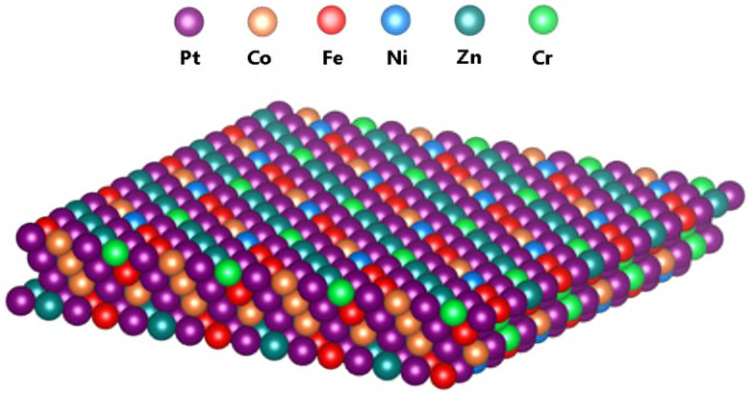

Figure S48. The PZFCNC-HEI (111) surface reference models of Figure 46a.

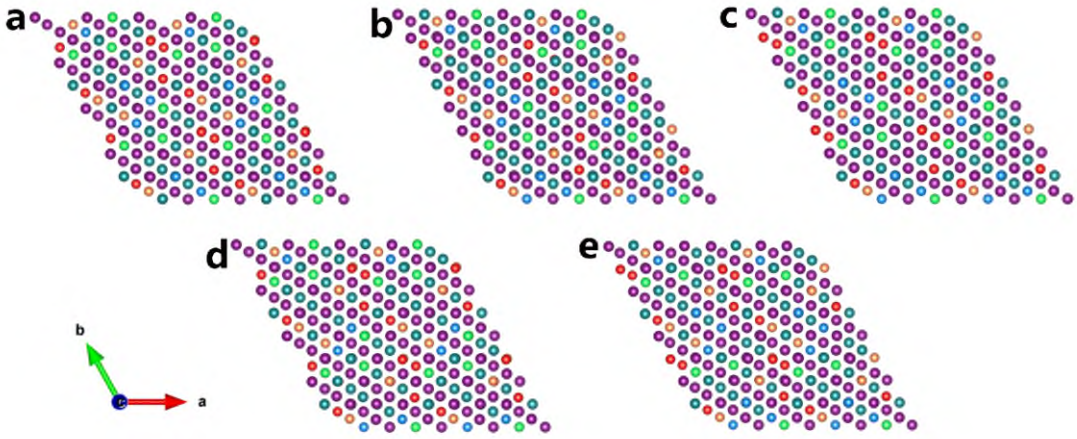

Figure S49. Constructed a series of PD-PFCNZ-HEI (111) surface models. where (a)–(e) represent the antisite defect models with Pt atom substituting Zn, Fe, Co, Ni, and Cr sites, respectively.

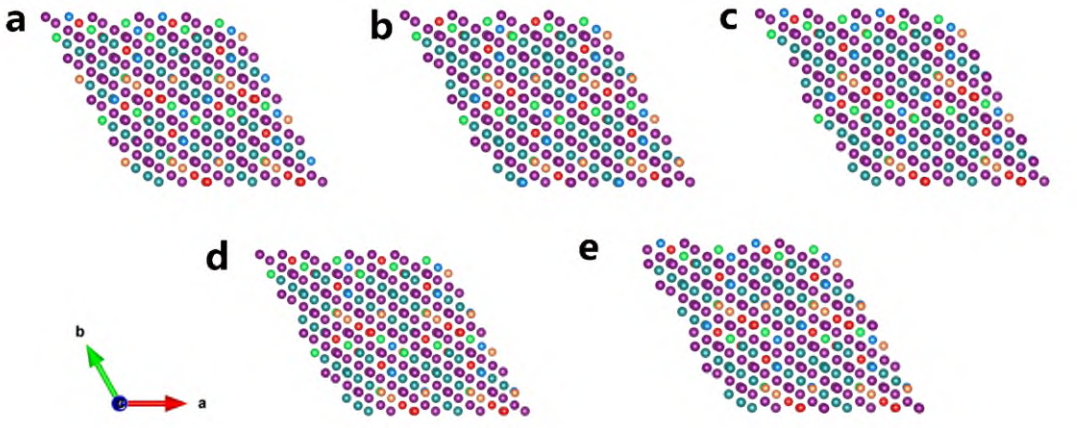

Figure S54. Constructed a series of PD-PFCNZ-HEI (111) surface models based on Figure 46j. where (a)–(e) represent the antisite defect models with Pt atom substituting Zn, Fe, Co, Ni, and Cr sites, respectively. The energies for these models were -382.10 eV, -382.07 eV, -373.02 eV, -378.81 eV, and -378.56 eV, respectively.

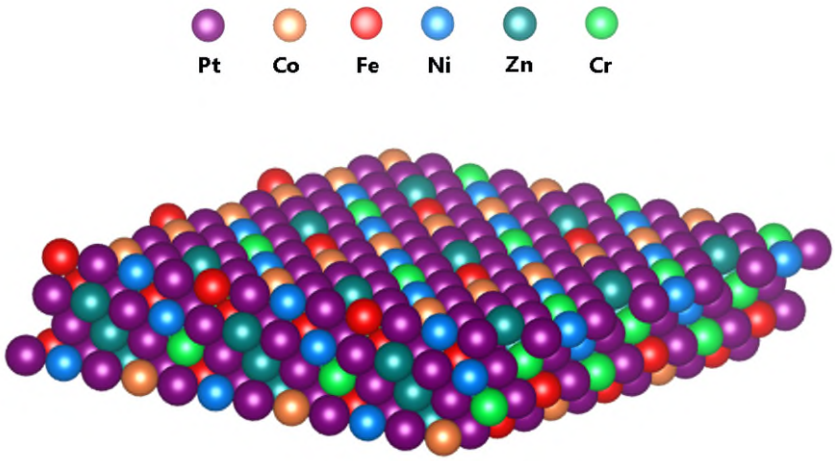

Figure S55. The PD-PZFCNC-HEI-2 surface reference models of Figure 53a.

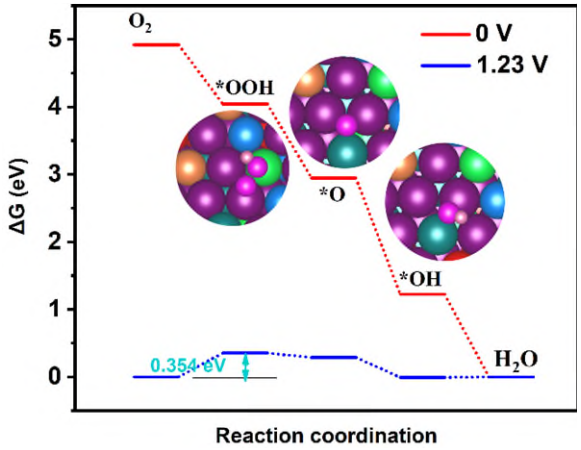

Figure S56. The free energies of intermediates of Pt sites on the PD-PZFCNC-HEI-2 surface for the ORR steps.

Changes made in the revised manuscript:

We added description "The high-entropy model was constructed using Python's pymatgen and random modules by randomly replacing the Fe sites in the PtFe (111) surface structure. Specifically, we first determined the atomic numbers and quantities of atoms in the optimized PtFe (111) surface structure. Based on the elemental ratios obtained from experimental characterization (Pt:Cr:Fe:Co:Ni:Zn = 1:0.137:0.171:0.123:0.115:0.445), we calculated the number of atoms to be replaced for each of the five elements (Cr, Fe, Co, Ni, Zn). We then used the random module to generate a random array of these five elements and employed pymatgen methods to perform the element substitution in the PtFe (111) surface structure, aiming to simulate the disordered distribution of multiple elements in a high-entropy structure. Using this random construction method, we generated 10 different (4 × 4 × 4) unit cells, with energy differences less than 0.5 eV, indicating that their distribution has minimal impact on the stability of the bulk structure, as shown in Figure S47a-j. By further comparing their energies, we selected the structure with the lowest energy, i.e., the thermodynamically most stable structure, to further construct the Pt-defective high-entropy structure." and "Supplementary Note 5: To further illustrate the impact of Pt defects on the performance of HEIs, we selected the defect-free HEI structure with the second-lowest Gibbs free energy, shown in Figure S47j. Based on this structure, we sequentially replaced non-precious metal atoms (Zn, Fe, Co, Ni, Cr) with Pt atoms to construct defect models, as shown in Figure S54a-e. Among these, the model with the lowest energy,

shown in Figure S54a, was selected for further exploration and designated as PD-PZFCNC-HEI-2, as detailed in Figure S55. By calculating the Gibbs free energy of the surface reaction intermediates for PD-PZFCNC-HEI-2, we found that the rate-determining step is the hydrogenation process of O_2, with an energy barrier of 0.354 eV, which is still significantly lower than the barrier for the Pt (111) surface (0.406 eV, Figure S50). This further supports the validation of the defect structure in enhancing catalytic activity." in the revised supporting information.

Figure S54, Figure S55 and Figure S56 were added in supporting information as follows:

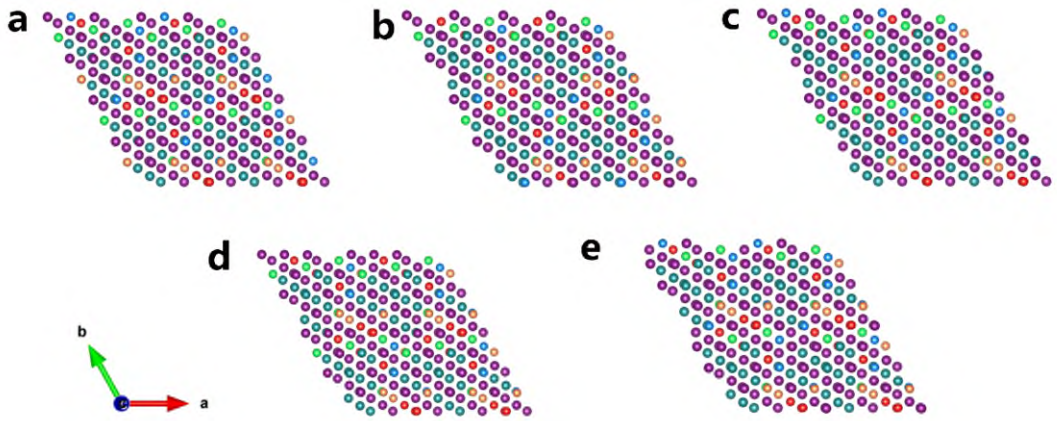

Figure S54. Constructed a series of PD-PFCNZ-HEI (111) surface models based on Figure 46j. where (a)–(e) represent the antisite defect models with Pt atom substituting Zn, Fe, Co, Ni, and Cr sites, respectively. The energies for these models were -382.10 eV, -382.07 eV, -373.02 eV, -378.81 eV, and -378.56 eV, respectively.

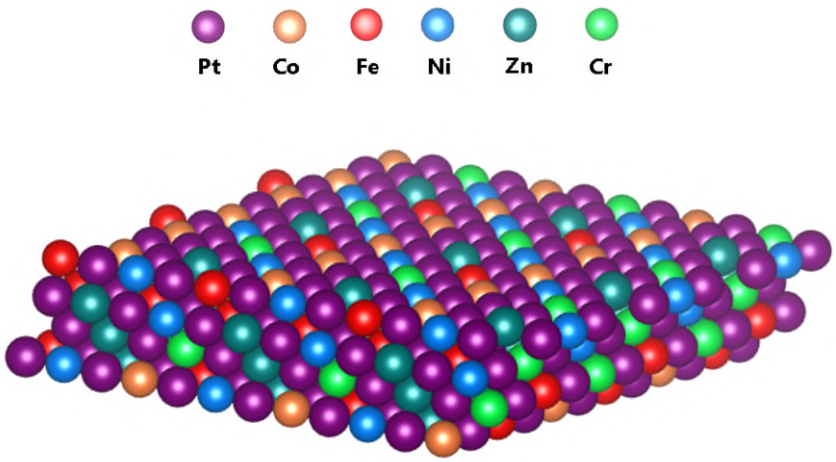

Figure S55. The PD-PZFCNC-HEI-2 surface reference models of Figure 53a.

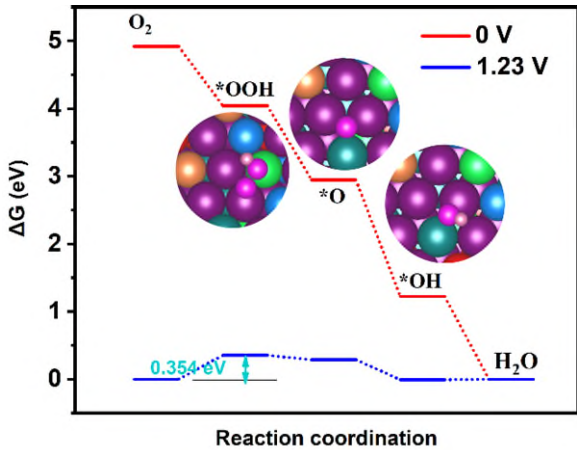

Figure S56. The free energies of intermediates of Pt sites on the PD-PZFCNC-HEI-2 surface for the ORR steps.

Comment 8: COHP calculations are performed for the adsorption of *OH, however it is unclear what insight they add. The meaning of the values is not explained, and in any case the rate limiting step is found to be the hydrogenation of O_2.

Response: We sincerely appreciate the reviewer's valuable comments. In our calculation of the COHP for the intermediates, we found that both O atoms in the O_2 and *OOH intermediate molecules undergo charge transfer with the PD-PZFCNC-HEI. Since the positions of these two O atoms are different on a local scale, their COHPs are also different. Therefore, the question arises: which O atom should be chosen to study the interaction between the oxygen-containing intermediates and the PD-PZFCNC-HEI surface? The choice of O may lead to different results. On the other hand, according to previous reports, there is a certain linear relationship between the adsorption energies of intermediates during the ORR process, so *OH intermediates are often studied to examine the correlation with the interface. Hence, we considered investigating the bonding interaction between the O atom in the *OH intermediate and the interface to infer the influence of the PD-PZFCNC-HEI surface on the adsorption of intermediates.

Comment 9: P2 L8: "However, the development of efficient oxygen reduction reaction catalysts hinders their practical applications." I think this sentence was intended to have the opposite meaning.

Response: We sincerely appreciate the reviewer's valuable comments. We have rephrased this sentence.

Changes made in the revised manuscript:

We replaced a description "However, the lack of efficient ORR catalysts significantly hinders their practical application." in the revised manuscript.

Comment 10: P7, line 2. "Pt occupies the non-metallic sites" There are no non-metallic sites?

Response: We sincerely appreciate the reviewer's valuable comments. This is an error in our expression. What we intended to describe was non-noble metal sites, not non-metallic sites. We have made the necessary corrections in the relevant sections.

Changes made in the revised manuscript:

We replaced a description "Along the wide green lines, Pt generally exhibits a periodic distribution trend; however, a small amount of Pt occupies non-noble metal sites, such as the weak peak between the two Pt peaks." in the revised manuscript.

Comment 11: P10: There are two references to Figure 40, this must be figure S40?

Response: We sincerely appreciate the reviewer's valuable comments. You are correct. We have made the necessary

revisions.

Changes made in the revised manuscript:

We replaced a description "Density functional theory (DFT) calculations were performed to gain insight into the superior ORR performance of the PD-PZFCNC-HEI. Initially, a series of defect-free PtZnFeCoNiCr intermetallic compound (PZFCNC-HEI) models were constructed based on the P4/mmm space group (Figure S47). We selected Figure S47a, which has the lowest energy, as the reference model for defect-free PZFCNC-HEI (Figure S48)." in the revised manuscript.

Comment 12: Figure 4a-b. There is no label for the colours of the different atoms.

Response: We sincerely appreciate the reviewer's valuable comments. We have added the atomic color annotations in Figure a-b.

Changes made in the revised manuscript:

We replaced Figure 4 as follow:

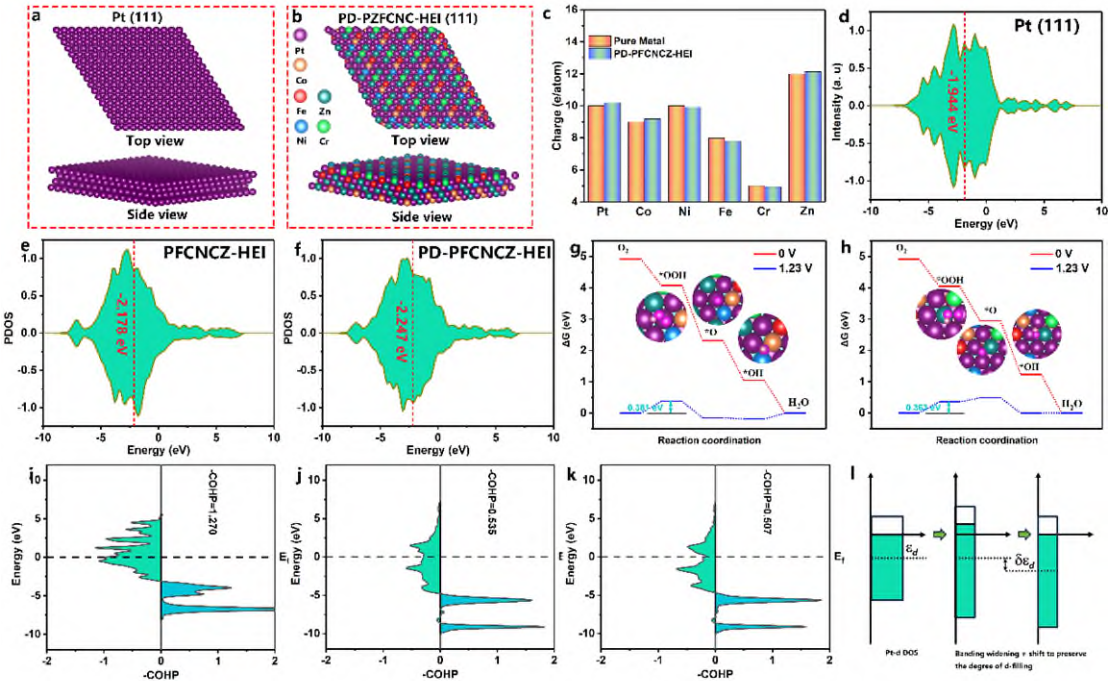

Figure 4. Mechanistic insights into the ORR catalytic reaction by PD-PZFCNC-HEI. The top and side views of the (a) Pt (111) and (b) PD-PZFCNC-HEI (111) surface models; (c) The number of outer electrons in the surface atoms of PD-PZFCNC-HEI and the corresponding pure metal from Bader charge analysis; Partial density of states (PDOS) of the d-band for the surface Pt atoms in (d) Pt (111), (e) PZFCNC-HEI and (f) PD-PZFCNC-HEI surface; The free energies of intermediates of (g) Pt and (h) Zn sites on the PD-PZFCNC-HEI surface for the ORR steps; COHP and ICOHP for *OH adsorption intermediates at (i) Pt (111), (j) the Pt and (k) the Zn sites on PD-PZFCNC-HEI; (l) Variation of Pt d-band structure with compressive strain

Refence:

1 Li, J. *et al.* Fe Stabilization by Intermetallic $L1_0$-FePt and Pt Catalysis Enhancement in $L1_0$-FePt/Pt Nanoparticles for Efficient Oxygen Reduction Reaction in Fuel Cells. *Journal of the American Chemical Society* **140**, 2926-2932 (2018). https://doi.org:10.1021/jacs.7b12829

2 K., W., L., W., Z., Y., L., Z. & al., e. Kinetic diffusion–controlled synthesis of twinned intermetallic nanocrystals for CO-resistant catalysis. *Science Advances* **8**, eabo4599 (2022). https://doi.org:10.1126/sciadv.abo4599

3 Wang, R. M. *et al.* Layer Resolved Structural Relaxation at the Surface of Magnetic FePt Icosahedral Nanoparticles. *Physical Review Letters* **100** (2008). https://doi.org:10.1103/PhysRevLett.100.017205

4 Wang, Y., Han, P., Lv, X., Zhang, L. & Zheng, G. Defect and Interface Engineering for Aqueous Electrocatalytic CO2 Reduction. *Joule* **2**, 2551-2582 (2018). https://doi.org:10.1016/j.joule.2018.09.021

5 Huang, H. *et al.* Understanding of Strain Effects in the Electrochemical Reduction of CO2: Using Pd Nanostructures as an Ideal Platform. *Angewandte Chemie International Edition* **56**, 3594-3598 (2017). https://doi.org:10.1002/anie.201612617

6 Li, Z.-A. *et al.* Chemically ordered decahedral FePt nanocrystals observed by electron microscopy. *Physical Review B* **89**, 161406 (2014). https://doi.org:10.1103/PhysRevB.89.161406

7 Chi, M. *et al.* Surface faceting and elemental diffusion behaviour at atomic scale for alloy nanoparticles during in situ annealing. *Nature Communications* **6**, 8925 (2015). https://doi.org:10.1038/ncomms9925

8 Chen, Y. *et al.* Pt Atomic Layers with Tensile Strain and Rich Defects Boost Ethanol Electrooxidation. *Nano Letters* **22**, 7563-7571 (2022). https://doi.org:10.1021/acs.nanolett.2c02572

9 Zhao, S. Lattice distortion in high-entropy carbide ceramics from first-principles calculations. *Journal of the American Ceramic Society* **104**, 1874-1886 (2021). https://doi.org:10.1111/jace.17600

10 Wang, Y. *et al.* Enhancing properties of high-entropy alloys via manipulation of local chemical ordering. *Journal of Materials Science & Technology* **180**, 23-31 (2024). https://doi.org:10.1016/j.jmst.2023.10.003

11 Wang, L., Maxisch, T. & Ceder, G. Oxidation energies of transition metal oxides within theGGA+Uframework. *Physical Review B* **73**, 195107 (2006). https://doi.org:10.1103/PhysRevB.73.195107

12 Söderlind, P., Landa, A. & Turchi, P. E. A. Comment on "Correlation and relativistic effects in U metal and U-Zr alloy: Validation ofab initioapproaches". *Physical Review B* **90**, 157101 (2014). https://doi.org:10.1103/PhysRevB.90.157101

13 Yan, Y. *et al.* Intermetallic Nanocrystals: Syntheses and Catalytic Applications. *Advanced Materials* **29**, 1605997 (2017). https://doi.org:10.1002/adma.201605997

14 Zhao, J. *et al.* Co NP/NC hollow nanoparticles derived from yolk-shell structured ZIFs@polydopamine as bifunctional electrocatalysts for water oxidation and oxygen reduction reactions. *Journal of Energy Chemistry* **27**, 1261-1267 (2018). https://doi.org:10.1016/j.jechem.2018.04.015

15 Choi, S. I. *et al.* Synthesis and characterization of 9 nm Pt-Ni octahedra with a record high activity of 3.3 A/mg(Pt) for the oxygen reduction reaction. *Nano Lett* **13**, 3420-3425 (2013). https://doi.org:10.1021/nl401881z

16 Zhevnenko, S. N., Petrov, I. S., Scheiber, D. & Razumovskiy, V. I. Surface and segregation energies of Ag based alloys with Ni, Co and Fe: Direct experimental measurement and DFT study. *Acta Materialia* **205**, 116565 (2021). https://doi.org:10.1016/j.actamat.2020.116565

Response to reviewers (NCOMMS-24-57617A)

We sincerely extend our heartfelt gratitude to the four reviewers for their recognition and support of our work. In response to the three issues raised by Reviewer 4, we have earnestly adopted and thoroughly considered his/her suggestions. Below, we address the reviewer's comments point by point and clearly indicate the corresponding revisions made.

Reviewers' comments:

Reviewer #4

Comment 1: I agree with the answer given by the authors – the adsorption site consists of several atoms. In the pictures shown in Figure 4, the adsorption sites primarily consist of Pt, which makes sense because Pt is close to the optimal activity for ORR. One could even speculate that the antisite defects are favorable because it gives rise to more hollow sites with two Pt atoms + one non-noble metal. However, the text currently reads:

"Notably, even for non-noble metal sites, such as the Zn12 site, the energy barrier for the ratelimiting step is only 0.363 eV (Figure 4h), which is lower than that of Pt (111). To our knowledge, Zn is not typically considered a highly active element in the ORR. However, it was activated as a highly active site in PD-PZFCN-HEI. These results indicated the presence of multiple active sites on the PD-PZFCNC-HEI surface."

This statement is not correct and should be rewritten to reflect that Zn might be part of the active site but is not solely responsible for the activity. Furthermore, given that the active site contains more than one atom, many different combinations of elements are possible, and the calculated sites are not necessarily representative. While I appreciate that a thorough investigation of representative configurations might be beyond the scope of this work, I believe that this should also be conveyed to the reader.

Response: Thanks for reviewer's professional suggestions. We wholeheartedly concur with your perspective. Indeed, for the ORR process, the adsorption of oxygen-containing intermediates on the PD-PZFCNC-HEI surface is not governed by a single metal site but rather by the synergistic interaction between the central metal atom and its surrounding metal atoms, as illustrated in Figure S54b. Consequently, our previous description of the metal sites may have been inaccurate and potentially misleading. In light of this, we have revised the corresponding descriptions in the manuscript to better reflect this understanding. We employ the abbreviated notation M_c–$M_1M_2M_3M_4M_5M_6$ to delineate the reactive sites, wherein M_c signifies the central metallic atom, and M1 through M6 denote the adjacent metallic atoms. This nomenclature effectively encapsulates the central site along with all the coordinating metallic atoms in its vicinity.

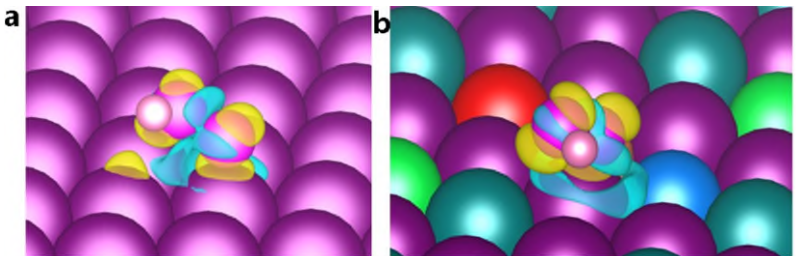

Figure S54. Differential charge density ($\Delta\rho = \rho_{*OOH} - \rho_{*} - \rho_{OOH}$) of *OOH adsorbed system at (a) Pt (111) and (b) the PD-PFCNCZ-HEI. The isosurface in blue and yellow represent charge accumulation and depletion, respectively.

Changes made in the revised manuscript:

In the revised manuscript, we added description: "Given that the interaction between the high-entropy intermetallic surface and oxygen-containing intermediates is characterized by multi-metal synergistic coupling rather than single-metal adsorption,[54] the sites on the PD-PZFCNC-HEI surface are denoted as M_c–$M_1M_2M_3M_4M_5M_6$, representing a central metal

atom (M_c) and six adjacent metal atoms (M_1-M_6). At an equilibrium potential of 1.23 V vs. RHE, the rate-limiting step for the reaction pathway of *O at the top site on Pt(111) is the hydrogenation of O_2 to form the *OOH intermediate with a ΔG of 0.406 eV (Figure S50). The rate-determining energy barriers for the bridge and hollow sites are 1.0517 eV (Figure S51a) and 1.053 eV (Figure S51b), respectively. Similarly, the rate-limiting step at the Pt-PtCoNiPtPtZn site on the PD-PZFCNC-HEI surface is also the O_2 hydrogenation step, corresponding to a ΔG value of 0.381 eV (Figure 4g), which is lower than the rate-limiting steps of all Pt(111) surface reaction pathways. Moreover, the integrated projection of the crystal orbital Hamiltonian population values (ICOHP) of the Pt–*OH bond of the Pt-PtCoNiPtPtZn (Figure 4j) and Zn-CrPtPtPtPtPt (Figure 4k) sites on the PD-PZFCNC-HEI surface were calculated to be 0.535 and 0.507, respectively, both lower than the value of 1.270 for Pt (111) (Figure 4i)." and "Notably, even for non-noble metal sites, such as the Zn-CrPtPtPtPtPt site, the energy barrier for the rate-limiting step is only 0.363 eV (Figure 4h), which is lower than that of Pt (111)."

The title of Figure 4 has been revised as follows:

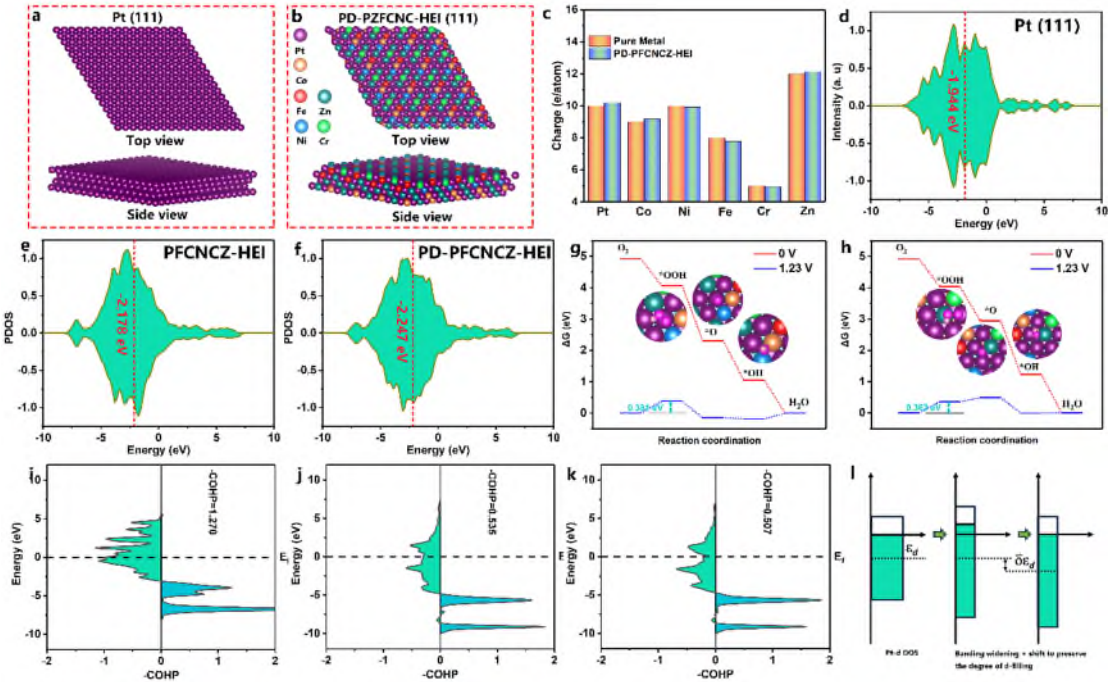

Figure 4. Mechanistic insights into the ORR catalytic reaction by PD-PZFCNC-HEI. The top and side views of the (a) Pt (111) and (b) PD-PZFCNC-HEI (111) surface models; (c) The number of outer electrons in the surface atoms of PD-PZFCNC-HEI and the corresponding pure metal from Bader charge analysis; Partial density of states (PDOS) of the d-band for the surface Pt atoms in (d) Pt (111), (e) PZFCNC-HEI and (f) PD-PZFCNC-HEI surface; The free energies of intermediates of (g) Pt-PtCoNiPtPtZn and (h) Zn-CrPtPtPtPtPt sites on the PD-PZFCNC-HEI surface for the ORR steps; COHP and ICOHP for *OH adsorption intermediates at (i) Pt (111), (j) the Pt-PtCoNiPtPtZn and (k) the Zn-CrPtPtPtPtPt sites on PD-PZFCNC-HEI; (l) Variation of Pt d-band structure with compressive strain.

Comment 2. Yes, in principle the adsorbate should move to the site that is most stable, however this will not always happen due to symmetry constraints (which might be present on pure Pt but not on the HEI surface) or because the top site is a local maximum with no gradient. However, on a real Pt surface diffusion between different surface sites should be thermally accessible. The Pt energy diagram should therefore consist of the adsorbates in their most stable adsorption site for a fair comparison with the HEI structures. There are plenty of examples in the literature that can be used for comparison. In this respect it would also be useful if the authors included in the methods section how the free energies were calculated, e.g. following ref 5?

Response: Thanks for reviewer's professional suggestions. Based on your suggestion, we calculated the reaction pathways

for the *O intermediate at different sites (top, bridge, and hollow) on the Pt (111) surface, as shown in Figure S51, Figure S52a, and Figure S52b, respectively. It can be observed that the reaction energy barriers on the PD-PZFCNC-HEI surface (Figure 4g and h), whether at the Pt-PtCoNiPtPtZn (0.381 eV) or Zn-CrPtPtPtPtPt (0.363 eV) sites, are lower than those of all reaction pathways on Pt (111). This further validates the high catalytic activity of PD-PZFCNC-HEI.

Regarding the density functional theory (DFT) computations pertaining to the oxygen reduction reaction (ORR), we opted for the associative mechanism involving a four-electron pathway. In conjunction with this, we employed the computational standard hydrogen electrode framework, as introduced by Nørskov and colleagues, to assess the theoretical ORR efficacy of the relevant slab models[1]. In summary, the free energy change for each reaction step can be represented by the subsequent equations:

$\Delta G_1 = E(*) - E(\mathrm{HOO}*) + E_{\mathrm{O2}} + 1/2E_{\mathrm{H2}} + (\Delta ZPE - T\Delta S)_1 - eU$ (1)

$\Delta G_2 = E(\mathrm{HOO}*) - E(\mathrm{O}*) - E_{\mathrm{H2O}} + 1/2E_{\mathrm{H2}} + (\Delta ZPE - T\Delta S)_2 - eU$ (2)

$\Delta G_3 = E(\mathrm{O}*) - E(\mathrm{HO}*) + 1/2E_{\mathrm{H2}} + (\Delta ZPE - T\Delta S)_3 - eU$ (3)

$\Delta G_4 = E(\mathrm{HO}*) - E(*) - E_{\mathrm{H2O}} + 1/2E_{\mathrm{H2}} + (\Delta ZPE - T\Delta S)_4 - eU$ (4)

The total energies of the pristine surface and the surface with adsorbed intermediates are denoted as $E(*)$, $E(\mathrm{HOO})$, $E(\mathrm{O}*)$, and $E(\mathrm{HO}*)$, respectively. The energies calculated for H_2O, H_2, and O_2 molecules are represented by E_{H2O}, E_{H2}, and E_{O2}, respectively. The ΔZPE values were derived from the vibrational frequencies obtained through computation, while the -eU term signifies the external bias U applied at each stage. To circumvent the DFT-based calculation of O_2, the free energy change for the overall reaction $H_2O \rightarrow 1/2O_2 + H_2$ was set at the experimentally determined value of 2.46 eV per water molecule. The theoretical overpotential for the reaction (η_{ORR}) can be determined by assessing the disparity between the minimum voltage required for ORR (1.23 V) and the voltage necessary to render all free-energy steps energetically favorable, which can also be expressed by the following equation:

$\eta_{\mathrm{ORR}} = 1.23 - \min(\Delta G_{1\text{-}4})$ (5)

where $\min(\Delta G_{1\text{-}4})$ is the step with the smallest ΔG value in $\Delta G_{1\text{-}4}$.

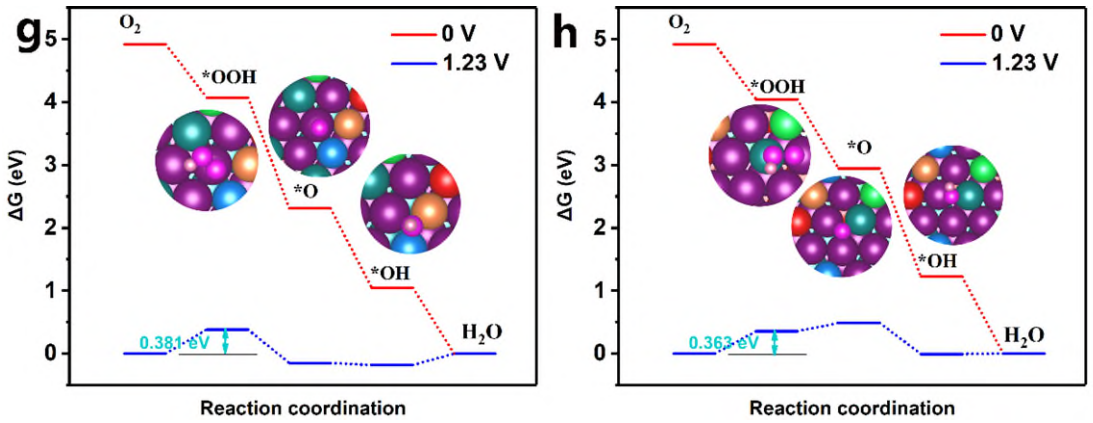

Figure 4g-h: The free energies of intermediates of (g) Pt-PtCoNiPtPtZn and (h) Zn-CrPtPtPtPtPt sites on the PD-PZFCNC-HEI surface for the ORR steps.

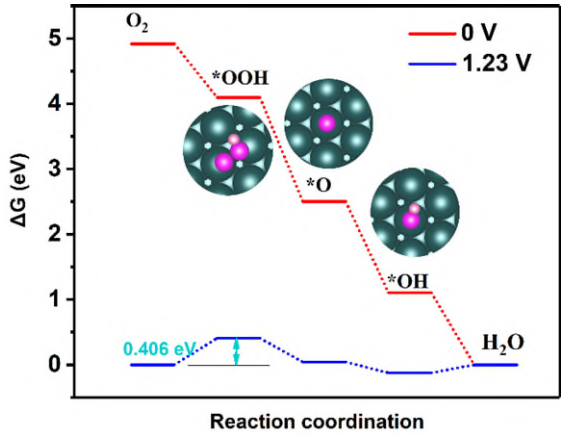

Figure S51. The free energies of intermediates on the Pt (111) surface for the ORR steps. (*O intermediate is in the top position)

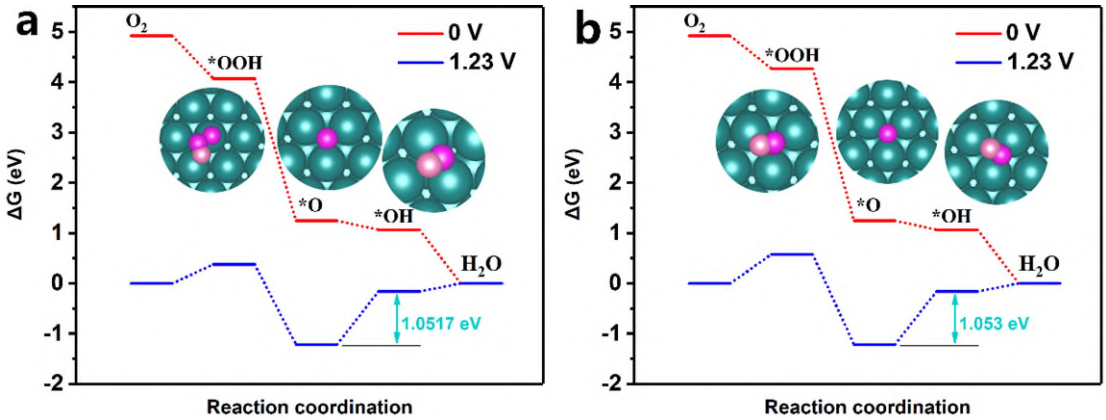

Figure S52. The reaction pathways for the intermediate *O on the Pt (111) surface at (a) the bridge site and (b) the hollow site during the ORR.

Changes made in the revised manuscript:

In the revised manuscript, we changed a description: "At an equilibrium potential of 1.23 V vs. RHE, the rate-limiting step for the reaction pathway of *O at the top site on Pt (111) is the hydrogenation of O_2 to form the *OOH intermediate with a ΔG of 0.406 eV (Figure S51). The rate-determining energy barriers for the bridge and hollow sites are 1.0517 eV (Figure S52a) and 1.053 eV (Figure S52b), respectively. Similarly, the rate-limiting step at the Pt-PtCoNiPtPtZn site on the PD-PZFCNC-HEI surface is also the O_2 hydrogenation step, corresponding to a ΔG value of 0.381 eV (Figure 4g), which is lower than the rate-limiting steps of all the Pt (111) surface reaction pathways."

In the supporting information, a descript was added: "Regarding the density functional theory (DFT) computations pertaining to the ORR, we opted for the associative mechanism involving a four-electron pathway. In conjunction with this, we employed the computational standard hydrogen electrode framework, as introduced by Nørskov and colleagues, to assess the theoretical ORR efficacy of the relevant slab models[1]."

Figure S52 was replaced in supporting information as follows:

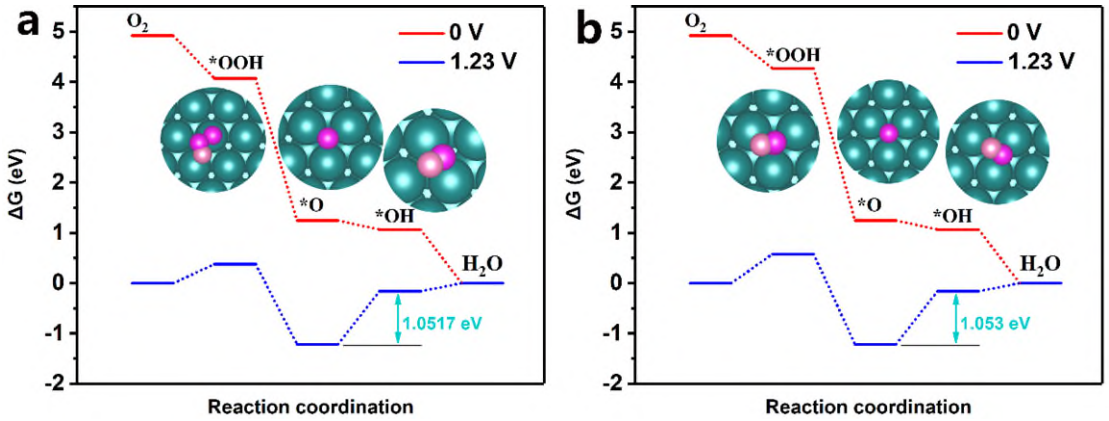

Figure S52. The reaction pathways for the intermediate *O on the Pt (111) surface at (a) the bridge site and (b) the hollow site during the ORR.

Comment 3. Total energies can be compared only if the structures being compared have the same number of atoms of each element. It is unclear to me if this has been considered for the defect structures? If the defect structures are formed by replacing one Zn with one Pt in one structure and one Cr with one Pt in another, the energies cannot be compared. Instead an appropriate reference should be used to say anything about the relative energies of replacing each of the non-noble metals. Therefore, please consider if the following statement is correct:

"The energies of these models were -382.18 eV, -377.76 eV, -376.15 eV, -381.19 eV, and -375.02 eV, respectively. It can be inferred that the inverse defect structure where Zn sites are replaced has the lowest energy and the most stable structure."

Response: We sincerely appreciate the reviewer's positive comments on our work. Based on your suggestion, for the construction of the Pt antisite defect model, we first built the PtFe (111) surface structure based on the P4/mmm space group of the PtFe bulk phase. Subsequently, by randomly substituting Fe sites in the PtFe (111) surface structure with other non-precious metal elements, we obtained the defect-free PZFCNC-HEI reference model, with elemental ratios derived from experimental results (Pt:Cr:Fe:Co:Ni:Zn = 1:0.137:0.171:0.123:0.115:0.445). Following this, we generated 10 different defect-free (4 × 4 × 4) PZFCNC-HEI unit cells, with energy differences of less than 0.5 eV, indicating that their distribution has minimal impact on the stability of the bulk structure, as shown in Figures S47a-j. Among these models, we selected Figure S47a, which has the lowest energy (-477.76 eV) and is therefore considered the most stable structure, as the PZFCNC-HEI model, with its surface depicted in Figure S48. Considering that Pt antisite defects can replace any non-precious metal atom, we sequentially constructed Pt antisite defect models by substituting Zn, Fe, Co, Ni, and Cr sites on the PZFCNC-HEI (111) model surface. These models were then optimized, and each exhibited stable energy convergence.

Since the substitution of different elements results in slight deviations in the number of each element in the defect models, we chose to compare the substitutions of each element separately. For example, since the PZFCNC-HEI surface in Figure S48 has three Zn atoms at different positions, we replaced each of these Zn atoms with Pt to obtain three different PD-PZFCNC-HEI defect models (Figures S49a-c). Among these, Figure S49a exhibited the lowest energy, and thus, we selected it as the representative PD-PZFCNC-HEI defect model with Pt substitution at Zn sites for further calculations. The energy barriers of the rate-determining steps calculated based on this model (Figures 4g, h) were found to be lower than those of the Pt(111) surface (Figure S51). To further validate the advantages of Pt antisite defects, we continued calculations based on the PD-PZFCNC-HEI-2 defect model (Figure S50a), where Pt replaces Fe to form an antisite defect. The energy barrier of the rate-determining step obtained from this model (Figure S55) was also lower than that of the Pt (111) surface (Figure S51). Therefore, it can be further inferred that antisite defects play an optimizing role in the ORR process.

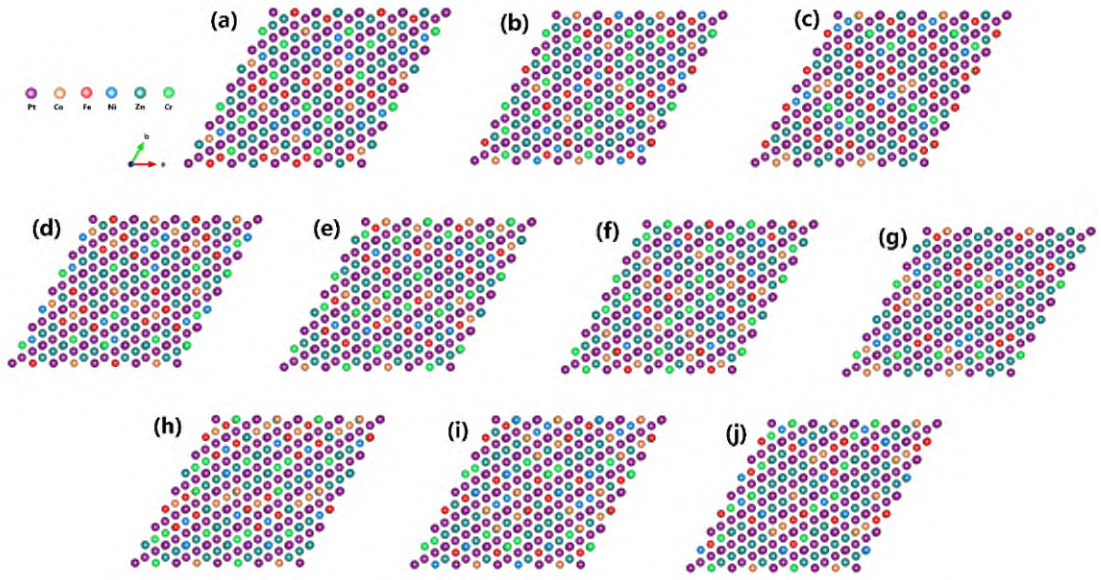

Figure S47. Constructed a series of defect free PFCNZ-HEI (111) surface models. The energies for (a)-(j) were -377.69 eV, -376.53 eV, -376.74 eV, -376.09 eV, -377.33 eV, -374.75 eV, -376.59 eV, -375.51 eV, 377.37 eV, -377.6 eV, respectively.

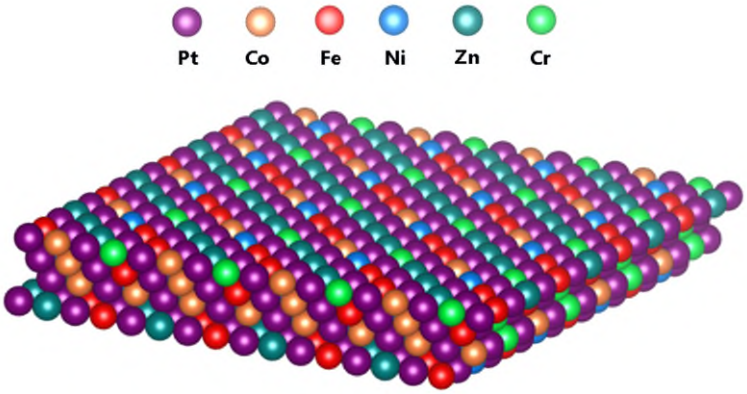

Figure S48. The PZFCNC-HEI (111) surface reference models of Figure S47a.

Figure S49. (a-c) A series of defect PD-PFCNZ-HEI (111) surface models were constructed by replacing the three different Zn sites on the surface with Pt. The energies of these three models are: -382.18 eV, -382.02 eV, and -377.76 eV, respectively. Therefore, Figure S49a was selected as the most stable Pd-PFCNZ-HEI (111) model with Zn sites substituted by Pt antisite defects.

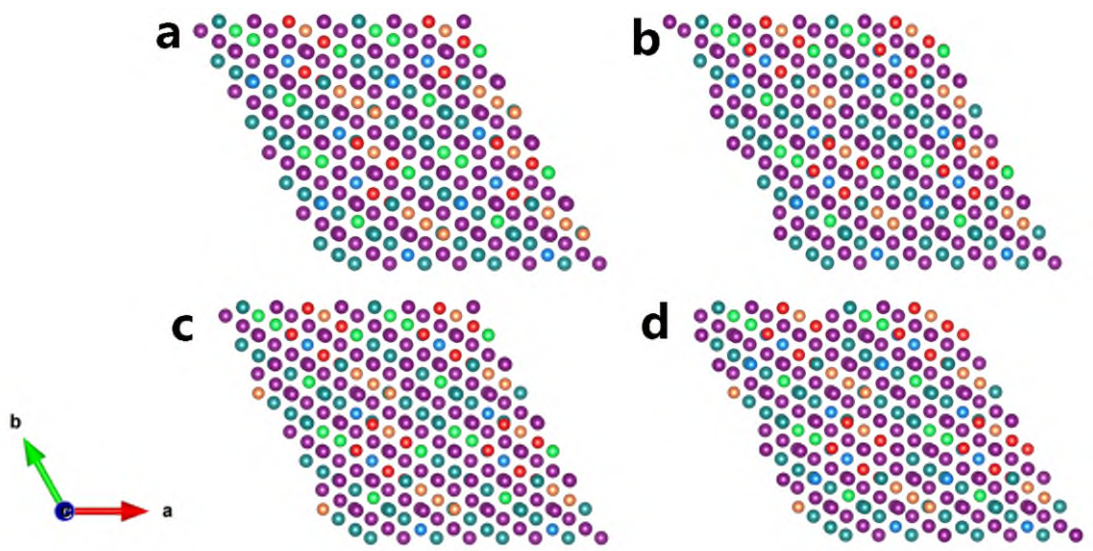

Figure S50. Constructed a series of PD-PFCNZ-HEI (111) surface models. where (a)–(d) represent the antisite defect models with Pt atom substituting Fe, Co, Ni, and Cr sites, respectively.

Considering the possibility of Pt atom antisite defects replacing any non-noble metal atom, we sequentially constructed Pt antisite defect models by substituting Fe, Co, Ni, and Cr sites on the (111) surface. Subsequently, the models were optimized, and each model exhibited stable energy convergence. The energies for these models were -377.76 eV, -376.15 eV, -381.19 eV, and -375.02 eV, respectively.

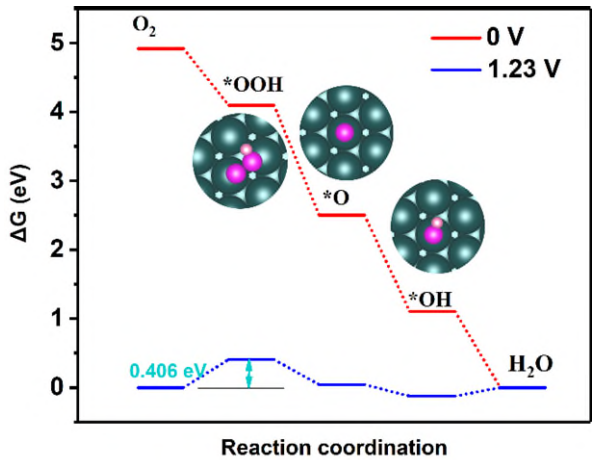

Figure S51. The free energies of intermediates on the Pt (111) surface for the ORR steps. (*O intermediate is in the top position)

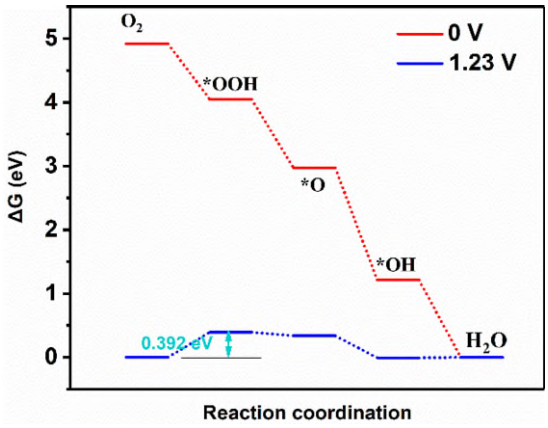

Figure S55. Free energy of intermediates in the ORR steps on the PD-PZFCNC-HEI-2 surface formed by Pt substitution at the Fe site.

Changes made in the revised manuscript:

In the revised manuscript, we changed a description: "Based on this model, we constructed anti-site defect models by sequentially replacing each outermost non-noble metal atom with a Pt atom (Figure S49 and S50). After optimization, the most stable antisite defect model, PD-PZFCNC-HEI, formed by Pt substitution at the Zn site, was selected as a case for analysis (Figure 4b and Figure S49a)."

In the supporting information, we added a description: "Supplementary Note 5: For the construction of the Pt antisite defect model, we first built the PtFe (111) surface structure based on the P4/mmm space group of the PtFe bulk phase. Subsequently, by randomly substituting Fe sites in the PtFe (111) surface structure with other non-precious metal elements, we obtained the defect-free PZFCNC-HEI reference model, with elemental ratios derived from experimental results (Pt:Cr:Fe:Co:Ni:Zn = 1:0.137:0.171:0.123:0.115:0.445). Following this, we generated 10 different defect-free (4 × 4 × 4) PZFCNC-HEI unit cells, with energy differences of less than 0.5 eV, indicating that their distribution has minimal impact on the stability of the bulk structure, as shown in Figures S47a-j. Among these models, we selected Figure S47a, which has the lowest energy (-477.76 eV) and is therefore considered the most stable structure, as the PZFCNC-HEI model, with its surface depicted in Figure S48. Considering that Pt antisite defects can replace any non-precious metal atom, we sequentially constructed Pt antisite defect models by substituting Zn, Fe, Co, Ni, and Cr sites on the PZFCNC-HEI (111) model surface. These models were then optimized, and each exhibited stable energy convergence. Since the substitution of different elements results in slight deviations in the number of each element in the defect models, we chose to compare the substitutions of each element separately. For example, since the PZFCNC-HEI surface in Figure S48 has three Zn atoms at different positions, we replaced each of these Zn atoms with Pt to obtain three different PD-PZFCNC-HEI defect models (Figures S49a-c). Among these, Figure S49a exhibited the lowest energy, and thus, we selected it as the representative PD-PZFCNC-HEI defect model with Pt substitution at Zn sites for further calculations. The energy barriers of the rate-determining steps calculated based on this model (Figures 4g, h) were found to be lower than those of the Pt(111) surface (Figure S51). To further validate the advantages of Pt antisite defects, we continued calculations based on the PD-PZFCNC-HEI-2 defect model (Figure S50a), where Pt replaces Fe to form an antisite defect. The energy barrier of the rate-determining step obtained from this model (Figure S55) was also lower than that of the Pt (111) surface (Figure S51). Therefore, it can be further inferred that antisite defects play an optimizing role in the ORR process."

Figure S49, S50 and S55 was replaced in supporting information as follows:

Figure S49. (a-c) A series of defect PD-PFCNZ-HEI (111) surface models were constructed by replacing the three different Zn sites on the surface with Pt. The energies of these three models are: -382.18 eV, -382.02 eV, and -377.76 eV, respectively. Therefore, Figure S49a was selected as the most stable Pd-PFCNZ-HEI (111) model with Zn sites substituted by Pt antisite defects.

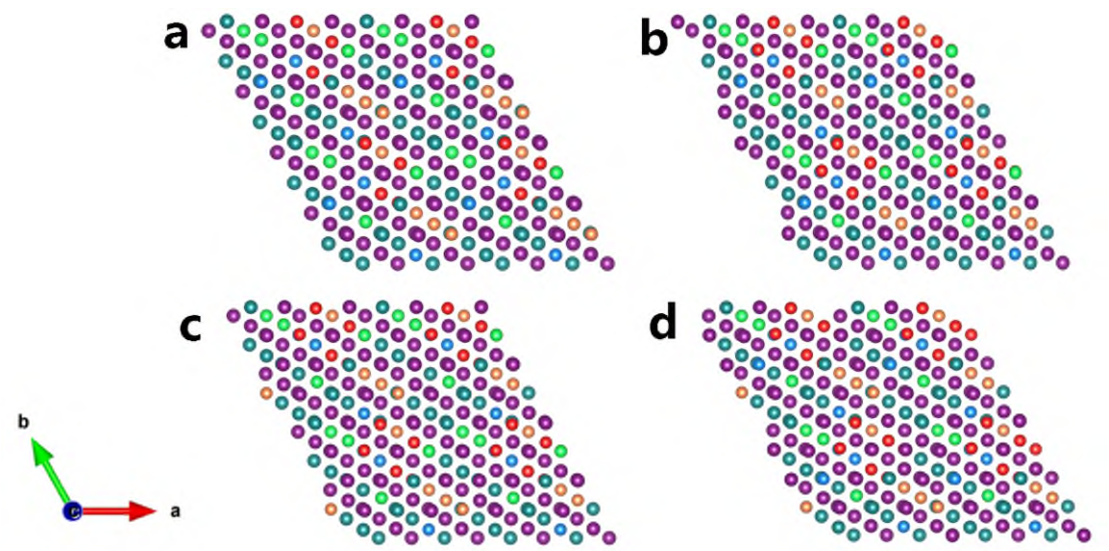

Figure S50. Constructed a series of PD-PFCNZ-HEI (111) surface models. where (a)–(d) represent the antisite defect models with Pt atom substituting Fe, Co, Ni, and Cr sites, respectively. Considering the possibility of Pt atom antisite defects replacing any non-noble metal atom, we sequentially constructed Pt antisite defect models by substituting Fe, Co, Ni, and Cr sites on the (111) surface. Subsequently, the models were optimized, and each model exhibited stable energy convergence. The energies for these models were -377.76 eV, -376.15 eV, -381.19 eV, and -375.02 eV, respectively.

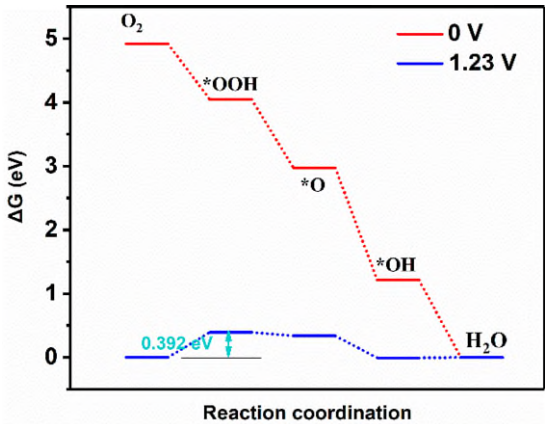

Figure S55. Free energy of intermediates in the ORR steps on the PD-PZFCNC-HEI-2 surface formed by Pt substitution at the Fe site.

Refence:

1 K., N. J., J., R., A., L. & L., L. Origin of the Overpotential for Oxygen Reduction at a Fuel-Cell Cathode. *J. Phys. Chem. B* **108**, 17886-17892 (2004). https://doi.org:10.1021/jp047349j

Overall, the revision has improved the manuscript and answered some of my concerns. However, a few points should be corrected or conveyed more clearly in the paper before it can be published. New comments, related to the answers to my previous comments, are written in blue.

Comment 5: The insets in Figure 4g-h are likewise too small. However, if you zoom in it can be seen that the adsorbates are not in the same adsorption sites. Notably, the diagram which is stated to be a Zn adsorption site (Figure 4h) shows pictures where the adsorbates are never bound to Zn only. The other diagram (Figure 4g) appears to have *OH in a site that is not present in the pictures for *O and *OOH. Are these pictures taken from the optimized structures? Is the reason that Zn sites are found to be surprisingly active perhaps that the adsorbates move during optimisation?

Response: We sincerely appreciate the reviewer's valuable comments. Based on your suggestion, we have enlarged the 4g and Figure 4h illustrations. As can be seen, the intermediates are not fully localized at their corresponding sites, as we have provided the optimized structure. The improvement in catalytic activity is certainly related to the final optimized adsorption positions of the species, so presenting the optimized positions is the most reasonable approach. In fact, the adsorption process of intermediates at each site on the high-entropy intermetallic surface is not isolated, but rather influenced by multiple metal atoms. As shown in Figure S53, when *OOH adsorbs on the Pt reactive sites of the PD-PZFCNC-HEI surface, charge transfer occurs not only between *OOH and Pt but also between *OOH and neighboring non-precious metal atoms. This also explains that part of the high catalytic activity of PD-PZFCNC-HEI results from the synergistic effect of multiple elements.

I agree with the answer given by the authors – the adsorption site consists of several atoms. In the pictures shown in Figure 4, the adsorption sites primarily consist of Pt, which makes sense because Pt is close to the optimal activity for ORR. One could even speculate that the antisite defects are favorable because it gives rise to more hollow sites with two Pt atoms + one non-noble metal. However, the text currently reads:

"Notably, even for non-noble metal sites, such as the Zn12 site, the energy barrier for the rate-limiting step is only 0.363 eV (Figure 4h), which is lower than that of Pt (111). To our knowledge, Zn is not typically considered a highly active element in the ORR. However, it was activated as a highly active site in PD-PZFCN-HEI. These results indicated the presence of multiple active sites on the PD-PZFCNC-HEI surface."

This statement is not correct and should be rewritten to reflect that Zn might be part of the active site but is not solely responsible for the activity.

Furthermore, given that the active site contains more than one atom, many different combinations of elements are possible, and the calculated sites are not necessarily representative. While I appreciate that a thorough investigation of representative configurations might be beyond the scope of this work, I believe that this should also be conveyed to the reader.

Comment 6: For the pure Pt reference (figure S43) all adsorbates are positioned on top, while for the HEIs a mixture of top, bridge and hollow site adsorption sites are shown. On Pt, *O is usually more stable in th. For the pure Pt reference (figure S43) all adsorbates are positioned on top, while for the HEIs a mixture of tope hollow site, while on a HEI the most stable site will depend on the neighbouring atoms, and the adsorbate will not necessarily relax to this position. Thus, different adsorption sites (top, bridge, hollow) as well as different adsorption environments for the HEI should be tested to be able to conclude anything. This is especially true considering the small energy differences presented here. Furthermore, it could provide substance to the claim that the Pt antisite defects are important.

Response: We sincerely appreciate the reviewer's valuable comments. Based on your suggestion, in order to consider the reaction sites for *O more comprehensively, we have also calculated the reaction pathways for the *O intermediate at the bridge and hollow sites on Pt (111), as shown in Figure S51. As can be seen, the reaction barriers for *O at the bridge and hollow sites are higher than that at the top site, indicating that the reaction pathway on the top site will still be preferred on the Pt (111) surface.

On the other hand, for PD-PZFCNC-HEI, the reaction intermediates undergo natural optimization relaxation, and theoretically, they will relax to their most stable positions. Therefore, the *O intermediate could be at the bridge site (as shown in Figure 4g) or at the hollow site (as shown in Figure 4h). It can be stated that during the optimization process, the adsorbates naturally move to more stable adsorption positions, and whether or not the adsorbates were initially placed at the bridge or hollow sites on the high-entropy surface model does not affect our current results. Moreover, the current results are sufficient to explain the existing experimental observations.

Yes, in principle the adsorbate should move to the site that is most stable, however this will not always happen due to symmetry constraints (which might be present on pure Pt but not on the HEI surface) or because the top site is a local maximum with no gradient. However, on a real Pt surface diffusion between different surface sites should be thermally accessible. The Pt energy diagram should therefore consist of the adsorbates in their most stable adsorption site for a fair comparison with the HEI structures. There are plenty of examples in the literature that can be used for comparison. In this respect it would also be useful if the authors included in the methods section how the free energies were calculated, e.g. following ref 5?

Comment 7: It is unclear how the surface formation energies are calculated? The values are very large. For the calculation of antisite defects, as I understand it a random atom has been swapped for Pt in the original surface model. However, the defect formation energy depends on the local environment, and conclusions cannot be made based on a single defect structure.

Response: We sincerely appreciate the reviewer's valuable comments. This is an error in our statement. What we calculated are the structural energies of these structures, not the surface formation energies. Surface formation energy refers to the energy required to transform a material from its bulk state to a surface state, which requires the energy information of the bulk phase. However, the models we have constructed here are primarily based on the (111) crystal plane to study the catalytic process on this surface[16]. Therefore, surface formation energy cannot be calculated in this case. Instead, we computed the energies of the constructed structures to identify the most stable structural model.

For the construction of the Pt antisite defect model, we first built the PtFe (111) surface structure based on the P4/mmm space group of the PtFe bulk phase. Then, by randomly substituting Fe sites in the PtFe (111) surface structure with other non-precious metal elements, we obtained the defect-free PZFCNC-HEI reference model, with elemental ratios derived from experimental results (Pt:Cr:Fe:Co:Ni:Zn = 1:0.137:0.171:0.123:0.115:0.445). Next, we generated 10 different defect-free (4 × 4 × 4) PZFCNC-HEI unit cells, with energy differences of less than 0.5 eV, indicating that their distribution has minimal impact on the stability of the bulk structure, as shown in Figure S47a-j. Among these models, we selected Figure S47a, which has the lowest energy (-477.76 eV) and is therefore considered the most stable structure, as the PZFCNC-HEI model, with its surface shown in Figure S48. Considering that Pt antisite defects can replace any non-precious metal atom, we sequentially constructed Pt antisite defect models by substituting Zn, Fe, Co, Ni, and Cr sites on the PZFCNC-HEI (111) model surface. Subsequently, these models were optimized, and each exhibited stable energy convergence, as shown in Figure S49. The energies of these models were -382.18 eV, -377.76 eV, -376.15 eV, -381.19 eV, and -375.02 eV, respectively. It can be inferred that the inverse defect structure where Zn sites are replaced has the lowest energy and the most stable structure. Therefore, the model shown in Figure S47a was selected as the defect model PD-PZFCNC-HEI for subsequent studies.

To further illustrate the impact of Pt defects on the performance of HEIs, we selected the defect-free HEI structure with the second-lowest Gibbs free energy, shown in Figure S47j. Based on this structure, we sequentially replaced non- precious metal atoms (Zn, Fe, Co, Ni, Cr) with Pt atoms to construct defect models, as shown in Figure S54a-e. Among these, the model with the lowest energy, shown in Figure S54a, was selected for further exploration and designated as PD-PZFCNC-HEI-2, as detailed in Figure S55. By calculating the Gibbs free energy of the surface reaction intermediates for PD-PZFCNC-HEI-2, we found that the rate-determining step is the hydrogenation process of O2, with an energy barrier of 0.354 eV, which is still significantly lower than the barrier for the Pt (111) surface (0.406 eV, Figure S50). This further supports the validation of the defect structure in enhancing catalytic activity.

Total energies can be compared only if the structures being compared have the same number of atoms of each elements. It is unclear to me if this has been considered for the defect structures? If the defect structures are formed by replacing one Zn with one Pt in one structure and one Cr with one Pt in another, the energies cannot be compared. Instead an appropriate reference should be

used to say anything about the relative energies of replacing each of the non-noble metals. Therefore, please consider if the following statement is correct:

"The energies of these models were -382.18 eV, -377.76 eV, -376.15 eV, -381.19 eV, and -375.02 eV, respectively. It can be inferred that the inverse defect structure where Zn sites are replaced has the lowest energy and the most stable structure."